Ana Raquel Ribeiro Fernandes

Degree in Biochemistry

Live cell biosensors for detection and quantification of viral pathogens

Dissertation to obtain Master's Degree in

Biochemistry for Health

Supervisor: Ana Sofia Coroadinha, PhD, ITQB NOVA/iBET

Co-Supervisor: Miguel Ricardo Guerreiro, PhD, ITQB NOVA/iBET

December 2020

Ana Raquel Ribeiro Fernandes

Degree in Biochemistry

Live cell biosensors for detection and quantification of viral pathogens

Dissertation to obtain Master's Degree in

Biochemistry for Health

Supervisor: Ana Sofia Coroadinha, PhD, ITQB NOVA/iBET

Co-Supervisor: Miguel Ricardo Guerreiro, PhD, ITQB NOVA/iBET

December 2020

Acknowledgements

It is not only the end of a long and challenging journey, but also the beginning of a new chapter. As it should be, I would like to express my gratitude to all the amazing people who helped me during this year.

My first words of acknowledgement go to my supervisor, Dr. Ana Sofia Coroadinha, for giving me the opportunity to work in the Cell Line Development and Molecular Virology group of the Animal Cell Technology Unit at iBET. For always providing a good work environment, constant support, scientific guidance, and most of all, for teaching me to always look for the positive side.

A special acknowledgment goes to Miguel Guerreiro for everything he taught me. For being the most dedicated and tireless teacher, I have ever had. For all the patience and understanding. For helping and guiding me. For shaping who I believe will turn into a great scientist! This would not be possible without you! Thank you, Miguel.

To my colleagues of the CLD&MV Lab: Ana Isabel, Miguel, Filipa, Sofia, Catarina, Maria, Rodrigo, Tiago, Elisa, and Mariana; thank you for all the support, availability, encouragement and knowledge. Most importantly, thank you for the great work environment.

A special thanks goes to my beloved “cremosas” Maria João e Joana for being the best lab partners ever. For being the best friends Lisbon could ever give me. For all the laughter, tears, concerns and coffees shared. For the best sleepovers. For being the truest friends when I needed the most. For being my family here. But most of all, for all the times they babbysitted my cells :)

Aos meus pais e ao meu irmão, por sempre apoiarem os meus sonhos, por acreditarem em mim e no meu potencial e por me darem as melhores ferramentas para um futuro risonho. Por serem peças fundamentais na construção daquilo que sou hoje. Isto é tanto meu como vosso.

Ao Daniel, por ser o melhor ouvinte e o meu maior pilar. Por viver as minhas batalhas como se fossem dele. Por me apoiar de forma incondicional e por me mostrar sempre o lado positivo. Por ser a melhor pessoa que poderia ter ao meu lado e por nunca, em alguma circunstância, me falhar. Acima de tudo, por me encorajares. Sem ti não estaria aqui.

À Helena, por dar a Lisboa um gosto a lar Vimaranense.

A todos os meus amigos e família próxima, por saberem que apesar de longe, estou perto. Por serem pessoas magníficas e me relembrarem sempre o quão bom é estar de volta a casa.

Abstract

Every year, thousands of human lives are lost due to viral pathogen infections, namely Zika and Chikungunya. Currently, no vaccines or antivirals are available to prevent and treat these infections. This current and imperative medical necessity is detained by the urgent need for reliable tools to study these viruses in both fundamental and applied research.

To tackle the presented problems, we developed, (i) a platform relying on a cell-based approach for viral detection and (ii) a virus-based tool for antiviral screenings. For the cell-based approach, split-GFP with prevented transcomplementation by single – embedment in an eglin c molecule (eGFP11) or intein cyclization (cyGFP11) – or dual distortions – using coiled-coils (ccGFP10+ccGFP11) – was used. Proteolysis, here performed by proof of concept viral protease TEVp, relieves the introduced distortions, promoting fragments re-assembly and fluorescence emission. As virus-based tool, pseudotyped chimeric rVLPs harboring mCherry, TEVp (single strategies) or both proteins (dual strategy) were developed for separate or concomitant monitoring of cell entry (mCherry) and viral proteolytic activity (TEVp).

Of the cell-based sensors tested, coiled-coils distortions presented the best performance, with a signal-to-noise ratio up to 97 ± 21. A cell line stably expressing this sensor – 293cc11/10 – was established. Transient studies showed sensor activation, in contrast to stable cells. Single and dual chimeric rVLPs were characterized, revealing similar transfection, sensor activation and production performances. Hence, VSV-G enveloped rVLPs incorporating mCherry or/and TEVp were produced and used to infect 293cc11/10 cells. While mCherry incorporation did not substantially affect rVLP production yields and enabled effective monitoring of particle cell entry, TEVp incorporation hampered rVLP production, reducing titers to 1.40%. Kinetic studies with the rVLPs showed successful protein delivery and high mCherry signal intensity at 24 hours post-infection.

Overall, we developed a cell-based sensor system and rVLPs enabling pseudotyping, providing promising tools for virus detection and antiviral screenings.

Keywords: Zika, Chikungunya, Cell-based biosensor, protease, virus detection, chimeric retrovirus-like particles, antiviral screenings.

Resumo

Atualmente, milhares de vidas humanas são perdidas devido a infeções virais, nomeadamente Zika e Chikungunya. Como resultado da falta de métodos confiáveis para estudar estes virus, não existem vacinas ou antivirais para prevenção ou tratamento.

Posto isto, desenvolvemos (i) uma plataforma baseada em células para deteção de vírus e (ii) uma ferramenta baseada em vírus para rastreios antivirais. Na primeira abordagem, foi usada Split-GFP com transcomplementação impedida por incorporação de distorções únicas – embebimento na molécula eglina c (eGFP11) ou ciclização por uma inteína (cyGFP11) – ou distorção dupla – usando bobinas enroladas (ccGFP10+ccGFP11). A proteólise, realizada pela protéase viral de prova de conceito TEVp, alivia as distorções, promovendo complementação dos fragmentos e emissão de fluorescência. Na segunda abordagem, rVLPs quiméricas pseudotipadas albergando mCherry, TEVp (estratégias simples) ou ambas as proteínas (estratégia dupla) foram desenvolvidas para monitorização em separado ou concomitante de entrada na célula (mCherry) e atividade proteolítica viral (TEVp).

As distorções introduzidas por bobinas enroladas apresentaram o sensor com melhor desempenho (rácio sinal-ruído de 97 ± 21). Uma linha celular expressando estavelmente o sensor (293cc11/10) foi estabelecida. Ao contrário de estudos em células estáveis, estudos transientes mostraram ativação do sensor. A caracterização das rVLPs quiméricas revelou desempenhos semelhantes na transfecção, ativação de sensor e produção. Assim, rVLPs envelopadas com VSV-G incorporando mCherry e/ou TEVp foram produzidas e usadas para infetar as células 293cc11/10. Enquanto a incorporação de mCherry não afetou substancialmente os rendimentos de produção e permitiu a monitorização eficaz da entrada nas células, a incorporação de TEVp dificultou a produção de rVLPs, reduzindo os títulos para 1.40%. Estudos cinéticos com as rVLPs mostraram sucesso na entrega de proteínas e elevada intensidade de sinal mCherry 24 horas após a infeção.

Neste trabalho foi desenvolvido um biossensor para deteção viral e rVLPs passíveis de pseudotipagem, providenciando ferramentas promissoras para deteção de vírus e rastreios antivirais.

Palavras-chave: Zika, Chikungunya, biossensor, protéase, deteção de virus, partículas retrovirais quiméricas, rastreios antivirais.

Contents

Figure Index

Table Index

Abbreviations

293	Human embryonic kidney 293 cells
293T	Human embryonic kidney 293T cells
2CMC	2'-C-methylcytidine
7DMA	7-deaza-2'-C-methyladenosine
ALB	Albumin
ANOVA	One-way analysis of variance
ATCC	American type culture collection
AVP	Adenovirus protease
BCA	Bicinchoninic acid
BHK	Baby hamster kidney cells
BHK-21	Baby hamster kidney cells 21
BSA	Bovine serum albumin
BSL	Biosafety level
CDC	Centers for Disease Control and Prevention
cDNA	Complementar deoxyribonucleic acid
CHIKV	Chikungunya virus
CLD&MV	Cell line development and molecular virology laboratory
CMV	Cytomegalovirus
cPPT	Central polypurine tract
Ct	Cycle threshold
DAA	Direct-acting antivirals
DMEM	Dulbecco’s modified Eagle’s Medium
DNA	Deoxyribonucleic acid
E. coli	*Escherichia coli*
eGFP	Enhanced green fluorescent protein
EDTA	Ethylenediaminetetraacetic acid
ELISA	Enzyme-linked immunosorbent assay
EMCV	Encephalomyocarditis virus
ER	Endoplasmic reticulum
FACS	Fluorescence-activated cell sorting
FBS	Fetal bovine serum
FDA	Food and drug administration
GAG	Group-specific antigen
GFP	Green fluorescent protein
Gluc	*Gaussia* luciferase
GOI	Gene of interest
HIV-1	Human immunodeficiency virus 1

hPGK-1	Human phosphoglycerate kinase 1
HRP	Horseradish peroxidase
HTA	Host-targeting antivirals
IgG	Immunoglobulin G
IRES	Internal ribosomal entry site
JEV	Japanese encephalitis virus
LB	Lysogeny broth
LTR	Long terminal repeats
LV	Lentivirus
M-PER	Mammalian protein extraction reagent
MFI	Mean fluorescence intensity
MOI	Multiplicity of infection
Nab	Neutralizing antibody
ORF	Open reading frame
PBS	Phosphate buffer saline
PCR	Polymerase chain reaction
PEI	Polyethyleneimine
PFU	Plaque-forming units
PRNT	Plaque reduction neutralization test
qPCR	Real-time quantitative polymerase chain reaction
Rluc	*Renilla* Luciferase
RNA	Ribonucleic acid
RRE	Rev responsive element
RV	Retrovirus
RVPs	Reporter virus particles
rVLPs	Retrovirus-like particles
SDS	Sodium dodecyl sulfate
SDS-PAGE	Sodium dodecyl sulfate-polyacrylamide gel electrophoresis
SIN	Self-inactivating
SNR	Signal-to-noise ratio
SV40	Simian vacuolating virus 40
TB	Terrific broth
TBS	Tris-buffered saline
TBST	Tris-buffered saline with Tween 20
TEV	Tobacco etch virus
TEVp	Tobacco etch virus protease
VCN	Vector copy number
VCN-qPCR	Vector copy number quantitative polymerase chain reaction
VLPs	Virus-like particles
VRP	Virus replicon particle

VSV-G	Vesicular stomatitis virus G protein
WPRE	Woodchuck hepatitis virus post-transcriptional regulatory element
WT	Wild type
YFV	Yellow fever virus
ZIKV	Zika virus

1 Introduction

1.1 Neglected viral infectious diseases

Over the years, it has been observed a dramatic increase in the emergence and re-emergence of epidemic viruses responsible for serious infectious diseases [1]. This worrisome situation led to outbreaks affecting thousands of people and, consequently, not only the increasing of severe debilitating conditions but also the number of human deaths.

Among these life-threatening viruses are arthropod-borne viruses (arboviruses), which are responsible for a vast incidence of human infections [2]. As neglected diseases, arbovirus borne infections are more prevalent in tropical climates and are usually associated with precarious lifestyles, such as poor sanitation, absence of potable water supplies and little or no access to health care [3]. The association of these conditions to developing countries makes them often overlooked by government officials, public health programs, pharmaceutical companies, and media. Despite resulting in severe disabilities, they do not cause dramatic lethal outbreaks, making these diseases less visible all over the world. Nevertheless, recent outbreaks of dengue, yellow fever (YFV), zika (ZIKV) and chikungunya virus (CHIKV) have awakened society for the severity of the situation [2].

Due to the lack of effective prophylactic and therapeutic approaches, this work focused on the development of new virus- and cell-based tools and approaches to overcome some of the limitations in basic and applied research on ZIKV and CHIKV.

1.1.1 Epidemiology

ZIKV and CHIKV are mainly transmitted by the bite of *Aedes* mosquitoes vectors, namely *aegypti* and *albopictus* (**Figure 1.1**) [4]. The spread of these two arboviruses is made primarily through the sylvatic (animal-mosquito-human) and urban (human-mosquito-human) cycles of transmission [5,6]. These transmission chains, coupled with human growth, urbanization, and long-distance travelling, are the causes behind the major reported outbreaks. However, transmission by mosquitoes is not the only way to contract these viral infections, since it can also occur directly between vertebrates, vertically (mother-to-child), nosocomially, sexually and via transfusions or transplantations [2,7].

The emergence and re-emergence of these viruses is also closely related with their adaptation to new vectors and their propensity to acquire genetic mutations that can potentiate their infectious capacity [8]. Since the first time ZIKV fever was identified in humans in Nigeria in 1954, cases of infection have been noticed sporadically or associated to epidemics in Africa, the Americas, Asia, the Pacific and in Europe [7,9,10]. Until the first large outbreak, only approximately 12 cases of ZIKV infections were reported in Africa (Uganda and Nigeria) and Asia (Indonesia) by the early 2000s.

While the first large outbreak was reported in 2007 on the Yap island, a part of the Federated States of Micronesia, the second was registered almost 7 years later, between 2013 and 2014, in French Polynesia, spreading further to other neighboring islands in the South Pacific Ocean.

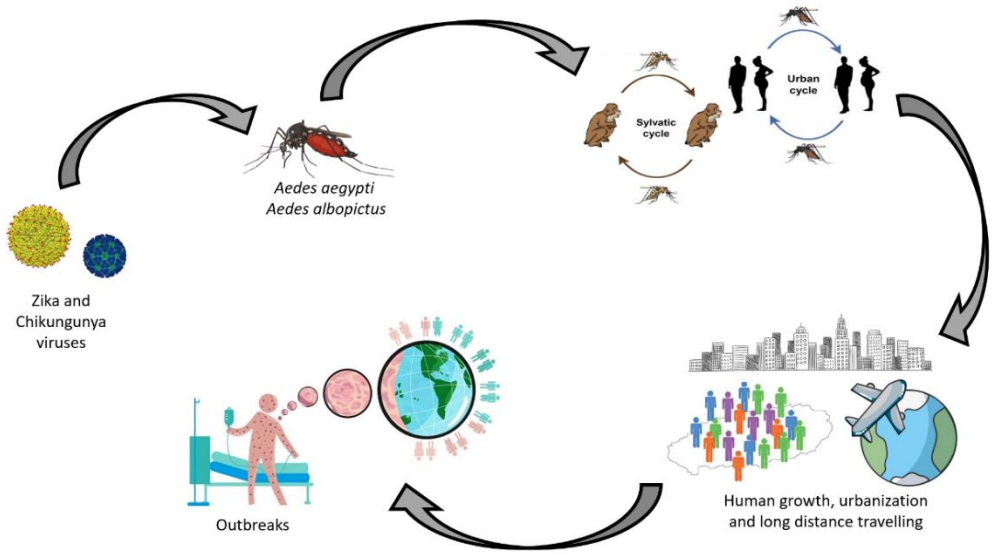

Figure 1. 1 – Cycle of Zika and Chikungunya virus transmission. Zika and Chikungunya viruses are mainly transmitted by the bite of *Aedes aegypti* and *Aedes albopictus* mosquitoes and spread through the sylvatic (animal-mosquito-human) and urban (human-mosquito-human) cycles of transmission. These transmission paths coupled to human growth, urbanization and long-distance travelling are the main causes behind major outbreaks.

In 2015, the third large outbreak of ZIKV infection was confirmed in Brazil, and by the end of the year, the first case outside of Brazil was reported in Colombia. By 2016, ZIKV was spreading at an alarming rate throughout much of Central and South America and the Caribbean, with the last outbreak registered to date occurring in 2018 in India [11,12] (**Figure 1.2**).

Regarding the epidemiologic situation in Europe, the first case of ZIKV infection was reported in 2013 [13] in Germany, and since then similar cases were observed in Portugal [14], Spain [15], and France [16]. According to the Centre for Disease Prevention and Control (CDC), as of April 29th of 2016, 452 new imported cases in 17 different countries were described, of which 23 represented pregnant women [17]. All the verified transmissions in Europe were a result of imported cases from affected countries, sexual, and vertical transmission, with no vector born origin [18,19].

Relatively to CHIKV, since the first reports of human infection in Tanzania (Africa) in 1952, sporadic and epidemic cases have occurred in Africa, Asia, the Americas and even Europe [20–22] (**Figure 1.3**) [23]. The first large outbreak was registered in 2004 in Kenya, and by January 2005 the viral epidemic had spread to the Comoros Islands (Grande Comore, Moheli, Anjouan, and Mayotte). This epidemic resulted later in the dispersion of this virus to the neighboring islands Seychelles and Mauritius by March of the same year. Another large outbreak was registered 3 years later in 2007 in La Reunion island, resulting in rapid spread to several countries in the Indian Ocean and India. In 2011 another massive outbreak was registered, this time in the Republic of Congo (Africa).

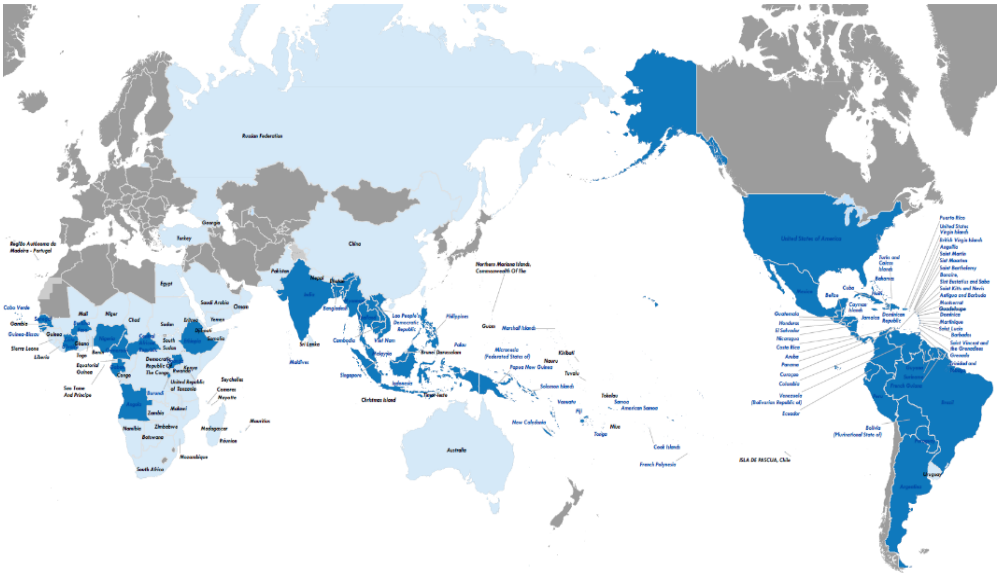

Figure 1. 2 – Countries and territories with current or previous Zika virus transmission by June 2019. Dark blue represents countries and territories with current or previous Zika virus transmission; Light blue represents countries and territories with established competent vector, but no known cases of Zika virus infection; Dark grey represents countries and territories with no known cases of Zika virus infection and no established competent vector; Light grey represents not applicable situations. This map does not include countries or territories where only imported cases have been documented [12].

CHIKV infections reached the European continent much earlier than ZIKV, registering the first case in 2006, when an outbreak in India and Indian ocean states infected European travelers [24–26]. This episode resulted in 17 cases in Italy [27], where a year later the first autochthonous outbreak was registered, with 205 cases in less than two and a half months [28–30]. CHIKV infection was also reported in France in 2010 [31], 2014 [32] and 2017 [33], however with a reduced number of cases.

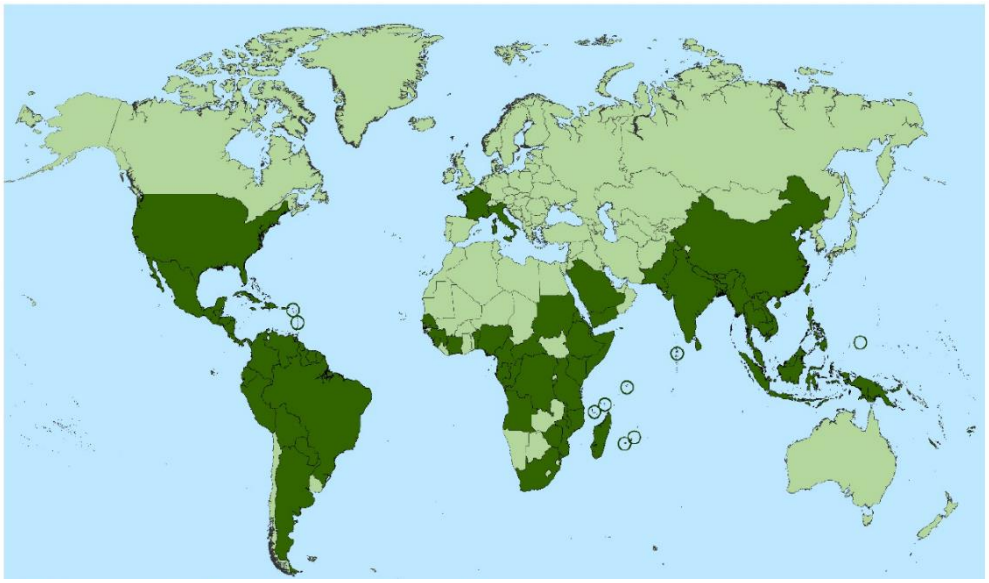

Figure 1. 3 – Current or previous local transmission of chikungunya virus by September 2019. Zones of transmission are represented in dark green. This map does not include countries or territories where only imported cases have been documented [23].

1.1.2 Clinical outcomes

Zika fever results, generally, in a clinical condition of acute febrile illness, to which symptoms like rash, fever, arthritis or arthralgia, conjunctivitis and myalgia are associated [5,7]. Human epidermal keratinocytes, dermal fibroblasts, immature dendritic cells, and cells of the central and peripheral nervous system are the types of cells that are permissive to this virus. As such, neurologic complications such as Guillain–Barré syndrome and adverse fetal outcomes resulting from the vertical mother-to-fetus transmission can also be observed. These adverse outcomes in fetal development are the consequence of ZIKV's capacity to penetrate the placental barrier and thus infect the fetus, resulting in teratogenic effects like microcephaly.

Regarding CHIKV, the permissiveness of epithelia and endothelial cells, primary fibroblasts, and monocyte-derived macrophages to infection can result in an asymptomatic condition or produce a variable spectrum of clinical manifestations [34]. Chikungunya fever can be presented through an acute stage of short-term manifestation, or through a chronic stage that can persist for months or even years [22,35]. Infection by this alphavirus can result in conditions like encephalitis, Raynaud syndrome, and endocrine and metabolic diseases, hence presenting symptoms like high fever, intense joint pain, fatigue, and rash.

1.2 Virus Biology

1.2.1 Zika Virus

First isolated in 1947 from a monkey in the Zika forest of Uganda, ZIKV is a member of the *Flaviviridae* family and *Flavivirus* genus [36]. Its genome is comprised of a positive sense single stranded RNA, of approximately 10.8 kilobases (kb) in size, with one open reading frame (ORF; **Figure 1.4**) [37]. ZIKV's ORF encodes a polyprotein processed into ten different proteins: three with a structural function – capsid (C), envelope (E) and membrane precursor (prM) proteins; and seven with non-structural functions – NS1, NS2A, NS2B, NS3, NS4A, NS4B, and NS5.

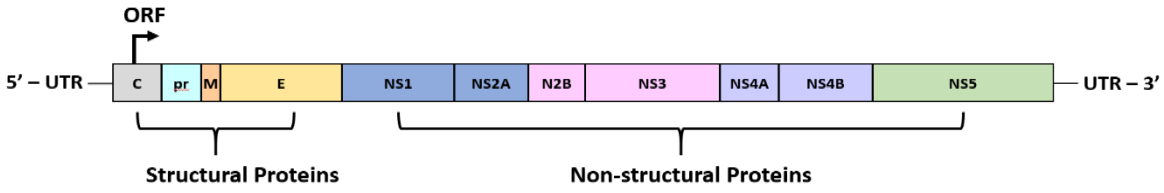

Figure 1. 4 – Representation of the Zika virus genome. Zika virus genome is comprised of a single open reading frame encoding a polyprotein processed into 10 viral proteins. Capsid (C), membrane precursor (prM) and envelope (E) are the proteins responsible for virus structure, while the remaining (NS1, NS2A, NS2B, NS3, NS4A, NS4B, and NS5) are responsible for non-structural functions.

ZIKV is a small (approximately 50 nm in diameter) enveloped and spherical virus whose surface proteins are arranged in an icosahedral-like symmetry (**Figure 1.5**) [37,38]. ZIKV particles present 180 copies of the membrane (M) and envelope (E) proteins – the latter consisting of 4 domains (stem-transmembrane domain pair, and ectodomains I, II and III) – in its viral membrane. ZIKV virions have the genomic RNA surrounded by capsid monomer proteins, forming the nucleocapsid. The basic organizational unit of E protein in mature *flaviviruses* like ZIKV is a dimer, with each E monomer within the dimer related to its neighbor by 2-fold symmetry. Three E proteins dimers lie parallel to one another in the so-called raft configuration, with the virion having a total of 30 rafts.

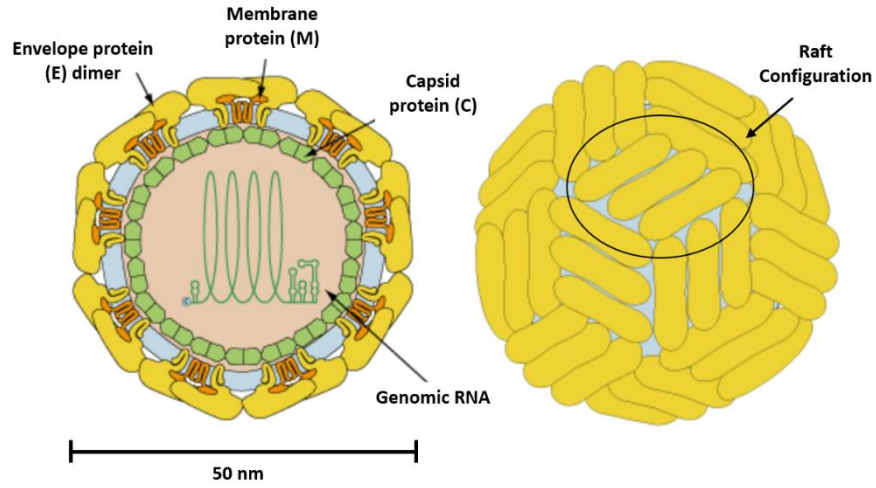

Figure 1. 5 – Zika virus structure. ZIKV is a 50 nm diameter icosahedral and enveloped virus. This particle presents membrane (M) and envelope (E) proteins in the viral membrane. Its basic organizational unit is the E dimer that forms the raft configuration when they lie parallel to one another. Genomic RNA is encapsulated by a nucleocapsid formed by capsid protein (C) monomers. Adapted from [38].

ZIKV life cycle is initiated by the low-affinity attachment of the virus E glycoprotein (**Figure 1.6**) [39,40]. This attachment is promoted by attachment factors such as the negatively charged glycosaminoglycans, to concentrate the virus on the cell surface. Afterwards, cell entry is promoted by the interaction of E proteins' N-glycans with the host cells' surface receptors and activated and driven by clathrin-mediated endocytosis. Irreversible conformational changes in protein E triggered by low pH, induce fusion between viral and endosomal membranes and, consequently, release of the viral RNA into the cytoplasm [37]. Once viral RNA is free in the cytosol, it is translated into a single polyprotein, later co- and post-translationally processed into 10 different proteins (**Figure 1.4**) by cellular and viral proteases. The next step in this virus life cycle is viral genome replication within endoplasmic reticulum (ER) associated vesicles and its packaging by capsid proteins to form nucleocapsids bearing viral genomic RNA [41]. Later, remaining structural proteins, prM and E, elicit nucleocapsids budding into the ER lumen, producing an immature virus particle. The new immature virion is posteriorly glycosylated in the ER and transported to the Golgi apparatus, where it is converted to its mature form. Finally, the new virion is released to the extracellular milieu by exocytosis.

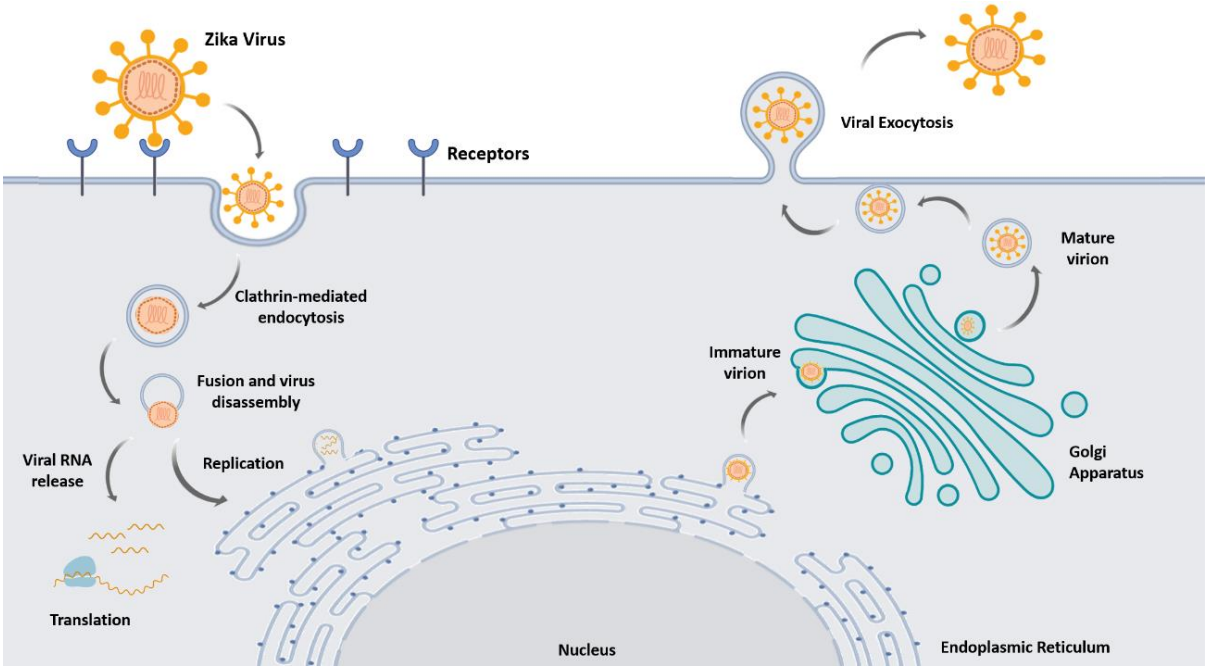

Figure 1. 6 – Zika virus life cycle in mammals. ZIKV life cycle initiates with its attachment to the surface of a host cell and consequent entry by clathrin-mediated endocytosis. Once inside the cell, viral and endosomal membranes fuse and the viral RNA is released into the cytoplasm. Free viral RNA is translated into a single polyprotein, later processed into 10 different proteins and the viral genome is replicated. Viral assembly takes place on virus-induced vesicle packages, derived, and closely tied to the surface of the endoplasmic reticulum. The immature virions are then transported to the golgi apparatus where they travel alongside the trans-golgi network, maturing and converting to their infectious form. Mature viruses are released from the cell by exocytosis.

1.2.2 Chikungunya Virus

First isolated in 1952 from febrile patients and mosquito species, CHIKV is a member of the *Togaviridae* family and *Alphavirus* genus [42]. It presents a positive sense single stranded genomic RNA with approximately 11.8 kb in size and two ORFs (**Figure 1.7**) [6,35]. The first ORF, in the 5' end, is 7 kb in size and is translated into two different polyproteins – P123 and P1234 – that are later processed into the non-structural proteins nsP1, nsP2, nsP3 and nsP4. This ORF presents a STOP codon upstream of the nsP4 protein, which leads to the formation of the P123 polyprotein. Termination suppression at that same codon leads to the formation of a P1234 polyprotein product [43]. The second ORF, at the 3' end, is 4 kb in size and encodes the structural polyprotein. This ORF is first transcribed into a structural polyprotein of 26S subgenomic RNA which is posteriorly translated into two different products – C-E3-E2-6k-E1 (major product) and C-E3-E2-TF (minor product) – due to the existence of a ribosomal frameshift. From this ORF, 6 different proteins are generated – capsid, E3, E2, 6K, TF, and E1 –the capsid (C) and the two viral envelope glycoproteins (E1 and E2) being the principal ones.

CHIKV is a small (approximately 70 nm in diameter) spherical virion with 240 copies of the capsid protein constituting the nucleocapsid (**Figure 1.8**) [44,45]. This structure involves the viral genomic RNA forming an icosahedral lattice, which is surrounded by a membrane and a lipid bilayer envelope. Embedded within the envelope are heterodimers of E1 and E2 glycoproteins arranged in 80 trimer-shaped spikes distributed in the viral surface.

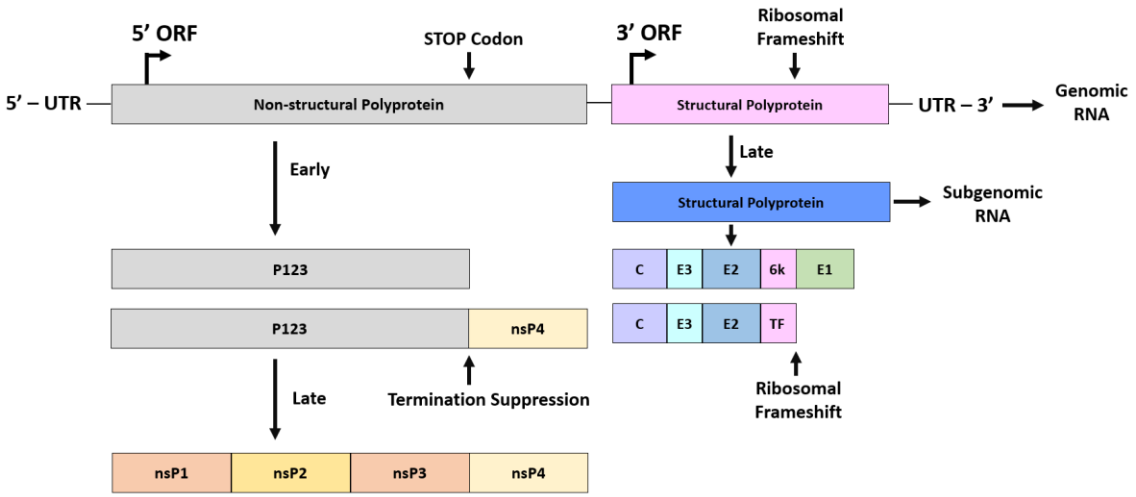

Figure 1. 7 – Representation of Chikungunya virus genome, encoded polyproteins, and respective proteins. Chikungunya virus genome is comprised of 2 open reading frames (ORFs) encoding 2 different polyproteins. The 5' ORF encodes the non-structural polyproteins P123 and P1234, which are processed into nsP1-4. The 3' ORF encodes the subgenomic structural polyproteins which is later processed into the products C-E3-E2-6k-E1 and C-E3-E2-TF.

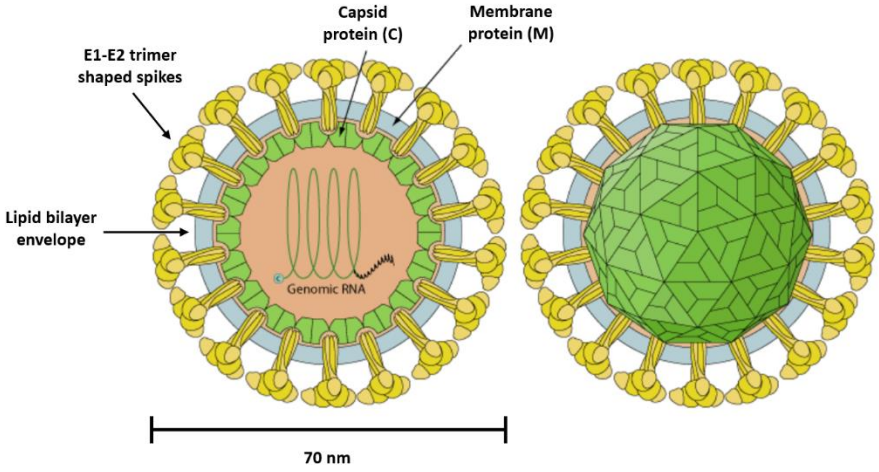

Figure 1. 8 – Chikungunya virus structure. Chikungunya is a 70 nm diameter icosahedral and enveloped virus. Embedded within its lipid bilayer envelope are heterodimers of the E1 and E2 glycoproteins arranged in trimers-shaped spikes. Genomic RNA is encapsulated by a nucleocapsid formed by capsid protein (C) monomers. Adapted from [44].

Similarly to ZIKV, CHIKV life cycle is initiated with E2 protein attachment to the host cells by glycosaminoglycans, which are expressed at the cell surface of most mammalian cell types. After attachment, cell receptor binding is promoted and receptor-bound particles are internalized, mainly by clathrin-mediated endocytosis (**Figure 1.9**) [45–47]. During endosome maturation, a reduction in pH triggers conformational changes in viral glycoproteins, exposing E1's fusion loop and inducing viral and endosomal membranes fusion and nucleocapsid release into the cytosol. Nucleocapsid disassembly promotes viral genomic RNA delivery and consequent non-structural polyprotein translation, inducing the formation of spherules, where viral (+)RNA replication occurs from a (-)RNA template and subgenomic RNA is transcribed [48]. When these structures are internalized, large cytopathic vacuoles

(CPV-I) are formed, to translate the structural polyprotein (**Figure 1.7**) from which the capsid protein is released by autoproteolysis, inducing the assembly of new viral nucleocapsids enclosing the viral RNA genome. The translation of structural polyproteins and their post-translational modifications culminates in the deposit of E2 and E1 proteins at the plasma membrane. Finally, the recruitment of the already assembled nucleocapsids to the membrane associated viral proteins, promotes virion assembly and budding from the cell, marking the first mode of viral release.

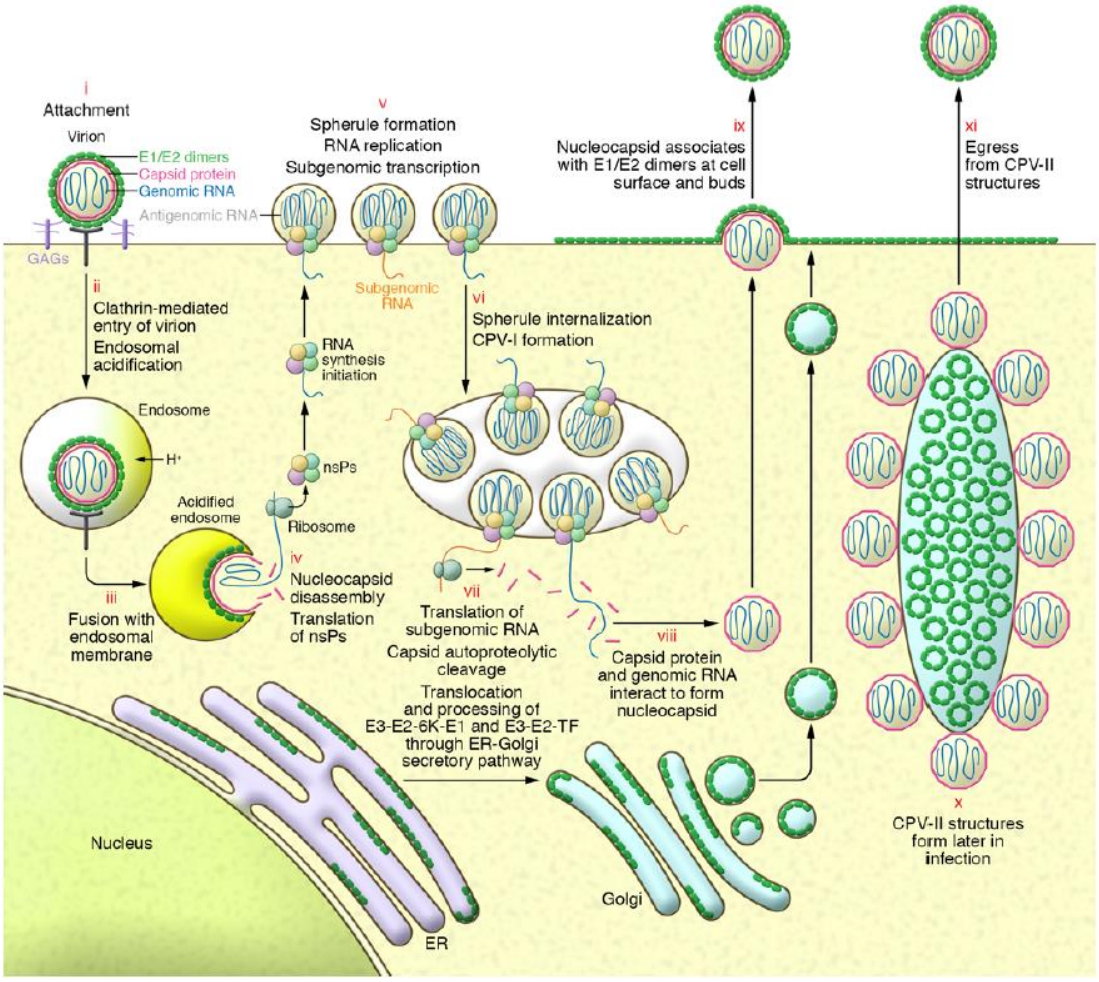

Figure 1. 9 – Chikungunya virus life cycle in mammals. Chikungunya virus life cycle initiates with (i) attachment to the host cell surface followed by (ii) cell entry through clathrin-mediated endocytosis. The endosome created by the endocytosis suffers acidification which induces (iii) fusion of the viral and endosomal membranes and consequent release of the nucleocapsid into the cytosol. (iv) The nucleocapsid disassembles liberating the genomic viral RNA and the translation of the non-structural proteins (nsPs) occurs. (v) Four nsPs (nsP1-4), together with genomic RNA and host proteins, assemble at the plasma membrane (PM) forming viral replication compartments (spherules) containing viral dsRNA. (vi) These spherules are internalized and form large cytopathic vacuoles (CPV-I) that house multiple spherules. The next step of this cycle is (vii) translation of subgenomic RNA, producing the structural polyprotein, followed by capsid autoproteolysis. The products of subgenomic RNA translation, E3-E2-6K-E1/E3-E2-TK polyproteins, are translocated to the ER, where E2/E1 are post-translationally modified and deposited at the PM. (viii) Interaction of capsid proteins and genomic RNA leads to the formation of icosahedral nucleocapsids which (ix) assemble with E2/E1 at the PM, resulting in budding of mature virions. (x) Later in infection, CPV-IIs studded with nucleocapsids and containing hexagonal lattices of E2/E1 are generated. These structures may (xi) serve as transport vehicles and assembly sites for structural proteins allowing the formation of mature virions and their egress [45].

In a later stage of the infection cycle, CPV-I's are substituted by another type of vacuole, the CPV-II [49,50], whose function and mechanisms are still not well understood. However, previous studies have pointed out their potential role in intracellular transport of glycoproteins from the trans-golgi network to the plasma membrane budding sites prior to mature virion budding. In addition, CPV-II may also provide a reservoir of glycoproteins destined to the plasma membrane for eventual assembly and budding. These findings suggested virion maturation may occur within these vesicles during the later stages of infection. This reveled CPV-II's ability to fuse with the cellular membrane and release matured CHIKV, functioning as exocytosis vesicles and marking the second mode of viral release.

1.3 Current therapies for ZIKV and CHIKV

At the present time, there are no vaccines or targeted antivirals to treat the diseases or prevent the infections caused by these two viruses [7,35,51]. Therefore, all the preventive procedures taken towards ZIKV and CHIKV infections are based on common prophylactic measures and symptoms relief. Prophylaxis is mostly practiced by the utilization of insecticides or repellents, minimization of skin exposure and mosquito breeding control [46]. On the other hand, symptoms relief is frequently done by using drugs like paracetamol. Therefore, it is extremely urgent to develop vaccines and/or antivirals to combat these viral infections.

1.3.1 Vaccines

There are several different types of platforms available, chosen according to their features, to develop vaccines with the desired characteristics [52]. Examples of these platforms are inactivated virus formulations, live attenuated virus vaccines, subunit vaccines, viral vectored vaccines, chimeric and nucleic acid (DNA or RNA) vaccines and virus-like particles (VLPs) based vaccines (**Figure 1.10**).

Over the years there have been numerous attempts to develop different vaccine platforms to fight these viral infections [53,54]. Amongst the different platforms available, VLPs-based vaccines have recently seen its interest increased due to their promising features [55]. VLPs are nanoparticles (20 to 200 nm) that resemble the organization and conformation of authentic native viruses but do not have the viral genomic material, precluding any possibility of mutation reversion or pathogenic infection [55,56]. One of the most important characteristics of these particles is their replication incompetence, which eliminates all the safety issues during manufacture and administration. In addition, their rigidity and repetitive presentation of antigens facilitates cross-linking of B cell receptors, allowing production of very high cellular and humoral immune responses, which is advantageous in vaccine development [57]. These nanoparticles are also very versatile, having more than 170 different host expression systems where they can be produced, namely bacteria, insect, yeast or mammalian cells [58]. However, it is important to highlight that the expression system chosen must consider the needs and characteristics of the VLP, hence taking into consideration the requirements for protein folding and post-translational modifications.

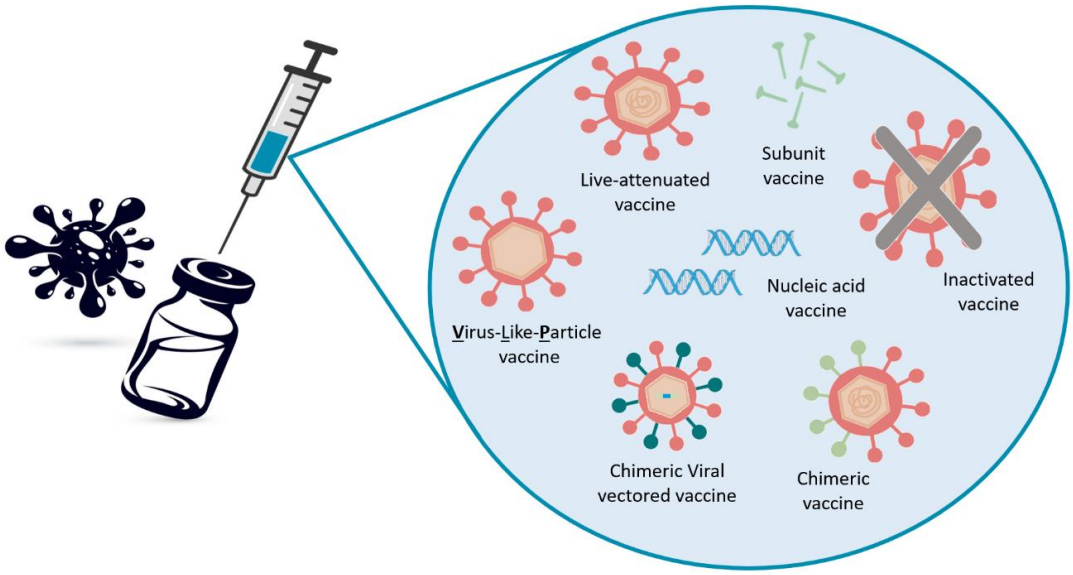

Figure 1. 10 – Types of vaccine platforms. Several different vaccine platforms are available for vaccine development, namely inactivated virus formulations, live attenuated virus vaccines, subunit vaccines, chimeric viral vectored vaccines, chimeric and nucleic acid (DNA or RNA) vaccines and virus-like particles (VLPs) based vaccines.

As the native viruses from which they derive, VLPs can have different structures and organizations, presenting one or several structural proteins that have the ability to self-assemble when recombinantly expressed [59]. These proteins can be arranged in single, double, or triple layers, and in some situations, have an external lipid envelope. In the last case, the structural protein core exits the cell through a budding process, enveloping the capsid within part of a cellular membrane. This process is another important event to take into consideration during the choice of the producer cell line, since the enveloped VLPs will contain the proteins expressed on the producer's membranes, possibly enhancing immunogenicity, and acting as an adjuvant.

For example, in 2017 a VLP-based vaccine for ZIKV was developed through the production of a 293T cell line constitutively expressing Zika prM-E VLPs (**Table 1.1**) [60]. For that, a construction consisting in ZIKV's structural proteins prM-E was delivered into 293T using lentiviral transduction and, after selection, a cell line stably expressing the desired VLPs was established. Another reported example, this time to produce CHIKV VLPs, takes advantage of the baculovirus-insect cell expression system, demonstrating the versatility of VLPs platforms [61]. In this case, recombinant baculoviruses expressing CHIKV's structural cassette (C-E3-E2-6K-E1) were produced using the bac-to-bac expression system and used to infect *Sf21* cells, which posteriorly secreted the desired VLPs into the supernatant. However, the utility of VLPs as a platform for vaccine development is not their only application, revealing to be excellent tools for protein delivery into target cells [62], glycoprotein display for antiviral screening [63], drug delivery and for surrogates in basic research [64]. For example, in 2020, the same group developed a multivalent VLP-based vaccine directed to 4 different arboviruses endemic in overlapping regions, ZIKV, CHIKV, YFV and Japanese encephalitis virus (JEV; **Table 1.1**) [65]. For that, VLPs expressing their native structural proteins – C-prM-E for ZIKV, YFV and JEV and C-E3-E2-6K-E1 for CHIKV – plus Zika's NS2B-NS3 protease for the flavivirus, were developed.

Table 1. 1 - Zika and chikungunya virus-like particles (VLPs) based vaccine candidates.

Vaccine	Expression system
ZIKV VLP vaccine: Safe, effective, and economical.	Mammalian cells (293T)
Multivalent VLP vaccine for ZIKV, CHIKV, YFV and JEV: Safe, effective, and scalable.	Mammalian cells (293T)
CHIKV VLP vaccine: Effective, safe, and scalable.	Baculovirus-insect cell (*Sf*21)

In a similar fashion to the ZIKV VLP, each native structural protein construction was delivered separately to 293T cells using lentiviral transduction. Hence, after the required selection steps, four different cell lines constitutively expressing each VLP were established. The inclusion of ZIKV protease in the VLPs design evidences their potentiality as protein delivery vehicles. Moreover, although in the present situation the protease was included for processing purposes, its delivery could have other applications, like for instance screening of potential protease inhibitors during antiviral studies.

1.3.2 Antivirals

Numerous classes of compounds targeting either viral (direct-acting antivirals, DAAs) or cellular (host-targeting antivirals, HTAs) factors have been studied [66]. Theoretically speaking, any compound targeting any step of the viral life cycle could have potential antiviral activity. However, an antiviral capable of fighting ZIKV and CHIKV must respond to some fundamental requirements: be active in cells of the nervous system; cross the blood-brain and placental barriers; and be safe for pregnant women and their fetuses [67]. It is important to highlight that HTAs, like the ones that inhibit viral entry, could be a better long-term solution as they are less impacted by viral genome mutations that increase the likelihood of drug resistant variants, frequently observed in RNA viruses [68].

Broad spectrum antiviral drugs, especially broad-spectrum nucleoside analogues such as 7-deaza-2'-C-methyladenosine (7DMA), 2'-C-methylcytidine (2CMC), ribavirin, favipiravir, and T-1105, have shown activity against both ZIKV and CHIKV by inhibiting, respectively, NS5 and nsP4 RNA-dependent RNA polymerases and thus viral replication [67,69].

Recent repurposing studies on FDA-approved drugs showed some with anti-ZIKV activity [70]. Of those, cancer drugs were the ones that more often showed antiviral activity, probably due to the existing crosstalk pathways. However, the need for clinical trials and the lack of knowledge about the mechanism of action are the reasons impairing their therapeutic application.

Another attractive target is the NS2B-NS3 protease, that has an essential role in the ZIKV life cycle [71]. Recent studies to elucidate the protease structure have been carried out to better understand it, and thus, discover how to interfere with its enzymatic activity. Research in this field has bet on peptide substrates and peptidomimetics development since they alleviate the oral bioavailability and pharmacokinetics issues.

Regarding antivirals against CHIKV infection, a vast number of compounds targeting different steps of the viral life cycle (DAAs) and host factors (HTAs) have been reported (**Table 1.2**) [72].

Table 1. 2 - Chikungunya antiviral candidates and their targets. Information adapted from [72].

Inhibition target	Compound
Viral entry	Chloroquine, Arbidol and 10H-phenothiazines.
Viral protein translation	iRNA, shRNA, Harringtonine and Homoharringtonine.
Viral replicase	5,7-Dihydroxyflavones, Prothipendyl, Daphnane diterpenoids, Inhibitors of CHIKV nsP2 and MADTP compounds.
Viral genome replication	Ribavirin, 6-Azauridine and Mycophenolic acid.
Viral glycoproteins maturation	Decanoyl-RVKR-chloromethyl ketone.
Modulators of host immune response	IFN-α, Polyinosinic acid and Polycytidylic acid.
Unknown Targets	Tigliane diterpenoids

Among these, a novel series of small molecules (the MADTP series) stands out by efficiently inhibit *in vitro* CHIKV replication [66]. This inhibition is accomplished by interfering with nsP1 and its functions in capping and methylation of the newly synthesized RNA. Another relevant antiviral target is the nsP2, which exhibits 4 different types of crucial functions in CHIKV life cycle, including protease activity. Furthermore, it is involved in important tasks like host cell mRNA transcription and translation shut off and cellular antiviral response inhibition, making it an excellent target. Researchers have designed a series of nsP2 inhibitors that were already proven to be mildly effective. During one of these studies, Bassetto et al. have discovered, among the 5000 screened compounds, a lead that showed anti-CHIKV activity [73]. Structure-activity relationship (SAR) analysis, conducted in the same studies with structural analogs, has proven the importance of the lead's cyclopropylic moiety and hydrazone group in anti-CHIKV activity.

Focusing on viral entry targets, a few inhibitors were reported for CHIKV (**Table 1.2**). Of these, chloroquine stands out for its antiviral activity against ZIKV too, a shared feature among antimalarial drugs [68,74]. In every case, screenings were performed by infecting a susceptible cell line with CHIKV or ZIKV and further submitting it to different compound dosages [75–77]. Infectious clone isolates were used in all cases, except for 10H-phenothiazines, where a virus-based assay comprising a recombinant CHIKV was applied. Viral entry constitutes an advantageous target for viral inhibition. Not only the damage introduced by virulence factors during intracellular viral replication is minimized, but also, as the targets are more accessible, the required dosages are lower, which limits the cytotoxic effects [72]. Hence, compounds targeting viral entry might constitute an attractive therapeutical strategy for antiviral screenings.

Developments in the virology research fields are widely dependent on both fundamental and applied research. Without fundamental research it would not be possible to advance applied research, since the knowledge about the virus biology, like its structure and life cycle, are crucial in vaccine and

antiviral development. Both investigation areas are dependent on fast, reliable, accurate and robust detection and quantification methods. Unfortunately, there is a lack of such methods, namely the functional ones, which becomes an obstacle in the progression towards new effective antivirals.

1.4 Viral detection and quantification methods

Viral detection and quantification methods are broadly divided into two different categories: functional and non-functional methods [78]. Functional methods give information about viral functionality, measuring virions that can successfully infect a cell [79]. On the other hand, non-functional methods do not take the infectious capacity into account, therefore, they are based in quantification of the physical particles present in a viral sample, whether by measuring viral components (e.g. nucleic acids and proteins) or directly count of virus particles. Regarding non-functional methods, only serological – enzyme-linked immunosorbent assays (ELISA), indirect immunofluorescence assays and hemagglutination inhibition (HI) – and molecular approaches – nucleic acid amplification-based techniques – have been reported to detect ZIKV and CHIKV. The inability to assess particles infectious capacity and the possibility of titer overestimation associated with non-functional methods represent major limitations in viral research progress. Hence, functional assays emerged as the principal methods required to make progress in both fundamental and applied viral research. Considering this, henceforth we focused on functional methods and the constant search for new and improved assays.

1.4.1 Functional Methods

Regarding functional methods for detection and quantification of ZIKV and CHIKV, the first developed approaches relied on plaque assays and virus isolation, which were recognized throughout the years as gold standards. The limitations associated to these traditional methods were responsible for the search of new and improved approaches. Hence, virus and cell-based reporter approaches emerged as alternatives. Hereafter a more detailed description of these methods is provided.

1.4.1.1 Viral plaque assays

Viral plaque assays were the very first methods available for ZIKV and CHIKV detection and quantification, being acknowledged as the “gold standard” assay for many years [80,81]. Briefly, it relies on viruses ability to cause cytopathic effects in infected host cells (**Figure 1.11**), manifested through apoptosis in the case of CHIKV and ZIKV [79,82]. In this assay, plaques are formed as a result of cell infection by a single virus, originating plaque forming units (PFUs). Therefore, when calculating PFUs per milliliter in the original sample, one is in fact calculating the number of infectious particles [79,83].

Despite being the gold standard for viral detection and quantification, this technique presents several drawbacks. Viral plaque assays are not only time-consuming, having an approximate duration of 8 days, but are also very laborious and ambiguous since they depend on the interpretation of different morphologies by different researchers [79]. In addition, it is important to point out that absence of plaques is not always a synonym of viral infection inexistence, leading to misleading results [81].

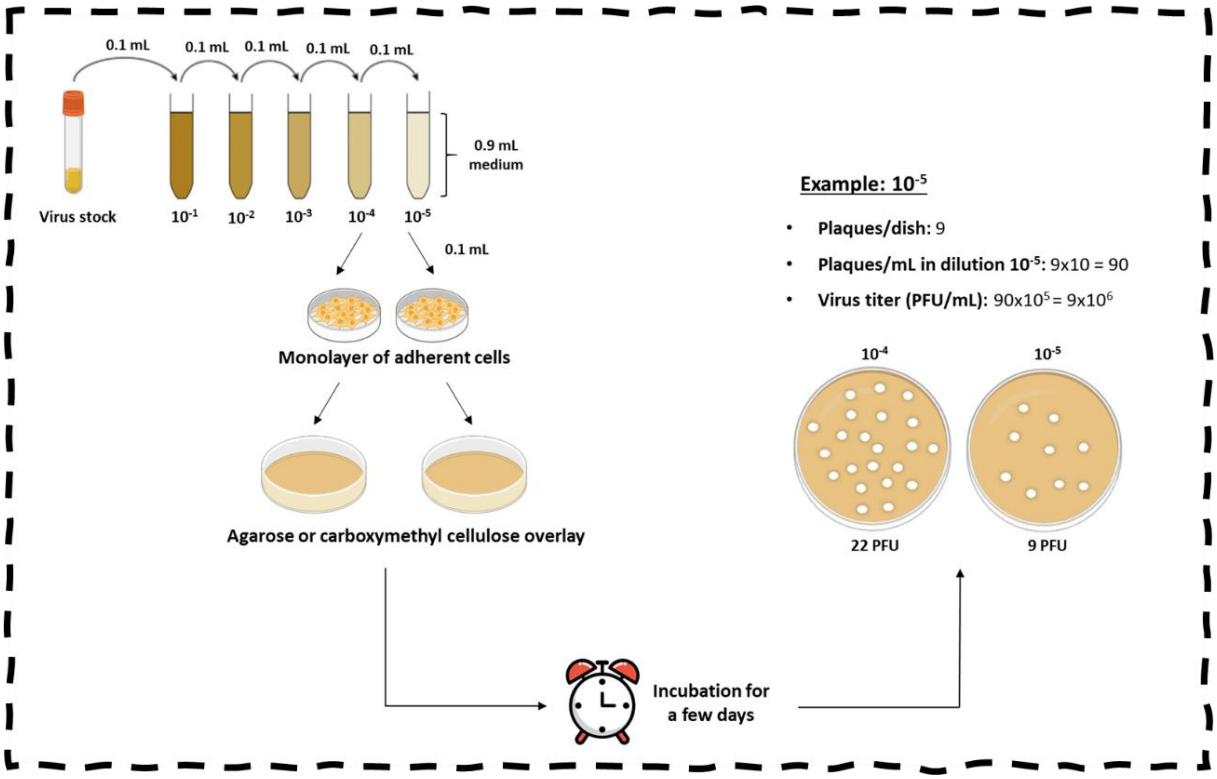

Figure 1. 11 – Schematic representation of viral plaque assays. Confluent monolayers of adherent cells are infected with serially diluted viral inoculum. After infection, cell colonies are covered with a semi solid gel (agarose or carboxymethyl cellulose), to prevent indiscriminate diffusion of viral infection, and normally incubated for 8 days, until a cytopathic effect is noticeable by plaque formation. In fact, when the plates are incubated, infected cells lyse and spread the infection to the nearby cells where the infection-to-lysis process repeats. Therefore, each infectious particle produces a circular zone of infected cells – a plaque – which can be observed either by naked eye, staining or light microscopy. Finally, assuming that each PFU is the result of cell infection by a single virus, the number of infectious particles or PFUs per milliliter in the original sample can be calculated taking into account the dilution factor applied, the volume of infection and the number of plaques present on the plate.

1.4.1.2 Virus isolation

ZIKV detection through isolation was first performed by mouse intracerebral inoculation and followed by inoculation in mosquitoes (*Toxorhynchites speldens* and C6/C36), mammalian (Vero, rhesus monkey kidney (LLC-MK2), or pig kidney (PS-C1) cells [84–86]. Regarding CHIKV, it can also be isolated through inoculation with susceptible mosquito (C6/36) or mammalian (BHK-21, HeLa and Vero cells) cell lines or by intracerebral inoculation of 1-day-old mice at the early phase of infection [20].

These methods are highly specific and present a detection limit of a single viable virus [87,88]. However, they require highly trained operators and are dependent on the sample integrity as well as on the short viremia period. In addition, viral isolation requires a significant amount of time to obtain results. Therefore, this approach is more applied in surveillance rather than diagnosis.

1.4.1.3 Virus-based reporter assays

Since the discovery of reporter proteins, they have been widely applied in several studies as a tool for visualization and monitoring of intracellular events, namely protein localization, trafficking, and

interactions, signaling pathways and gene expression levels [89]. These applications have become of great interest and utility in the viral research fields, which employed engineered virus encoding reporter proteins to detect and quantify the viral pathogens. Hence, reporter proteins have revolutionized the viral research field by introducing an alternative to the traditional time-consuming and laborious methods resulting in what we call virus-based assays [90–92]. Due to the lack of functional methods for both ZIKV and CHIKV studies, and the limitations associated to the existent ones, several virus-based assays have been reported for these arboviruses.

In 2013, a virus replicon particle (VRP) based CHIKV neutralization assay was developed to determine CHIKV neutralization potency, a valuable tool for validation of vaccine efficiency [93]. Briefly, CHIKV reporter VRPs were produced by co-electroporating a CHIKV replicon with all the structural genes replaced by a *Gaussia* luciferase (Gluc) reporter gene and two helper plasmids (to provide the structural functions withdrawn by the replacement) in baby human kidney cells 21 (BHK-21). These reporter particles were further used for incubation with neutralizing antibodies and posterior infection of BHK-21 cells. Considering that non-neutralized VRPs entered the target cells, and that Gluc bioluminescence is secreted into the supernatant, this procedure permitted the determination of the neutralization potency/percentage of infection by an easy readout of Gluc bioluminescence. This assay allows easy and faster readings and the possibility of high-throughput analysis, without manipulating infectious particles.

In 2016, a stable replication-competent and infectious enhanced green fluorescent protein (eGFP) reporter CHIKV (eGFP-CHIKV) with a similar replication efficiency to the wild type (WT) CHIKV, was constructed not only to develop a neutralization assay but also to detect and quantify CHIKV replication [94]. During this work, it was shown that eGFP expression levels in cells infected by eGFP-CHIKV reporter were correlated with viral replication, allowing its direct visualization. In addition, studies with different ribavirin concentrations (which is a known CHIKV's replication inhibitor) in cells infected by eGFP-CHIKV, demonstrated that eGFP expression levels and viral titer were reduced in a dose-dependent manner. This correlation feature enabled the development of a new reliable neutralization assay, useful for vaccine efficiency validation, following the same rational as the aforementioned VRP-based approach. This new method revealed to be more advantageous, since it guarantees easier productions, lower costs, scalability, and higher throughputs.

In the same year, a *Renilla* luciferase (Rluc) reporter ZIKV was developed by engineering the reporter gene into the viral capsid coding sequence of an infectious cDNA clone through reverse genetics [95]. After production, the reporter was used to infect Vero cells that upon treatment with a panflavivirus inhibitor exhibited a dose-dependent inhibition of the luciferase signals, revealing its potential use for antiviral drug screenings in a high-throughput manner. In addition, since this infectious clone is coupled to a reporter, this approach also facilitates the tracking of viral replication *in vivo*, as well as the study of viral virulence and mosquito transmission. However, it is important to highlight that viral genome modification to produce this recombinant virus resulted in virus attenuation, affecting assay reliability.

Still in 2016, a robust method with great applicability was developed for the rapid generation of a recombinant ZIKV expressing green fluorescent protein (GFP) [96]. This infectious reporter assembled

in Vero cells, consisted in an eGFP fused in frame with the first 33 amino acids of ZIKV protein C and followed by a sequence encoding the protease 2A factor, responsible for reporter excision from the polyprotein. The good GFP expression levels obtained after reporter infection in mosquito and mammalian cells, demonstrated the reliability of this tool for ZIKV viral replication monitoring in both cell types. Furthermore, the reduction of GFP positive cells obtained by fluorescence-activated cell sorting (FACS) analysis when infected cells were previously or posteriorly treated with antivirals, demonstrated the suitability of this virus-based approach for antiviral compound screening. However, the genomic stability of this reporter only lasted for two passages on Vero cells, as eGFP is excluded from the genomic RNA. In addition, like the last two mentioned approaches, this assay requires the manipulation of infectious viruses, which is a major drawback concerning virus-based assays.

Later in 2019, this same ZIKV-GFP reporter was used to develop a flow cytometry-based neutralization test, which emerged as an alternative to the conventional plaque reduction neutralization test (PRNT) [97]. Briefly, a viral variant with improved GFP expression in infected cells was selected, incubated with serum containing anti-ZIKV antibodies and added to a monolayer of BHK-cells. These cells' GFP expression was measured by flow cytometry analysis and 100% infectivity was obtained with the number of GFP positive cells without incubation with serum. Face to this, neutralizing antibody (Nab) titer was calculated by nonlinear, dose-response regression analysis, considering the reduction of GFP expression given by flow cytometry analysis. As expected, a higher number of neutralizing antibodies will result in a higher number of antibodies binding to the ZIKV-GFP reporter and neutralizing its entry in the cells. When measuring neutralization by flow cytometry, higher percentages will correspond to less Nab and thus more viral reporter entry, whereas lower percentages will correspond to a higher neutralization rate and consequently, a higher number of Nab. This time-saver format of the conventional PRNT method without the requirement of PFU provided a reliable platform not only for epidemiologic cohorts but also for ZIKV vaccine development studies.

In 2017, a rapid quantitative GFP-based microneutralization assay emerged as an optimization of current approaches making use of flow cytometry for GFP positive cell analysis [60]. Briefly, reporter virus particles expressing (RVPs) ZIKV C-prM-E polyprotein, were developed to measure the neutralizing immune response given by vaccine candidates, namely VLPs. For that, 293T and Vero cells were infected with the RVPs and posteriorly fixed and analyzed by fluorescence microscopy to count the number of GFP positive cells, whether by using an automated software or manually. To complement the work, tests were made to determine if this assay could detect RVPs neutralization, by infecting cells after previous Nab incubation, and thus determine neutralization potency through GFP positive cells.

Overall, virus-based approaches provide simple, fast, sensitive, and high-throughput detection and quantification of recombinant viruses, revealing to be valuable tools for viral studies, vaccine development and antiviral screenings. However, virus-based approaches still present some decisive drawbacks [98,99]. In the first place, some of the approaches rely on infectious virus, which in the existent case of CHIKV, is extremely virulent. Therefore, manipulation of these particles may require high biosafety level laboratories (BSL 3), which are not always available and require trained personnel. Although not all the virus-based approaches present this problem, there are also other limitations. One of them is that the insertion of large reporter genes into the viral genome may introduce genetic instability

and impair viral growth. Indeed, depending on the locus where the gene is inserted, essential RNA structural elements can be disrupted, resulting in viral replication attenuation. Furthermore, the reporters used can present immunogenicity risks, which is the case of the highly used GFP, impairing their application in vaccines [100]. Also, this type of assays requires extensive knowledge of the molecular aspects of the virus, which in this case is very limited.

Therefore, it is imperative to find solutions to these negative aspects and thus, discover new approaches that could substitute traditional methods.

1.4.1.4 Cell-based reporter assays

The disadvantages associated to virus-based reporter assays and the continuous need for methods capable of elucidating virus biology and pathogenesis mechanisms, highlight the urgency for new methods. In this respect, methods based on live reporter cells have emerged as an attempt to overcome those disadvantages and thus enhance the understanding in this field. In a general way, one can say that in these assay types the reporter gene is incorporated in the cells in a "sentinel" state until its activation is induced by viral presence. This feature presents a great advantage over virus-based assays since there is no need for virus-labeling and consequently, one can detect and quantify both label-free recombinant virus and WT viruses. Moreover, it is important to emphasize that, since the cells are constitutively expressing the reporter in a "sentinel" state, and its activation is induced by viral presence, viral detection and quantification will be direct. Also, these approaches are easily adaptable to high-throughput strategies. Overall, cell-based reporter assays provide a simple, fast, and reliable tool for viral detection and quantification. Some examples of ZIKV and CHIKV assays are described below.

In 2011, a stable BHK cell line harboring a non-cytotoxic CHIKV replicon was generated and adapted as a screening tool to identify inhibitors of CHIKV's replication [77]. To generate this cell line, a selection marker (puromycin acetyltransferase) and two reporter genes (*Renilla* luciferase and eGFP) were inserted into a CHIKV replicon sequence. In addition, a mutation was introduced into the protease-encoding section (nsP2), reducing the cytotoxicity of the WT CHIKV replicon, and producing a biosafe surrogate model. BHK-21 cells stably expressing the replicon were exposed to a total of 356 compounds with potential CHIKV replication inhibition to assess dose-dependent suppression of the marker genes (eGFP and Rluc). With this protocol, compound inhibition capacity was evaluated, providing a new platform for antiviral screenings. Importantly, in the case of a replicon cell-line based assay, antiviral agents are expected to suppress the activity of already established replication complexes, whereas in the case of an infectious virus assay they are evaluated against a system in which the virus is establishing its replicative machinery after entering the host cell.

In another study in 2013, a cell-based assay for CHIKV infection detection in mosquitoes was developed using a subgenomic reporter RNA system [101]. For that, a subgenomic reporter consisting of the first 143 residues of nsP1 (to provide conserved RNA sequence elements), a subgenomic promoter sequence upstream of a mCherry reporter protein and 50 adenosines at the 3' terminus was inserted into an *Aedes* mosquito genome for constitutive expression. This assay was founded on the fact that expression of proteins encoded on subgenomic RNA is dependent on the viral non-structural protein

replication complex, providing a mechanism for expressing foreign genes only upon virus infection. Therefore, upon CHIKV infection the virus inducible promoter induces subgenomic RNA transcription and, consequently, reporter protein translation, resulting in red fluorescence within CHIKV infected mosquitoes' cells. This approach demonstrated to be a very useful tool for rapid and simple detection of WT alphaviruses, as well as for CHIKV infection monitoring. Additionally, this system is not only applied to mosquito cell cultures but also to live *Aedes aegypti* transgenic mosquitoes. The sensitivity and quick detection provided by this method turns it into a potential application for diagnosis purposes, allowing quick and accurate identification of viral infection. Furthermore, this method can further permit monitoring of viral infection dissemination and transmission from mosquitoes to mammalian hosts, increasing the knowledge about the viral transmission cycle.

Later, in 2018, a fluorescent cell-based reporter assay for live imaging of ZIKV infected cells was developed by establishing an A549 cell line stably expressing a ZIKV reporter [102]. The reporter is comprised by ZIKV's NS4B and the first ten amino acids of NS5 non-structural proteins – possessing a Zika protease (NS2B-NS3) cleavage site in the NS4B-NS5 polyprotein junction – followed by a nuclear localization signal and a GFP reporter. When cells stably expressing the reporter are infected by ZIKV, the viral protease cleaves the reporter in the NS4B-NS5 polyprotein junction, resulting in nuclear translocation of GFP and permitting to identify, in real-time through fluorescence microscopy, if a cell is infected by ZIKV. This method is advantageous since it can be used not only for ZIKV detection but also for antiviral efficiency screenings and biology and infection pathogenesis studies. However, one major limitation of this method is the inability to use high-throughput cell sorting for downstream analysis as this reporter measures subcellular localization changes that are not distinguishable by FACS.

In 2020, the first fluorescence-activatable cell-based molecular reporter system for live-cell imaging of flavivirus infection was developed [103]. Briefly, a genetically encoded flavivirus molecular reporter named FlaviA-GFP, which consisted of a GFP followed by a linker containing the internal NS2B-NS3 cleavage site and a quenching peptide was constructed and stably expressed in BHK-21 cells. When infected by flaviviruses like ZIKV, this reporter suffers viral protease cleavage at the linker's NS2B-NS3 cleavage site, resulting in the removal of the quenching peptide and promoting the development of a fluorescent signal. This strategy allowed not only ZIKV detection and quantification but also infection kinetics monitoring at a single-cell level by live-cell imaging. This fluorescence-activable reporter system allows an easier interpretation of the results and simplifies the image analysis when compared with systems based on fluorescent signal relocalization across cellular compartments. Furthermore, in addition to presenting low fluorescence background, it makes use of a single recombinant construct that codifies for a single fluorescent protein with intramolecular quenching, which is very advantageous when comparing to other difficult to optimize strategies. Moreover, reporter's validation with reference strains and clinical isolates of different flavivirus species other than ZIKV, made it suitable for a wide application range. In the follow up of this work, the developed molecular system was suited to be used in plaque assays simultaneously with molecular sensors of other cellular or viral-induced processes, like chromatin condensation and cell death. To that end, a far-red version of the FlaviA-GFP - FlaviA-mNeptune - was developed and established in mammalian cells. This reporter cell line allowed the study of viral plaques development kinetics with unlabeled native flavivirus strains. Additionally, the

incorporation of the mentioned molecular sensors, enabled the attainment of multiparametric data from single viral plaques. This multireporter platform not only allowed primary screens to detect infection types but also revealed to have an important role in antiviral compound screenings. Importantly, these plaque reduction tests allow a readout of the possible cytotoxic effects induced by the tested compounds in a single experiment.

Despite all the advantages associated to these approaches, there are still some drawbacks limiting their utilization. One of the greatest disadvantages is the requirement of expensive and complex equipment and software either for raw data direct attainment or for further processing. Furthermore, when the detection and/or quantification is accomplished by single cell fluorescence microscopy analysis without automatization, manual cell count could be labor-intensive and introduce errors between different operators. On top of that, adaptation to higher throughputs is widely precluded.

1.5 Aim and strategy

To respond the emergence of infectious viral diseases such as ZIKV and CHIKV and the imperative need for prophylactic or therapeutic agents to combat them, new platforms for both fundamental and applied viral research are compulsory. To tackle these problems, we proposed to develop a new fast and reliable platform to not only detect viral infection but also screen potential antivirals.

In a first approach, we wanted to escape the required BSL (3) to handle CHIKV using a strategy based in VLPs for viral protein display. Thus, one of the major objectives of this thesis was to develop retrovirus-like particles (rVLPs), which have been highly studied in the Cell Line Development and Molecular Virology Laboratory (CLD&MV), suitable for heterologous envelope pseudotyping (**Figure 1.12A** and **Figure 1.12B**). Concomitantly, these rVLPs will also be developed to bear a viral protease to attain a double virus-based system to test potential antiviral compounds targeting both entry and protease mechanisms (**Figure 1.12C**). To test these rVLPs infection capacity, and the potential WT ZIKV and CHIKV pseudotyped ones, our second major objective was to establish a cell-based reporter consisting of distorted split-GFPs, which remain in a "sentinel" state until rVLPs infection (**Figure 1.12E**). Upon infection, proteolytic activity triggers sensor activation. To first validate this double strategy as a proof of concept, we established rVLPs with capsid associated mCherry, for entry visualization, and/or the highly active Tobacco etch virus protease (TEVp) for biosensor activation.

With the development of chimeric rVLPs, a promising tool will be available to screen potential antiviral peptides and thus advance the antiviral development field. In addition, the biosensing system will permit the establishment of a new fast and reliable method for detection and quantification of viral pathogens. This new functional method will overcome the adversities of the existing methods and provide the so desired tool to make progress in viral studies, namely in the scope of LIVES project, - "Live cell sensors for virus detection: enabling drug and vaccine development for neglected diseases." Funded by Fundação para a ciência e a Tecnologia Ref. PTDC/BTM-SAL/30577/2017 - aiming to develop therapeutic and prophylactic solutions to treat ZIKV and CHIKV infections.

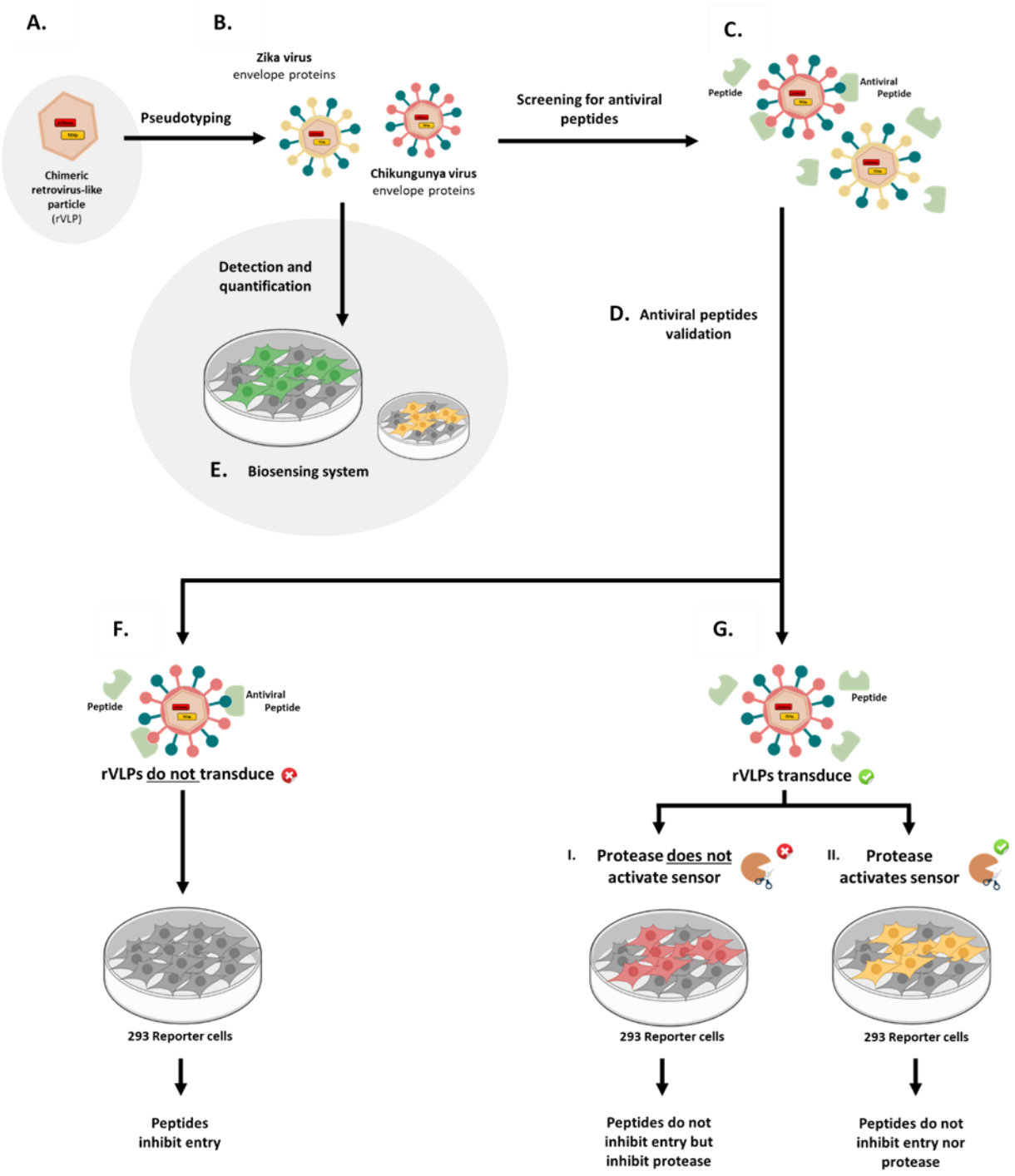

Figure 1. 12 – Overview of the thesis work within the scope of LIVES project. **(A)** Chimeric retrovirus-like particles (rVLPs) harboring mCherry and TEVp proteins and **(B)** pseudotyped with Zika or Chikungunya envelope glycoproteins will be developed to **(C)** screen an in-house library of peptides with potential antiviral activity. **(D)** This antiviral activity will not only be tested against viral entry, by targeting envelope proteins, but also against the viral life cycle, by targeting the viral protease. **(E)** In addition, a biosensing system based in a genetically encoded split Green Fluorescent Protein to detect and quantify viral pathogens was envisioned. This system not only presents a helpful tool to detect and quantify the developed rVLPs or any other viral pathogen, but also to validate the peptides with potential antiviral activity. In conjunction, these two platforms present a promising tool for antiviral screenings. When rVLPs are challenged with peptides, three different outcomes are expected. **(F)** peptides have antiviral effect against envelope proteins, inhibiting viral entry and consequently preventing any fluorescent signal; **(G-I)** peptides do not have antiviral properties against viral entry but inhibit protease - red fluorescence emission; **(G-II)** peptides do not have antiviral properties against viral entry nor protease - red and green (yellow) fluorescence emission. This thesis work falls in part A and E, development of rVLPs able to be pseudotyped with different viral envelopes and development of the sensor genetic backbone to detect viral proteases (highlighted in grey).

2 Materials and methods

2.1 Plasmids

The constructs encoding the designed biosensors and TEVp were cloned into a modified lentiviral vector transgene backbone (**Figure 2.1A**). Briefly, pRRLSIN.cPPT.PGK-GFP.WPRE (Addgene plasmid No. 12252, kindly provided by Didier Trono through the Addgene plasmid repository, Watertown, MA, USA) is a self-inactivating (SIN) third generation transgene backbone with human immunodeficiency virus-1 (HIV-1) long terminal repeat (LTR) sequences flanking the transgenes, enabling the plasmid integration in the host genome. This system backbone contains: cPPT (central polypurine tract), that increases transduction efficiency and transgene expression; Rev responsive element (RRE); HIV-1 packaging signal Psi (Ψ) for RNA encapsidation in the lentiviral nucleocapsid; and a Woodchuck Hepatitis Virus Post-Transcriptional Regulatory Element (WPRE) to stimulate transgene expression via increased nuclear export [104]. This backbone was previously modified at the CLD&MV (**Figure 2.1B**) to substitute the human phosphoglycerate kinase 1 (hPGK-1) promoter and GFP by a cytomegalovirus (CMV) promoter, the gene of interest (GOI), and an encephalomyocarditis virus (EMCV) internal ribosomal entry site (IRES; amplified from pIRESGALEO [105]) driving the expression of *Sh ble* (amplified from pMONO-zeo-mcs; Invivogen, San Diego, CA, USA) or *pac* genes (amplified from pSELECT-puro; Invivogen).

Figure 2. 1 – Schematic representation of plasmid backbones. A) Addgene original plasmid backbone modified in the Cell Line Development and Molecular Virology Laboratory by substituting hPGK and GFP by **B)** CMV, GOI, EMCV and *Sh ble* or *pac genes*, generating the final backbone used to construct Split-GFP and TEVp plasmids. LTR: long terminal repeat; Psi (Ψ): HIV-1 packaging signal; RRE: Rev responsive element; cPPT: central polypurine tract; hPGK: human phosphoglycerate kinase 1 promoter; GFP: green fluorescent protein; CMV: cytomegalovirus promoter; GOI: gene of interest; EMCV: encephalomyocarditis virus; IRES: internal ribosomal entry site.

The plasmids used for VLP expression were designed in pMLV-GP plasmid (**Figure 2.2**), which drives the expression of Murine leukemia virus (MLV) *gag-pro-pol* (GP) through a composite promoter – human Elongation Factor-1α (hEF1α) promoter and 5' untranslated region of the Human T-Cell Leukemia Virus (HTLV) – derived from pSELECT-blasti-mcs (Invivogen, San Diego, CA, USA).

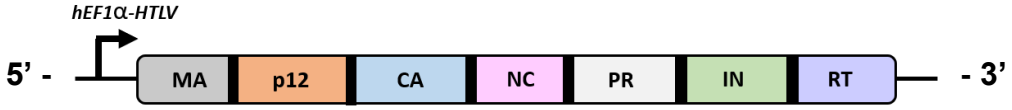

Figure 2. 2 – Schematic representation of pMLV-GP plasmid backbone. Murine leukemia virus (MLV) *gag-pro-pol* plasmid. Cassette expression is driven by hEF1α-HTLV composite promoter. Retrovirus protease cleavable sequences are represented in bold. hEF1α: human Elongation Factor-1α promotor; HTLV: Human T-Cell Leukemia Virus; MA: matrix; p12: protein 12; CA: capsid; NC: nucleocapsid: PR: protease; IN: integrase; RT: reverse transcriptase.

Primers and templates used for all the constructed plasmids are listed in **Table 6.1** in supplementary information.

2.1.1 Biosensors

To express the split-GFP11 fragment distorted by embedment in an eglin c with a TEVp recognition site (eGFP11), a plasmid previously designed at CLD&MV coding for GFP11 embedded in an eglin c with an adenovirus protease (AVP) recognition site – pRRLSIN.CMV.eLRGAG.v2.IRES.Puro.WPRE.v2 – was used. Therein, direct mutagenesis was performed to replace the AVP cleavage sequence – LRGA↓G (arrow denoting the scissile bond) – by a TEVp cleavage sequence – ENLYFQ↓S – generating the plasmid pRRLSIN.CMV.eENLYFQS.IRES.Puro.WPRE.v2 (**Figure 2.3A**) – hereafter referred to as eGFP11 plasmid for simplicity.

Split-GFP11 fragment distorted by cyclization promoted by *Nostoc punctiforme* DnaE (*Npu* DnaE) split intein and harboring a TEVp cleavage site (cyGFP11) was generated by using another previously developed plasmid at CLD&MV – the pRRLSIN.CMV.cLRGAG-GFPS11.IRES.Puro.WPRE.v2. Like the previous plasmid, the AVP cleavable sequence was replaced by ENLYFQ↓S by site directed mutagenesis, generating the pRRLSIN.CMV.cENLYFQS-GFPS11.IRES.Puro.WPRE.v2 plasmid (**Figure 2.3B**) – hereafter denominated cyGFP11 plasmid.

The GFP10 and GFP11 fragments distorted by coiled-coils with TEVp cleavage sequences were generated using two of the CLD&MV plasmids. The two plasmids used, pRRLSIN.CMV.E5-GFPS10-GLRGAG-GGS-K5.IRES.Zeo.WPRE.v2 and pRRLSIN.CMV.K5-GFPS11-GLRGAG-E5.IRES.Puro.WPRE.v2, had heterodimerizing coiled coils E5 and K5 flanking each fragment and also presented an AVP recognition sequence. In each plasmid, the AVP cleavage sequence was replaced by that of TEVp, generating respectively, the plasmids pRRLSIN.CMV.E5-GFPS10-ENLYFQS-GGS-K5.IRES.Zeo.WPRE.v2 (**Figure 2.3C**) – ccGFP10 plasmid – and pRRLSIN.CMV.K5-GFPS11-ENLYFQS-E5.IRES.Puro.WPRE.v2 (**Figure 2.3D**) – ccGFP11 plasmid.

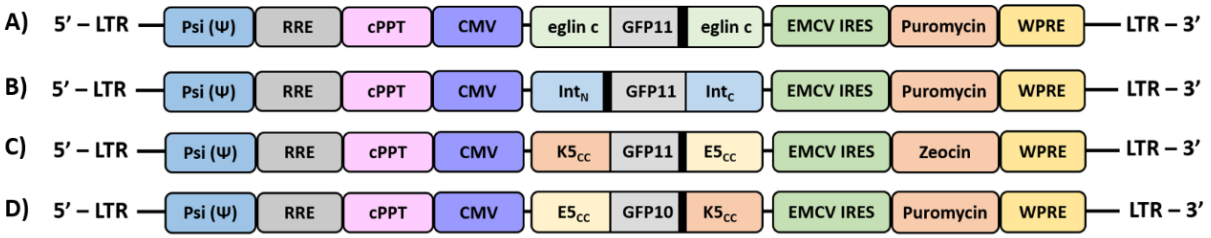

Figure 2. 3 – Schematic representation of split-green fluorescent protein (GFP) plasmids generated in this thesis. Plasmid constructs coding for **A)** eGFP11 **B)** cyGFP11 **C)** ccGFP11 and **D)** ccGFP10 are under the control of CMV promoter. GFP11 is flanked by the N- and C-terminal ends of **A)** the eglin c protein and **B)** the *Npu* DnaE intein. E5-K5 coiled-coils are flanking **C)** GFP11 and **D)** GFP10. TEVp cleavable sequences are represented in bold. EMCV IRES is promoting the expression of the antibiotic resistance genes – **A,B,D)** Puromycin and **C)** Zeocin. LTR: long terminal repeat; Psi (Ψ): HIV-1 packaging signal; RRE: Rev responsive element; cPPT: central polypurine tract; CMV: cytomegalovirus promoter; EMCV: encephalomyocarditis virus; IRES: internal ribosomal entry site; WPRE: Woodchuck Hepatitis Virus Post-Transcriptional Regulatory Element.

2.1.2 TEV protease

TEVp was expressed from the backbone original plasmid pRRLSIN.cPPT.CMV.Adenain-MVGLG-VIc.EMCVIRES.Zeo.WPRE (previously constructed at CLD&MV) modified to code for AVP. Hence, AVP coding sequence was eliminated through restriction and the sequence coding for TEVp, obtained from pRRLSIN.EF1a.TEVp.IRES.Puro.WPRE.v2 (previously constructed at CLD&MV) through polymerase chain reaction (PCR), was inserted into the mentioned backbone by In-Fusion cloning, generating the pRRLSIN.cPPT.CMV.TEVp.EMCVIRES.Zeo.WPRE plasmid (**Figure 2.4**) – hereafter referred to as TEVp plasmid.

Figure 2. 4 – Schematic representation of tobacco etch virus protease (TEVp) coding plasmid. TEVp is under the control of the CMV promoter while EMCV IRES is promoting the expression of the zeocin resistance genes. LTR: long terminal repeat; Psi (Ψ): HIV-1 packaging signal; RRE: Rev responsive element; cPPT: central polypurine tract; CMV: cytomegalovirus promoter; TEVp: Tobacco etch virus protease; EMCV: encephalomyocarditis virus; IRES: internal ribosomal entry site; WPRE: Woodchuck Hepatitis Virus Post-Transcriptional Regulatory Element.

2.1.3 Retrovirus-Like particles plasmids

All the plasmids constructed for VLP expression related work were derived from the CLD&MV plasmid, pMLV-GP. The genes of interest were inserted between sequences coding for retrovirus matrix (MA) and p12 proteins in the *gag* (group-specific antigen) polyprotein coding sequence, which contains the viral core structural proteins (**Figure 2.5**). Retrovirus protease native cleavage sequences (PRSSLY↓PALTP) were also added to flank the GOIs to permit their processing and subsequent individualization. The GOIs inserted were mCherry (**Figure 2.5A**), using the plasmid pPuro_mCherry as template, and TEVp (**Figure 2.5B**), using pRRLSIN.EF1a.TEVp.IRES.Puro.WPRE.v2 as template, generating the plasmids pMLV-GP-mCherry and pMLV-GP-TEVp, respectively.

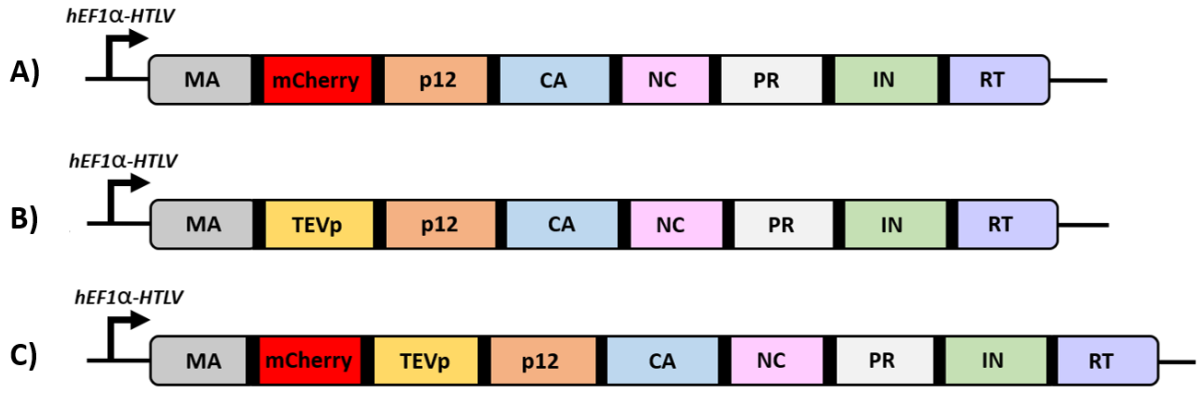

Figure 2. 5 – Schematic representation of retrovirus-like particles packaging plasmids. A) mCherry **B)** TEVp and **C)** mCherry and TEVp proteins are inserted between the Murine leukemia virus (MLV) matrix and p12 proteins of the g*ag-pro-pol* plasmid. Cassette expression is driven by hEF1α-HTLV composite promoter. Retrovirus protease cleavable sequences are represented in bold. hEF1α: human Elongation Factor-1α promotor; HTLV: Human T-Cell Leukemia Virus; MA: matrix; p12: protein 12; CA: capsid; NC: nucleocapsid: PR: protease; IN: integrase; RT: reverse transcriptase.

A third plasmid was also constructed with mCherry and TEVp separated by an additional retrovirus native cleavage sequence (**Figure 2.5C**), originating pMLV-GP-mCherry-TEVp plasmid.

2.2 Cloning procedures

All PCR reactions were performed using Phusion High-Fidelity DNA Polymerase [106] (Thermo Scientific, Waltham, MA, USA), in a Biometria T3 Personal Thermocycler (Biometria, Göttingen, Germany), as recommended by the manufacturer. All the PCR amplification conditions and steps were performed using Touchdown PCR [107] and were specifically designed for each fragment, taking amplicon-length, complexity, annealing temperatures and possible primer-primer and self-primer dimers in consideration.

PCR products were isolated through 0.8-2% (depending on fragment size) (w/v) agarose gel electrophoresis (NZYTech, Lisbon, Portugal), prepared in 1x Tris-Acetate-EDTA buffer (Fisher Bioreagents, Waltham, MA, USA) with 0.5 µL/mL RedSafe Nucleic Acid Staining Solution (INtRON Biotechnology, Hong Kong, China). After the run, gels were visualized in GelDoc XR+ system (BioRad, Hercules, CA,) and the fragments of interest excised using a scalpel. The excised fragments were purified using NucleoSpin Gel and PCR Clean-up kit (Macherey-Nagel, Düren, Germany), and quantified with a Nanodrop 2000C Spectrophotometer (Thermo Scientific).

Vector plasmids were linearized using the proper restriction enzymes (New England Biolabs, Ipswich, MA, USA) and CutSmart buffer (New England Biolabs) according to the manufacturer's instructions. The resulting restriction fragments were resolved by agarose gel electrophoresis and purified in the same conditions as above.

Cloning ligation reactions were performed using In-Fusion HD Cloning Kit (Takara Bio Inc., Mountain View, CA, USA), with a molar ratio of 2:1 insert to vector (with a minimum of 20 ng of insert) [108,109]. The ligated products were transformed in bacterial cells.

2.3 Bacterial strains and culture media

After the ligation reactions, two different *Escherichia coli* (*E. coli*) strains, NEB Stable (New England Biolabs) or Stellar (Takara Bio Inc.) competent cells were used for plasmid amplification according to the manufacturer's instructions. Liquid and agar cultures were performed using Luria Broth (LB) media (Fast-Media LB, Invivogen, San Diego, CA, USA) supplemented with Ampicillin or Blasticidin for bacteria selection and Terrific Broth (TB) media (Fast-Media TB, Invivogen), supplemented with Blasticidin. The media was prepared following the manufacturer's instructions and using sterile ultrapure water (Milli-Q, Merck Millipore, Billerica, MA, USA).

2.4 Plasmid purification and quality control

Plasmid recovery after transformation was performed in small scale using GeneJET Plasmid Miniprep Kit (Thermo Scientific Waltham, MA, USA)) and in large-scale with Genopure Plasmid Maxi Kit (Roche Applied Science, Basel, Switzerland), according to the manufacturer's instructions. Bacteria stocks for each construct were stored at -80 ºC in 15% (v/v) glycerol (Alfa Aesar, Haverhill, MA, EUA).

DNA concentration of the recovered plasmids was determined using a Nanodrop 2000C Spectrophotometer (Thermo Scientific) and purity measured through absorbance ratios 260/280 nm and 260/230 nm. Plasmids correct restriction pattern was confirmed by enzymatic restriction using the proper enzymes, followed by agarose gel electrophoresis, as previously described. All the plasmids obtained were sequenced by Eurofins Genomics services (Val Fleuri, Luxembourg) using the Sanger sequencing method.

2.5 Cell lines and culture conditions

Three different cell lines, 293, 293T and 293cc11/10 were used during the experimental work. 293 (American Type Culture Collection, ATCC; CRL-1573) is a cell line derived from human embryonic kidney. 293T (ATCC; CRL-3216) is a cell line derived from 293 that expresses the simian vacuolating virus 40 (SV40) large T antigen. 293cc11/10 is a cell line consisting in 293 cells stably expressing the split-GFP coiled-coils distorted biosensor, developed in the context of this thesis. 293T cell line was used for transient transfections and transient lentiviral vectors production while 293 cells were used for lentiviral vector titration and establishment of stable sensor populations. 293cc11/10 reporter cells were used for transient transfections. Cells were grown in Dulbecco's modified Eagle's Medium (DMEM; Gibco, Paisley, UK) supplemented with 10% (v/v) Fetal Bovine Serum (FBS; Gibco), under adherent conditions in tissue culture flasks. Additionally, 293cc11/10 reporter cells were also grown in the presence of 100 µg/mL of Zeocin and 1 µg/mL of Puromycin. All cells were cultured at 37 ºC in a humidified atmosphere with 8% CO_2.

2.6 Cell concentration and viability

Cell concentration and viability were determined by trypan blue exclusion assay, using a 0.1% (v/v) Trypan Blue (Sigma-Aldrich, St. Louis, MO, USA) solution in Phosphate Buffer Saline (PBS; Gibco). For cell counting a Fuchs-Rosenthal hemocytometer (Marienfeld-Superior, Lauda-Konigshofen, Germany) and an inverted microscope (Olympus, Tokyo, Japan) were used.

2.7 Biosensors initial characterization

To do an initial evaluation of the different split-GFP biosensor backbones and/or cleavable sequences, transient transfections with the genetically encoded biosensors were performed. 293T cells, seeded at 8×10^4 cells/cm^2 in 6-well plates the day before, were co-transfected with 5 µg of total DNA per 10^6 cells, using linear 25 kDa poly(ethylenimine) (PEI; Polysciences Inc., Hirschberg, Germany) with a DNA:PEI ratio of 1:1. Each biosensor coding plasmid was co-transfected with a plasmid coding for GFP10 (when needed for transcomplementation; previously constructed at CLD&MV), and either a TEVp-coding plasmid or a mock plasmid expressing mCherry (control). Medium was exchanged 24 h post-transfection. After 48 h, cells were observed by fluorescence microscopy (DMI6000; Leica, Wetzlar, Germany) and assessed by flow cytometry (CyFlow Space, Sysmex Partec GmbH, Görlitz, Germany).

2.8 Lentivirus vector production

Stable expression of split-GFP coiled-coils distorted biosensors in 293 cells was accomplished by lentivirus (LV) transduction.

First, LV stocks harboring as transgenes ccGFP10, ccGFP11, or GFP (as a control) were produced. 293T cells, seeded at 8 × 10^4 cells/cm^2 in tissue culture flasks with 75 cm^2 the day before, were transiently co-transfected using PEIpro® (Polyplus transfection, Illkirch, France) with the developed pRRLSIN plasmids coding for the respective split-GFP biosensors, and the plasmids pMDLg/pRRE (Addgene plasmid No. 12251), pRSV-Rev (Addgene plasmid No. 12253), and pMD2.G (Addgene plasmid No. 12259) which provided, respectively, the packaging functions *gag-pro-pol* and REV and the Vesicular stomatitis virus G (VSV-G) envelope [110]. After 24 h, medium was exchanged, and its volume reduced by half for LV concentration. After 48 h, LVs were harvested, filtered through 0.45 µm and stored in aliquots at -80 ºC.

2.8.1 Vector titration

To do LV titration, 293 target cells seeded at a density of 5 × 10^4 cells/cm^2 in 24-well plates the previous day were infected with 200 µL of serial dilutions (1:2, 1:20 and 1:200) of the viral samples in a medium with Polybrene (Sigma-Aldrich, St. Louis, MO, USA) in a final concentration of 8 µg/mL. Medium exchange was performed 4 h later, and cells incubated at 37 ºC for 48 hours. After the required incubation time, cells infected with control LV (harboring GFP as transgene) were analyzed by flow cytometry to determine the percentage of GFP positive cells. Lentiviral titer was determined using the following equation and considering only viral dilutions giving between 2% to 20% of GFP positive cells.

$$\textbf{Titer}\ (\textbf{T.U/mL}) = \frac{\%\text{GFP positive cells x number of cells at infection}}{100}\ \text{x}\ \frac{\text{viral dilution factor}}{\text{Infection volume (mL)}}$$

In addition to flow cytometry, viral load was also determined by integrated vector copy number quantitative polymerase chain reaction (VCN-qPCR).

2.8.2 Vector copy number quantitative PCR

LV stocks harboring the transgenes ccGFP10, ccGFP11 and a GFP control were also tittered by VCN-qPCR. This method determines the number of integrated LV genomes by quantitative PCR directly from transduced cell lysates, using the human albumin (ALB) as an internal reference gene.

Cells were transduced for flow cytometry and VCN q-PCR titration. At 48 hours post-transduction, cell extracts for VCN q-PCR titration were prepared by adding 100 µL of lysis buffer from Global UltraRapid Lentiviral Titering Kit (System Bioscience, Palo Alto, CA, USA) to each well. To help the lysis process, the plate was frozen at -80 °C and thawed after 30 minutes at room temperature for 15 minutes. Each well content was posteriorly homogenized, transferred to microtubes and heated at 95 °C for 10 minutes. After cooldown, the samples were centrifuged at 1200 x g for 5 minutes, distributed into aliquots and stored at -20 °C, until further use.

Integrated LV genomes and ALB reference gene were detected by qPCR using LightCycler 480 Probes Master mix (Roche Applied Science), ALB primer/probe mix (Thermo Scientific) and LTR probe (IDT, Coralville, Iowa, USA) and primers (**Table 6.2**).

Calibration curves were established with 10-fold serial dilutions of the plasmid pHR'-CMV-GFP-ALB, bearing the ALB gene and the plasmid pRRLSIN.CMV.K5-GFPS11-ENLYFQS-E5.IRES.Puro.WPRE.v2 bearing the transgene ccGFP11, ranging from 1×10^8 to 1×10^2 copies/µL. These calibration curves were used to establish a linear regression which correlates the cycle threshold (Ct) values with known concentrations of the standard plasmid. These linear regressions were used to calculate the number of copies/µL of the LTR and ALB sequences in each sample, by interpolating the linear regression equations with the Ct values obtained. VCN was subsequently determined by correlating the number of integrated LV sequences to the number of ALB, using the following equation:

$$\mathbf{VCN} = \frac{\text{LV sequence } \frac{\text{copies}}{\mu\text{L}}}{\text{Reference } \frac{\text{copies}}{\mu\text{L}}} \text{ x N}$$

"N" indicates the number of genomic copies of the reference gene per cell genome, which is assumed to be 2 in ALB's case. Having the VCN number, LV titers in integrative particles per mL (I.P./mL), were determined using the following equation:

$$\mathbf{Titer\ (I.P./mL)} = \frac{\text{VCN x C x D}}{\text{V}}$$

In this equation, "C" is the number of cells at infection, "D" the LV supernatant dilution used and "V" the volume of LV supernatant (in mL) used for transduction.

2.9 Cells transduction and selection

To accomplish the last step in the establishment of 293 sensor reporter cells, 293 cells seeded at a density of 6×10^4 cells/cm^2 in a 6-well plate the day before were transduced with LVs coding for ccGFP11 (previously titrated by VCN-qPCR) at a multiplicity of infection (MOI) of 5 in the presence of 8 µg/mL Polybrene (Sigma-Aldrich, St. Louis, MO, USA). After 48 h, cells were selected using 1.0 µg/mL Puromycin (Invivogen). The selected 293 ccGFP11 population was posteriorly transduced with LV stocks coding for ccGFP10 using the same MOI. After 48 h cells were selected using 100 µg/mL Zeocin (Invivogen), and the resulting populations characterized.

2.10 Chimeric retrovirus polyproteins initial characterization

To initially characterize the constructed chimeric RV polyprotein and their retroviral cleavage sites, 293T cells seeded at 8×10^4 cells/cm^2 in 6-well plates the day before, were transfected with 5 µg of either pMLV-GP, pMLV-GP-mCherry, pMLV-GP-TEVp or pMLV-GP-mCherry-TEVp per 10^6 cells, using linear 25 kDa PEI (Polysciences Inc., Hirschberg, Germany) with a DNA:PEI ratio of 1:1. After 48

h, cells were observed by fluorescence microscopy (DMI6000; Leica, Wetzlar, Germany), and assessed by flow cytometry (BD FACSCelesta™, BD Biosciences, San Jose, USA). To observe polyprotein cleavage by the retrovirus protease, and release of single proteins, a protein extraction protocol was performed in the transfected cells. The resultant protein extracts were quantified and used to perform western blot analysis.

2.10.1 Protein extraction, quantification, and western blot analysis

For protein extraction, cells seeded and transfected as described in 2.10 were collected, pelleted at 2500 x g for 10 minutes, washed in PBS (Gibco) and centrifuged again. The resultant cell pellets were lysed with Mammalian Protein Extraction Reagent (M-PER; Thermo Scientific) prepared with 1x cOmplete EDTA-free Protease Inhibitor Cocktail (Roche Applied Science), at a concentration of 100 µL of lysis solution per 1 x 10^6 cells, vortexed and incubated for 10 minutes at room temperature. Posteriorly, the lysate was centrifuged at 14000 × g for 10 minutes and the supernatant harvested, aliquoted and frozen at -20 ºC. Extracts' total protein was quantified according to the manufacturer's instructions using the Pierce BCA Protein Assay Kit (Thermo Scientific). To perform western blot analysis, the first step was to separate protein extracts by sodium dodecyl sulfate-polyacrylamide gel electrophoresis (SDS-PAGE). For that, equal amounts of total protein (20 µg) previously denatured at 95 °C for 5 minutes and prepared with NuPAGE LDS Sample Buffer (4X), NuPAGE Reducing Agent (10X) and mili-Q water in a final volume of 20 µL, were separated under denaturing conditions using NuPAGE 4-12% (w/v) Bis-Tris gel with NuPAGE MOPS SDS Running Buffer in XCell SureLock Mini-Cell electrophoresis system (Thermo Scientific). Gels ran initially at 80 V for 15 minutes, allowing sample entry into the gel, and afterwards at 180 V for 1 hour. SeeBlue Plus 2 Pre-Stained Protein Standard (Thermo Scientific) was used as molecular weight reference. The second step was to transfer the separated proteins from the gel to a nitrocellulose membrane using iBlot 2 Dry Blotting System (Invitrogen) following manufacturer's instructions. Membranes were blocked for 1 hour at room temperature with blocking solution 5% (w/v) non-fat dried milk (AppliChem GmbH, Darmstadt, Germany) prepared in Tris-Buffered Saline (TBS; Sigma-Aldrich) with 0.1% (w/v) Tween 20 (TBST; Sigma-Aldrich). After multiple washing steps with TBST, membranes were incubated under agitation overnight with primary antibodies: anti-α-Tubulin monoclonal antibody (Mouse, Sigma-Aldrich, #T1199, 1:2000); anti-mCherry monoclonal antibody (Mouse, Abcam, #ab125096, 1:2000); anti-TEVp polyclonal antibody (Rabbit, Novus Biologicals, NBP1-97669, 1:500) and anti-MLV p30 monoclonal antibody (Mouse, Abcam, #ab130757, 1:1500), all with their respective dilutions in 5% (w/v) Bovine Serum Albumin (BSA; Sigma-Aldrich) in TBST. After overnight incubation, membranes were submitted to multiple washing steps with TBST and incubated with gentle agitation for 2 hours at room temperature with Horseradish Peroxidase conjugated secondary antibodies, to further detect membrane-bounded primary antibodies. The secondary antibodies used were Amersham ECL sheep Anti-Mouse IgG (NA931; GE Healthcare, Little Chalfont, UK) to detect anti-α-Tubulin, anti-MLV-p30 and anti-mCherry primary antibodies and Amersham ECL donkey Anti-rabbit IgG (NA934; GE Healthcare, Little Chalfont, UK) to detect anti-TEVp primary antibodies, all diluted 1:5000 in blocking solution. Finally, membranes were revealed with Amersham ECL Prime Western Blotting Detection Reagent (GE Healthcare Amersham ECL), according

to the manufacturer's instructions, and chemiluminescence was detected with ChemiDoc XRS System (Bio-Rad).

2.10.2 Production and quantitation of non-enveloped retrovirus-like particles

To produce the rVLPs, transient transfections with each of the rVLP plasmids were performed. 293T cells, seeded at 8×10^4 cells/cm^2 in 6-well plates the day before, were transfected with 5 µg of either pMLV-GP, pMLV-GP-mCherry, pMLV-GP-TEVp or pMLV-GP-mCherry-TEVp per 10^6 cells, using linear 25 kDa PEI (Polysciences Inc., Hirschberg, Germany) with a DNA:PEI ratio of 1:1. Culture medium was removed 24 h post-transfection and replaced by DMEM 10% (v/v) FBS. After 48 h, supernatants were harvested, filtered through 0.45 µm, aliquoted and stored at -80 °C. Measurement of physical particle concentration was accomplished by MLV p30 ELISA using the QuickTiter™ MuLV Core Antigen ELISA Kit (Cell Biolabs, Inc, San Diego, USA), according to the recommendations and manufacturer's instructions. Viral supernatants underwent several dilutions performed in the assay diluent provided in the kit.

2.11 Initial characterization of 293cc11/10 reporter cells

To understand if the biosensing system could be used to detect and/or quantify the developed rVLPs, a transient transfection with the plasmids coding for coiled-coils distorted split-GFP biosensor and each VLP-coding plasmid was performed with the proper controls. For that, 293T cells seeded at 8×10^4 cells/cm^2 in 24-well plates the day before, were co-transfected with coiled-coils distorted split-GFP biosensor plasmids (i.e plasmids coding for ccGFP10 and ccGFP11) and either one of each VLP plasmid (pMLV-GP, pMLV-GP-mCherry, pMLV-GP-TEVp or pMLV-GP-mCherry-TEVp) or a TEVp-coding plasmid (positive control) or a mock plasmid expressing mCherry (control). Transfections were performed with 5 µg of total DNA per 10^6 cells, using linear 25 kDa PEI (Polysciences Inc., Hirschberg, Germany) with a DNA:PEI ratio of 1:1 and medium exchanged 24 h post-transfection. After 48 h, cells were observed by fluorescence microscopy (DMI6000; Leica, Wetzlar, Germany) and assessed by flow cytometry (BD FACSCelesta™, BD Biosciences, San Jose, USA).

2.12 Production of proof of concept retrovirus-like particles

VSV-G enveloped rVLPs with mCherry or mCherry-TEVp fusion insertion into *gag-pro-pol* were produced for control and proof of concept purposes. For that, 293T cells, seeded at 8×10^4 cells/cm^2 in tissue culture flasks with 150 cm^2 the day before, were transiently co-transfected with 5 µg of total DNA per 10^6 cells, using linear 25 kDa PEI (Polysciences Inc., Hirschberg, Germany) with a DNA:PEI ratio of 1:1. Co-transfection was made with the plasmids pMLV-GP-mCherry or pMLV-GP-mCherry-TEVp, pMD2.G (Addgene plasmid No. 12259) and pEMCGALEO which coded, respectively, for retrovirus (RV) *gag-pro-pol* with mCherry or mCherry and TEVp insertions, VSV-G envelope and a *LacZ* transgene. After 24 h, medium was exchanged and its volume reduced by half for RV concentration. After 48 h, VSV-G enveloped rVLPs were harvested, filtered through 0.45 µm and stored in aliquots at -80 ºC. In addition, cells were assessed by flow cytometry (BD FACSCelesta™, BD Biosciences, San Jose, USA).

2.12.1 Titration of proof of concept retrovirus-like particles using *LacZ*

To know the amount of integrative rVLPs per mL, viral supernatants were titrated using *LacZ* transgene. For that, 293 cells seeded at 8 × 10^4 cells/cm^2 in a 96 well-plate the previous day were infected with serial dilutions (10^{-0} to 10^{-7}) of the viral samples in medium with Polybrene (Sigma-Aldrich, St. Louis, MO, USA) in a final concentration of 8 µg/mL. Plate's old medium was removed, and 80 µL of viral dilutions added in triplicate and incubated at 37 ºC. Fresh medium was added 4 h post-infection. Forty-eight h post-infection cells were fixed and stained. For that, medium was removed from plates, wells washed with PBS and a fixing solution containing glutaraldehyde 25%, formaldehyde 37% and PBS was added. Fixing solution was incubated during 3 minutes at room temperature, wells washed 2 times with PBS and a staining solution containing X-gal 20 mg/mL in Dimethylformamide, 0.5 M $K_3Fe(CN)_6$, 0.5 M $K_4Fe(CN)_6$, 0.1 M $MgCl_2$ and PBS was added. Plate was incubated at 37 ºC for 24 h. Viral dilutions were observed on the microscope and blue cells were counted in wells containing between 10 to 90 blue cells. Titer was calculated using the following equation:

$$\textbf{Titer}\ (\textbf{I.P./mL}) = \frac{\text{Number of blue cells}}{\text{Volume of infection (mL)}}\ \text{x Viral dilution}$$

2.12.2 Titration of proof of concept retrovirus-like particles using mCherry

For rVLPs titration, 293 target cells seeded at a density of 1 × 10^5 cells/cm^2 in 24-well plates the previous day were infected with 200 µL of serial dilutions (1:2, 1:10, 1:20, 1:100 and 1:200) of the viral samples in medium with Polybrene (Sigma-Aldrich, St. Louis, MO, USA) in a final concentration of 8 µg/mL, and incubated at 37 ºC. Six h post-infection, cells were analyzed by flow cytometry (BD FACSCelesta™, BD Biosciences, San Jose, USA) to determine the percentage of mCherry positive cells. Titer was determined using the following equation and considering only viral dilutions giving between 2% to 20% of mCherry positive cells.

$$\textbf{Titer}\ (\textbf{T.U./mL}) = \frac{\%\ \text{mCherry positive cells x Cells at infection}}{100}\ \text{x}\ \frac{\text{Viral dilution factor}}{\text{Infection volume (mL)}}$$

2.12.3 Protein delivery kinetics of proof of concept retrovirus-like particles

To study the kinetics of protein delivery by the developed rVLPs, mCherry and mCherry-TEVp bearing rVLPs were used to transduce the previously developed reporter cell line 293cc11/10, and fluorescence was monitored for 72 h. For that, 293cc11/10 cells seeded at 1.25 × 10^5 cells/cm^2 in a 24 well-plate the day before and previously incubated on ice for 30 min, were transduced with 500 µL of each rVLP and a mock supernatant at a MOI of 3 in the presence of 8 µg/mL Polybrene (Sigma-Aldrich, St. Louis, MO, USA). Cells were harvested and analyzed by flow cytometry at the indicated time points.

2.13 Flow cytometry data acquisition and analysis

Flow cytometry was used to quantify percentage and geometric mean fluorescence intensity (MFI) of GFP and mCherry positive cells. Gates were set using non-transfected 293, 293T or 293cc11/10 cells as negative control, and percentage of GFP or mCherry positive cells and their MFIs were measured within the positive gate. Data analysis was performed with FlowJo Software for Windows, version 10.6.1 (Becton, Dickinson and Company, Ashland, OR, USA).

2.14 Data and statistical analysis

Results are shown as mean ± standard deviation (SD) of at least three independent experiments, except otherwise noted. Signal-to-noise ratio (SNR) was used to evaluate the performance of the developed sensors. Herein, SNR refers to the ratio of total accumulated GFP fluorescence (geometric mean fluorescence times the number of events measured by flow cytometry) upon sensor activation (signal), to total accumulated GFP fluorescence of mock or non-transfected controls (noise). Statistical analysis was performed using one-way analysis of variance (ANOVA) followed by Tukey's posthoc test. *P* values < 0.05 were considered statistically significant. Regarding rVLPs results, statistical significance was evaluated by comparing samples to their respective mock controls or between each other, using ANOVA followed by Tukey's posthoc test, or unpaired, two-tailed Student's t-test. *P* values < 0.05 were considered statistically significant.

3 Results

3.1 Design of split-GFP sensors activated by viral protease proteolysis

In this work, cell-based genetically encoded split-GFP biosensors were developed exploiting split-GFP intrinsic features. Split-GFP is a GFP divided into two non-fluorescent fragments - GFP10 (containing the first 10 β-strands of GFP) and GFP11 (containing the 11th β-strand) - that only reestablish its fluorescence when fragment complementation occurs [111]. A switch-on biosensor can be designed by preventing split-GFP fragment complementation and, consequently, fluorescence emission, until a virus of choice infects a host cell. To accomplish this, three types of structural distortions were assessed to impair correct fragment assembly (**Figure 3.1A**). The first strategy relied on embedding GFP11 fragment in the internal loop of the small eglin c protein (eGFP11 strategy) [112]. The second strategy involved cyclization induced by *Npu DnaE* split intein, where the N- and C-terminus of GFP11 fragment were respectively covalently linked to the C- and N-terminus of the *Npu DnaE* split intein (cyGFP11 strategy) [113]. Both eGFP11 and cyGFP11 strategies represent single distortion schemes – only one of the split-GFP fragments is distorted. As such, a dual distortion strategy – where both split-GFP fragments are distorted – was also assessed by the addition of the E5 and K5 heterodimerizing coiled coils to both split-GFP fragments [114]. For that, GFP10 was flanked by E5 in the N-terminus and K5 in the C-terminus (ccGFP10), and GFP11 was flanked with K5 in the N-terminus and E5 in the C-terminus (ccGFP11).

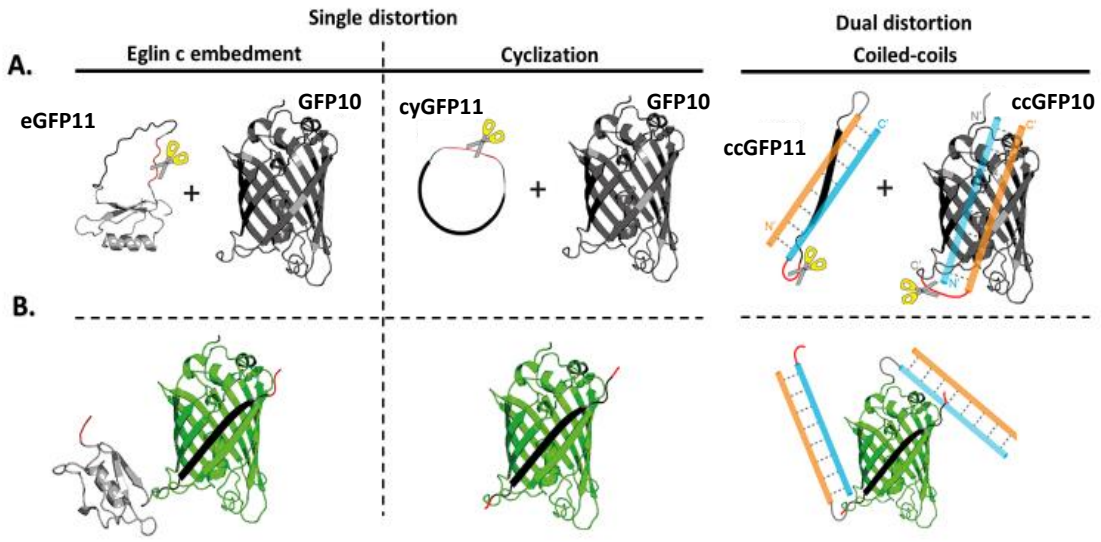

Figure 3. 1 – Schematic illustration of the designed structural distortions introduced into GFP10 and GFP11 split-GFP fragments. (A) eGFP11 was distorted by embedment in an eglin c molecule, cyGFP11 by split intein induced cyclization and ccGFP10 and ccGFP11 by coiled-coils introduction. These distorted fragments included also a TEVp cleavage sequence (in red) that upon cleavage by the protease allows **(B)** fragment distortion release and consequently split-GFP fragments complementation, reestablishing fluorescence.

For a virus-induced switch-on fluorescent sensor, we took advantage of site-specific recognition by viral proteases. As such, in addition to the above-mentioned structural distortions, cleavage sites specifically recognized by a protease of choice were added to the designed biosensors. For a first proof of concept and to evaluate the different distortion strategies, we took advantage of the highly specific and efficient TEVp [115]. When TEVp is present, the protease cleaves the introduced cleavage site, reestablishing the correct conformation of the split-GFP fragment, and allowing fragment complementation and fluorescence emission (**Figure 3.1B**).

3.1.1 Validation of the designed TEVp-dependent sensors

The plasmids encoding for the three proposed biosensing strategies, as well as the viral TEVp, were constructed as indicated in the materials and methods section. All the plasmid constructions were submitted to a restriction-based analysis (**Figure 3.2**) to confirm the correct restriction patterns. Since restriction analysis is not enough to confirm absence of mutations in the targeted area, especially in the case of the biosensors where only the restriction site was modified, all the constructions were also submitted to sequencing analysis.

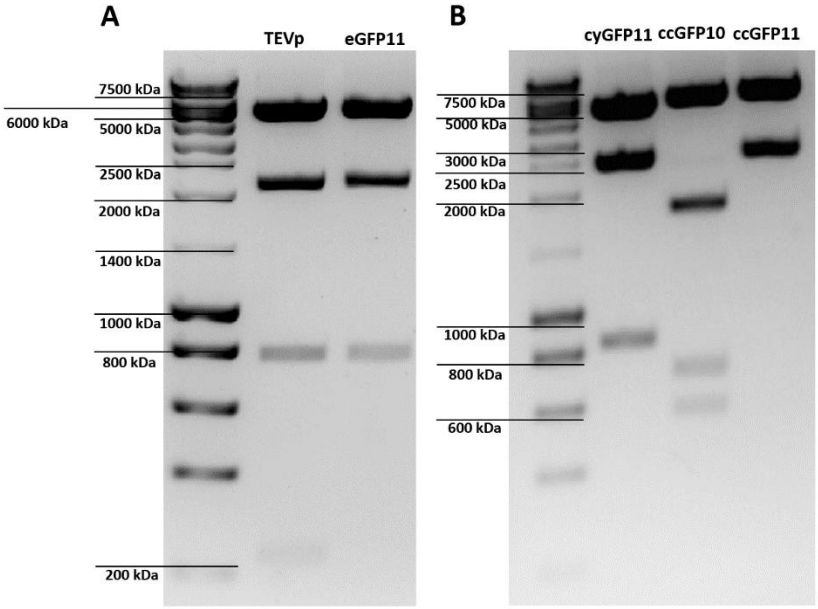

Figure 3. 2 – Restriction patterns of the constructed plasmids. The final plasmid constructs were submitted to a restriction-based analysis, showing the expected restriction patterns: 5315 bp + 2158 bp + 753 bp + 239 for TEVp; 5315 bp + 2158 bp + 753 bp for eGFP11; 5159 bp + 2539 bp + 836 bp for cyGFP11; 5567 bp + 1738 bp + 713 bp + 576 bp + 63 bp (out of the gel) for ccGFP10 and 5740 bp + 2539 bp for ccGFP11. **A)** Lane 1 and 2 represent respectively the plasmids coding for TEVp and eGFP11 biosensor, digested with the enzyme NcoI. **B)** Lanes 1, 2 and 3 represent respectively the plasmids coding for cyGFP11, ccGFP10 and ccGFP11 digested with the enzyme DraIII.

To validate the functionality of the proposed biosensors, the constructs bearing the distorted fragments (and the non-distorted GFP10 where necessary for complementation) were co-transfected into 293T cells together with either TEV protease or a mCherry mock control (**Figure 3.3A**). After 48

hours, transfected cells were observed by fluorescence microscopy for a qualitative analysis (**Figure 3.3B**).

As observed by the lack of fluorescence in the absence of protease, all strategies revealed to be effective in split-GFP inactivation (**Figure 3.3B, top panel**). When adding TEVp, eGFP11 strategy showed no fluorescence, suggesting the sensor was not being activated by proteolytic activity.

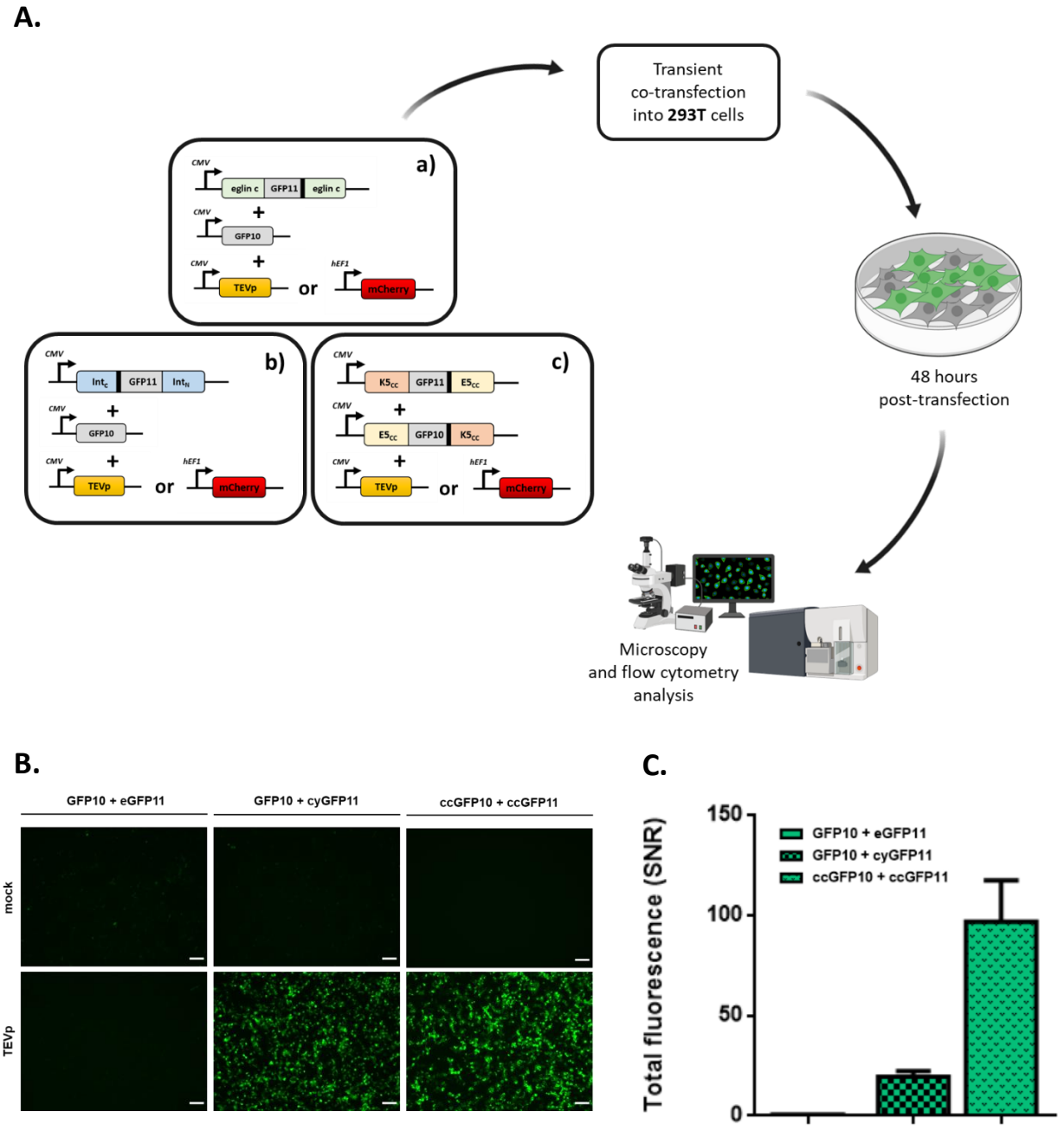

Figure 3. 3 – Evaluation of split-GFP biosensors triggered by TEVp activity performance. (A) 293T cells transiently co-transfected with **a)** GFP10 and eGFP11, **b)** GFP10 and cyGFP11 or **c)** ccGFP10 and ccGFP11, with either TEVp or mock plasmid, were analyzed 48 h post-transfection by **(B)** fluorescence microscopy and **(C)** flow cytometry. Data shown as mean ± SD of at least three independent experiments. Scale bar = 100 µm.

In addition, cells co-transfected with TEVp showed an unexpected lower fluorescence in comparison to the cells transfected with a mock plasmid. Relatively to cyGFP10 and ccGFP10 + ccGFP11 strategies, the presence of a highly distinct fluorescent signal confirmed sensor activation.

For a quantitative analysis, the transfected cells were also analyzed by flow cytometry (**Figure 3.3C**). This revealed that total fluorescence SNR of cells co-transfected with GFP10 and eGFP11 was low and, in presence of TEVp, lower than the background noise (SNR 0.56 ± 0.04), further demonstrating that the sensor was not being activated. Regarding the two remaining distortions, cyGFP11 and ccGFP10 + ccGFP11, flow cytometry data corroborated the results obtained by fluorescence microscopy, confirming sensor activation by proteolytic activity. Cells co-transfected with ccGFP10 + ccGFP11 presented a higher total fluorescence ratio (SNR 97 ± 21) than the ones co-transfected with GFP10 + cyGFP11 (SNR 20 ± 3), indicating a better performance of the biosensing system distorted by coiled-coils.

Since the distortions introduced by coiled-coils were the best performers, this was the biosensor chosen to further establish a cell line stably expressing the designed biosensing system. For that, 293 cells were infected with LVs bearing the adequate transgenes (ccGFP10 and ccGFP11) with a MOI of 5 and further submitted to antibiotic selection with Puromycin and Zeocin (as described in the Materials and Methods section) generating the 293cc11/10 cell line.

3.2 Design of chimeric retrovirus polyproteins

To develop a chimeric rVLP platform, monitoring virus entry in host cells and viral proteolytic activity – or their impairment – for applicability in screening of an in-house antiviral peptide library, a first proof of concept was conducted. To this end, we inserted mCherry and TEVp proteins into the *gag* polyprotein of the RV *gag-pro-pol* coding plasmid, more specifically between the matrix protein (MA) and the RNA-binding phosphoprotein p12 (P12) – as described in section 2.1.3. Retrovirus protease native cleavage sequences flanking the GOIs were also added to permit correct polyprotein processing and consequent individualization. These insertions were made between MA and P12 proteins since it has been reported that this is the place with a better compromise between relative titer and mean fluorescence intensity (MFI) [116]. While both mCherry and TEVp proteins allow rVLPs entry detection upon cell entry in the sensor reporter cells herein developed, TEVp additionally allows to assess viral proteolytic activity or its impairment (as a proof of concept protease). Two different single detection strategies, consisting of two different rVLPs, were designed: one carrying mCherry (for cell entry monitoring) and another carrying TEVp (for cell entry monitoring and reporter cells testing; **Figure 3.4A** and **Figure 3.4B**). The presence of such protease not only permits to evaluate if the reporter cells are able to detect the rVLPs presence, but also if they are suitable for further potential applications to WT viruses, functioning as a validation tool.

To combine the best of both worlds, an optimal strategy envisioning rVLPs harboring both fluorescent signal (mCherry) and protease (TEVp) was also created. This dual system allows simultaneous assessment of virus entry in the host cell (by mCherry fluorescence emission), and virus proteolytic activity (by biosensor fluorescence emission upon viral proteolysis; **Figure 3.4C**).

With this system, not only viral entry targeting antivirals could be tested, but also antivirals targeting protease activity.

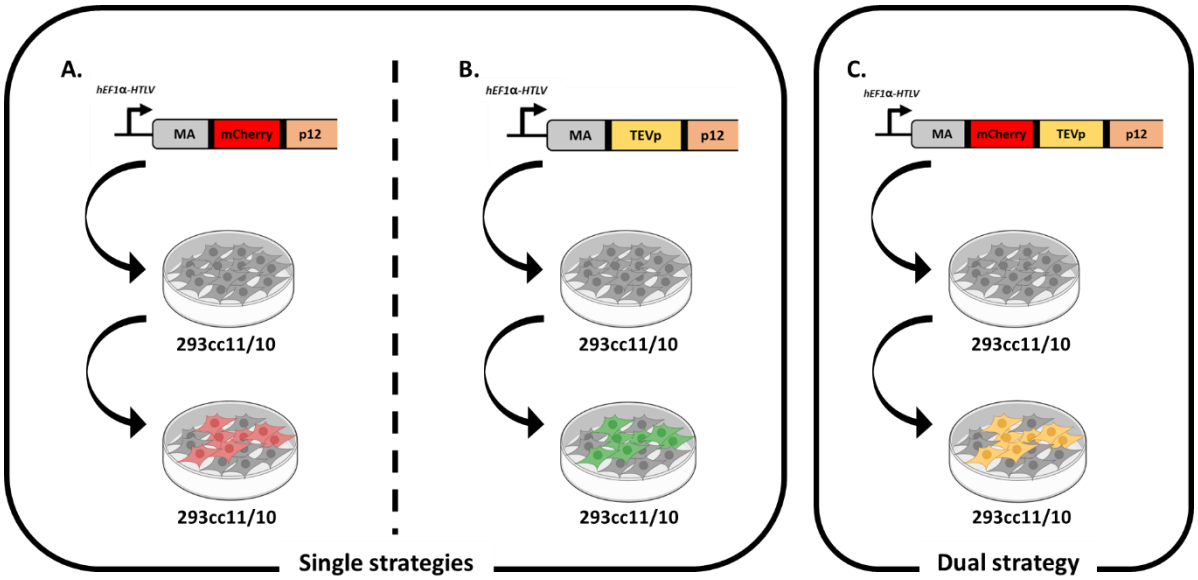

Figure 3. 4 – Schematic representation of retrovirus-like particles expression plasmids and their use for reporter cells activation. (A) mCherry **(B)** TEVp and **(C)** mCherry-TEVp flanked by retrovirus protease cleavage sequences (represented in bold), were inserted between the matrix (MA) and the RNA-binding phosphoprotein p12 (p12) in the retroviral *gag-pro-pol* coding plasmid. When these plasmids are transfected into 293 cells stably expressing the developed biosensor, they induce **(A)** red fluorescence prevenient from mCherry, indicating whether cells were transfected or not, **(B)** green fluorescence prevenient from sensor's activation by TEVp or **(C)** both, giving a fluorescent yellow color resultant from red and green colors superposition. While **(A)** and **(B)** represent separated (single) strategies, **(C)** combines the desired features into one single rVLP (dual).

3.2.1 Validation of the designed chimeric retroviral polyproteins

The developed chimeric *gag-pro-pol* plasmids were first validated and characterized in 293T cells. These plasmids were constructed as indicated in the Material and Methods section and analyzed by endonuclease restriction (**Figure 3.5**) to confirm they were correctly cloned. In addition, all the constructions were submitted to sequencing analysis.

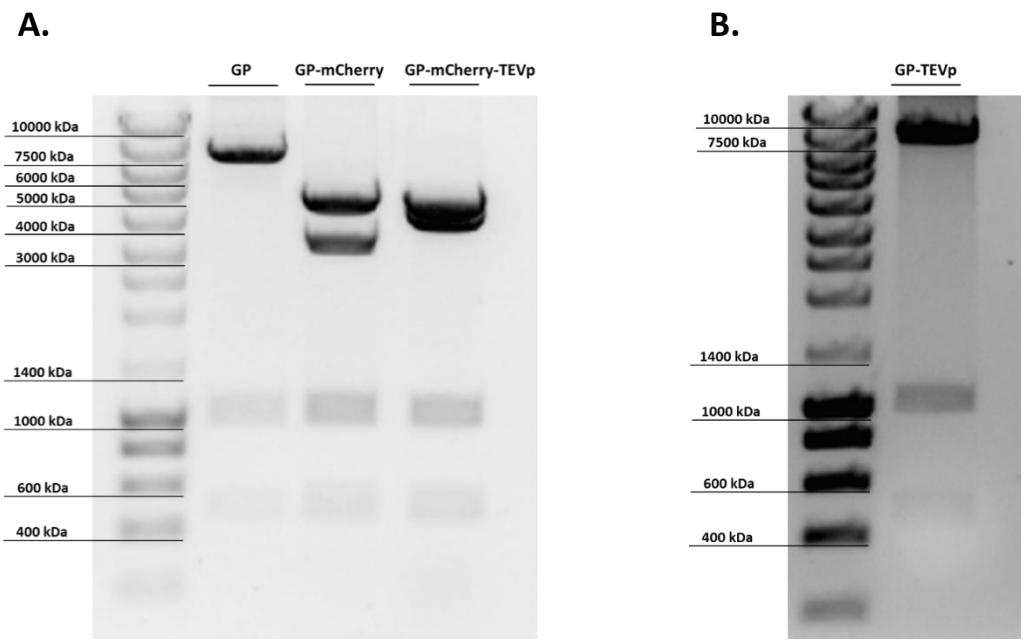

Figure 3. 5 – **Restriction patterns of chimeric retrovirus *gag-pro-pol* polyprotein coding plasmids.** The final constructs of chimeric retrovirus *gag-pro-pol* coding plasmids were submitted to a restriction-based analysis, revealing the expected restriction patterns: 6979 bp + 1011 bp + 499 bp for GP; 4564 bp + 3156 bp + 1011 bp + 499 bp for GP-mCherry; 4564 bp + 3900 bp +1011 bp+ 499 bp for GP-mCherry-TEVp and 7723 bp + 1011 bp + 499 bp for GP-TEVp. **(A)** Lane 1, 2 and 3 represent respectively the plasmids coding for RV *gag-pro-pol*, RV *gag-pro-pol* with a mCherry insertion and RV *gag-pro-pol* with a mCherry-TEVp insertion, digested with the enzyme NcoI. **(B)** represents the plasmid coding for RV *gag-pro-pol* with a TEVp insertion, digested with the same enzyme.

After confirming constructions sequence, plasmids were functionally characterized by performing transient transfections into 293T cells and analyzed after 48 h by fluorescence microscopy and flow cytometry (**Figure 3.6A**). In addition, cell protein content was extracted and submitted to western blot analysis.

Fluorescence microscopy (**Figure 3.6B**) and flow cytometry (**Figure 3.6C**) data demonstrated that transfection of GP-mCherry or GP-mCherry-TEVp plasmids resulted in red fluorescence emission, confirming the functionality of the fluorescent protein introduced in-between the retroviral polyprotein. As expected, no fluorescence was observed in cells transfected with GP and GP-TEVp coding plasmids. Regarding MFI, while GP-mCherry transfected cells showed an intensity value of 2273 AU ± 725, GP-mCherry-TEVp transfected cells demonstrated a significant inferior intensity value of 1313 AU ± 433 (**Figure 3.6D**).

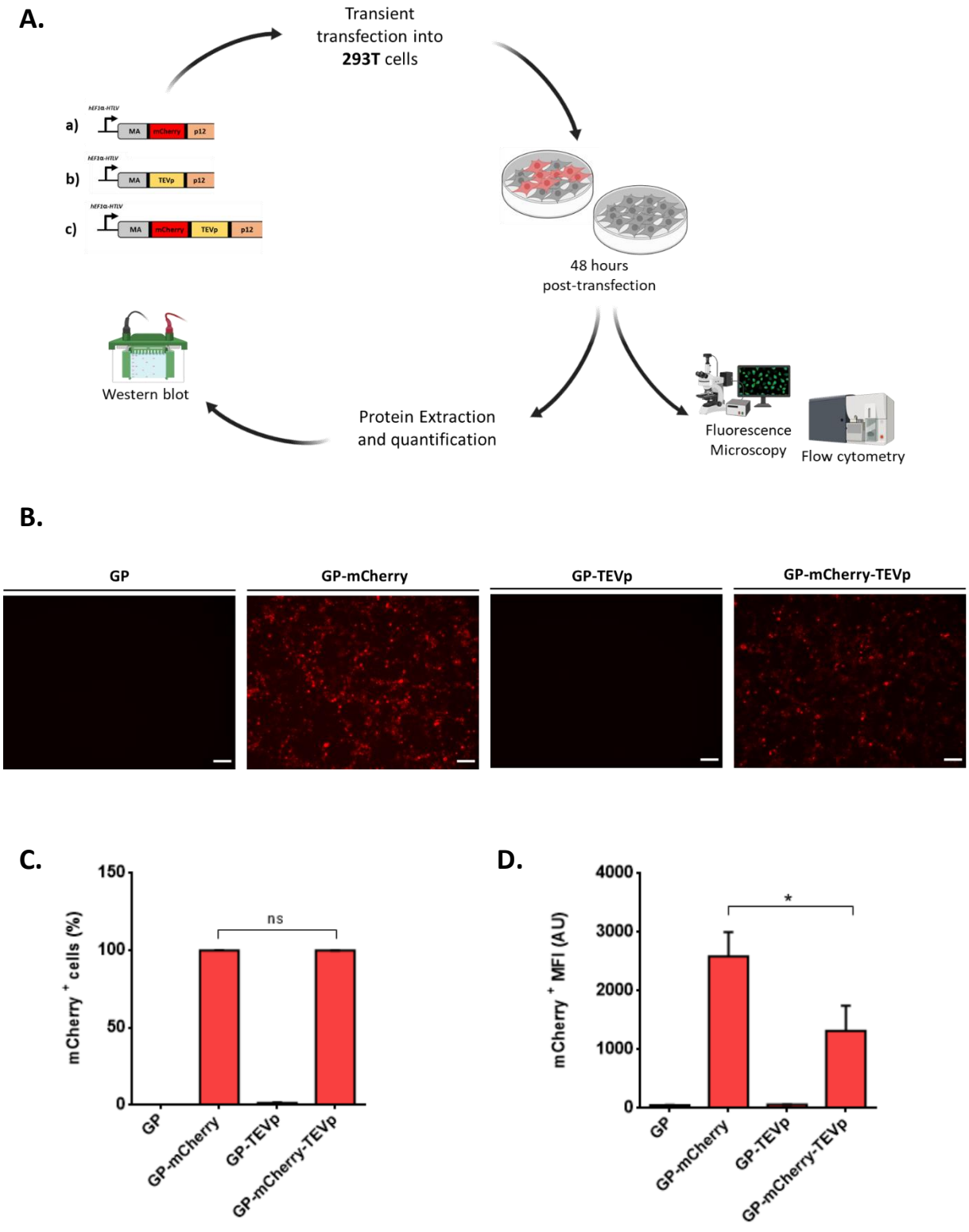

Figure 3. 6 – Validation of the proposed designs for chimeric retrovirus-like particles. (A) 293T cells transfected with **a)** GP-mCherry, **b)** GP-TEVp or **c)** GP-mCherry-TEVp, were analyzed 48 h post-transfection by **(B)** fluorescence microscopy and flow cytometry for **(C)** mCherry positive cells (%) and **(D)** their mean fluorescence intensity (MFI). Cell protein content was extracted and quantified for further western blot analysis. Data shown as mean ± SD of at least three independent experiments. Statistical analysis using unpaired, two-tailed Student's t-test. *, $P < 0.05$; ns, not significant; AU, arbitrary units. Scale bar = 100 µm.

Having confirmed plasmid functionality, the next step was to assess if the retrovirus protease was correctly processing the retroviral *gag-pro-pol* polyprotein, thus releasing mCherry (GP-mCherry), TEVp (GP-TEVp), mCherry and TEVp (GP-mCherry-TEVp), and capsid protein p30 as single proteins. For that, cell protein content was extracted and quantified to perform a western blot analysis using antibodies targeting either mCherry, TEVp, p30 or α-tubulin (the latter used as loading control; **Figure 3.7**).

When detecting mCherry, western blot results showed, as expected, no protein in GP (**Figure 3.7 lane 1**) and GP-TEVp (**Figure 3.7 lane 3**) transfected cells. On the other hand, unexpectedly, several different sized proteins were observed for GP-mCherry (**Figure 3.7 lane 2**) and GP-mCherry-TEVp (**Figure 3.7 lane 4**)**.** The pattern obtained in each case revealed that mCherry was not being released only as a single protein of 28 kDa but also in fusion with neighbor proteins of the *gag-pro-pol* polyprotein. A suggestion of the possible bands correspondence is presented in **Figure 3.7.** The bands highlighted with a square might correspond to mCherry fused to other neighboring protein parts due to potential site-unspecific cleavage by the protease. The remaining bands are of unknown origin. In addition, there is a notable variation in proteins intensity, which is an indicative of concentration. Face to this, in the case of GP-mCherry, we assume that although mCherry does not exist only as single protein, it is the most abundant form, followed by MA-mCherry-P12. Regarding GP-mCherry-TEVp, two forms seem to equally prevail – mCherry and MA-mCherry. Unfortunately, the performed western blots targeting TEVp and capsid protein p30 were not conclusive as the primary antibodies tested showed lack of specificity for the targeted proteins.

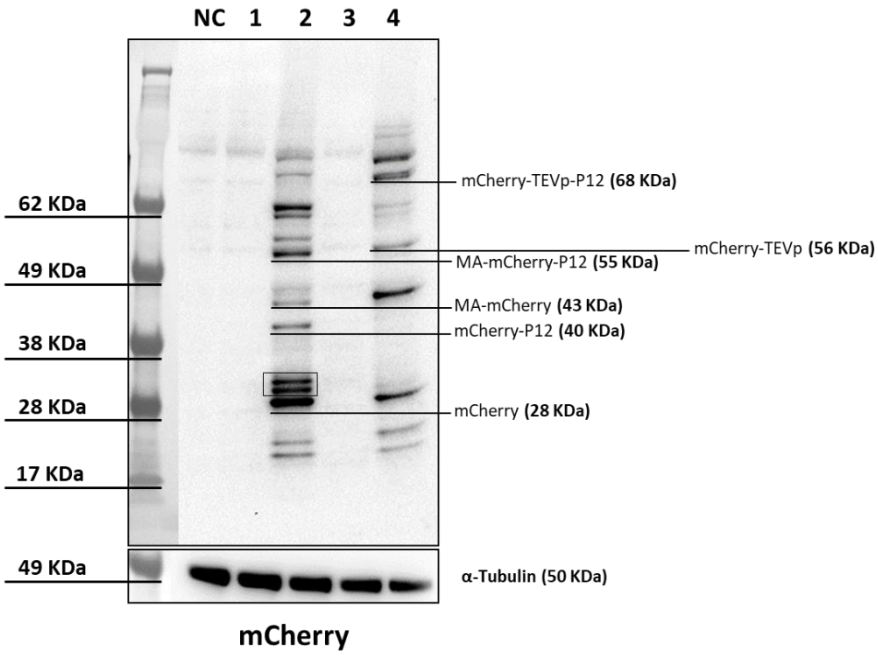

Figure 3. 7 – Western blot analysis for assessment of correct *gag-pro-pol* polyprotein processing. (1) GP, **(2)** GP-mCherry, **(3)** GP-TEVp and **(4)** GP-mCherry-TEVp transfected cells and non-transfected (negative control; NC) cells protein content was extracted and submitted to western blot analysis using a primary antibody targeting mCherry.

3.2.2 Production and characterization of chimeric rVLPs

Having verified chimeric polyproteins functionality and processing, the last validation step was to assess the impact of protein insertion in rVLPs production titers. For that, rVLPs coding plasmids were transiently transfected into 293T cells, and 48 h post-transfection, supernatants were harvested for further analysis by MLV p30 ELISA (**Figure 3.8A**). Cells were also assessed by fluorescence microscopy and flow cytometry to assess transfections efficiencies.

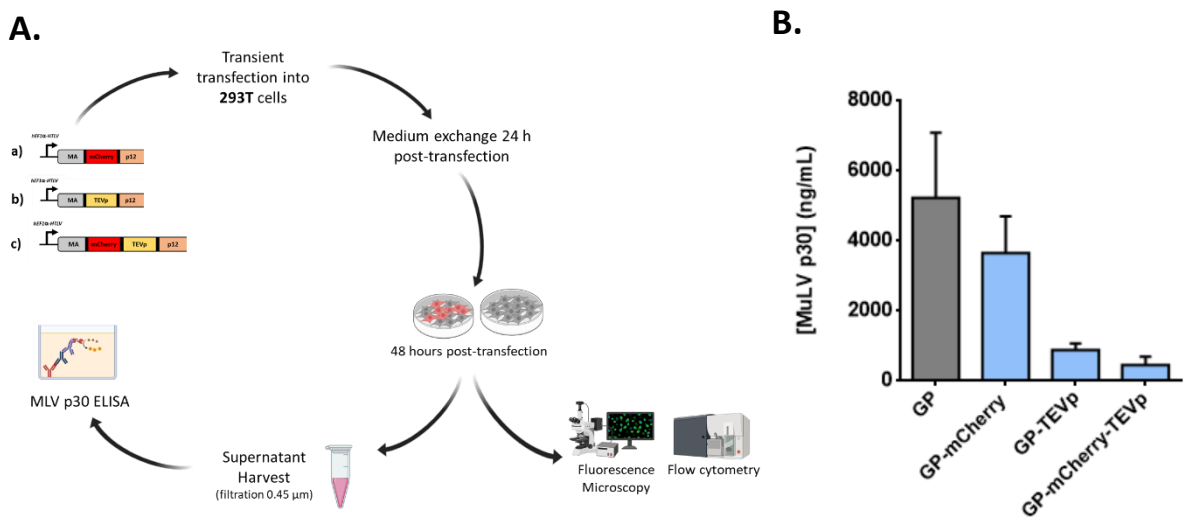

Figure 3. 8 – Quantification of retrovirus-like particles. (A) 293T cells were transfected with **a)** GP-mCherry, **b)** GP-TEVp or **c)** GP-mCherry-TEVp, and rVLPs containing supernatants were harvested and filtered through 0.45 µm 48 h post-transfection. Transfected cells were analyzed by fluorescence microscopy and flow cytometry. Supernatants were used to perform an enzyme-linked immunosorbent assay targeting Murine Leukemia Virus (MLV) rVLPs capsid protein 30. **(B)** represents the concentration obtained for each chimeric particle and the respective control (GP).

p30 quantification by ELISA showed a clear decay on physical particle production for all chimeric RV *gag-pro-pol* constructions in comparison to the parental control (GP; **Figure 3.8B**). Among the three tested designs, GP-mCherry was the one providing the most similar titers when compared to the control, corresponding to 70% of the GP rVLP production. On the other hand, GP-TEVp and GP-mCherry-TEVp evidenced a sharp decrease in physical particles production, resulting in 17% and 9% of the control total production. Although GP-mCherry-TEVp design presents almost half of the titer obtained for GP-TEVp, the expression of TEVp in these VLPs seems to have similar impact in the production titers.

3.3 Biosensor activation by the chimeric retroviral polyprotein

To do a first evaluation of rVLPs design on biosensor activation, each chimeric polyprotein was transiently co-transfected with plasmids coding for the developed biosensors, together with the proper controls (**Figure 3.9**).

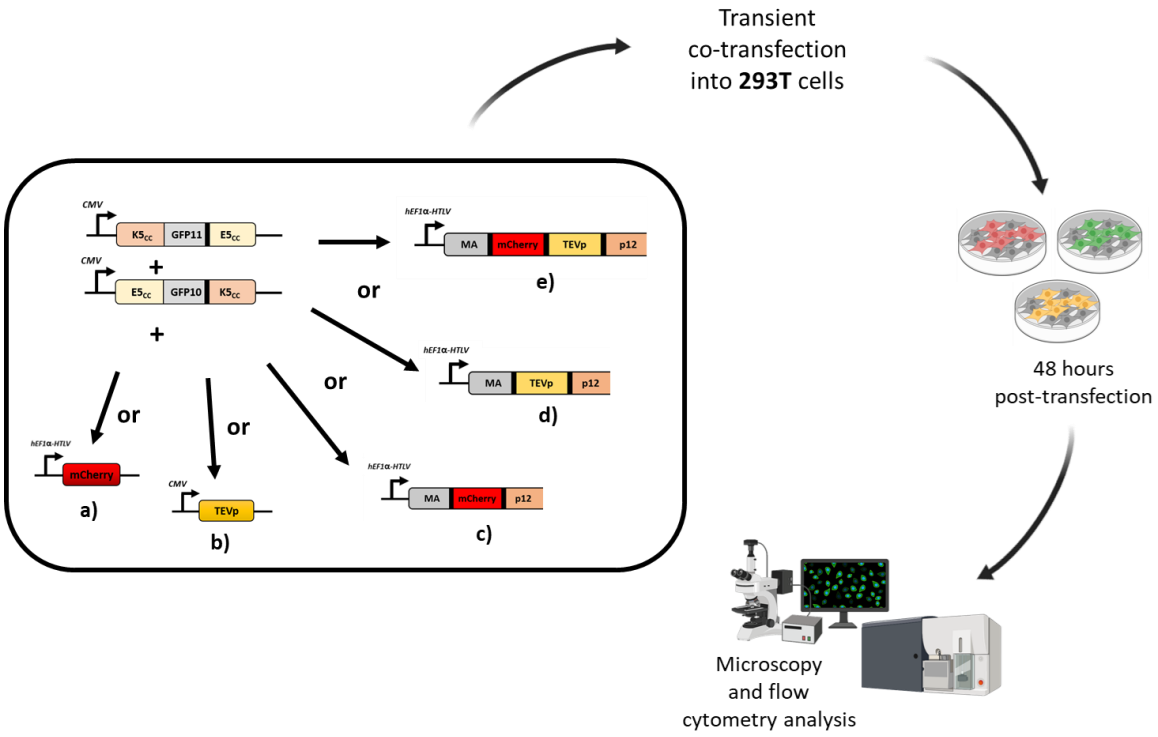

Figure 3. 9 – Schematic representation of the plasmids used for 293T cells transient co-transfection and performed analysis. 293T cells co-transfected with ccGFP10, ccGFP11 and either **a)** mock plasmid, **b)** TEVp **c)** GP-mCherry, **d)** GP-TEVp or **e)** GP-mCherry-TEVp, were analyzed 48 h post-transfection by fluorescence microscopy and flow cytometry.

As it was possible to assess by fluorescence microscopy images, transient co-transfection of the biosensor and chimeric RV *gag-pro-pol* coding plasmids seemed to result in a reduced level of both GFP positive cells and intensity, suggesting poor sensor activation (**Figure 3.10A**). In fact, flow cytometry data revealed that while sensor activation by TEVp (positive control) results in 57% ± 4 of GFP positive cells with an intensity of 2336 AU ± 809, GP-TEVp shows 44% ± 3 of activation with MFI of 890 ± 220 and GP-mCherry-TEVp 38% ± 14 with MFI of 882 ± 280 (**Figure 3.10B** and **Figure 3.10C**). The unexpectable fluorescence observed for sensor co-transfection with mock, GP and GP-mCherry coding plasmids, revealed the existence of background fluorescence. This background is the result of split-GFP complementary fragments re-assembly and was responsible for about 20 to 27% of GFP positive cells with signal intensities around 206 AU ± 45.

Regarding mCherry fluorescence results, a slight difference between mCherry containing *gag-pro-pol* plasmids intensities is verified, suggesting different mCherry signal performances between single and dual strategies. However, this difference was classified as non-significant by statistical analysis. Furthermore, a considerable difference is observed between these intensities and the one obtained for the mock control.

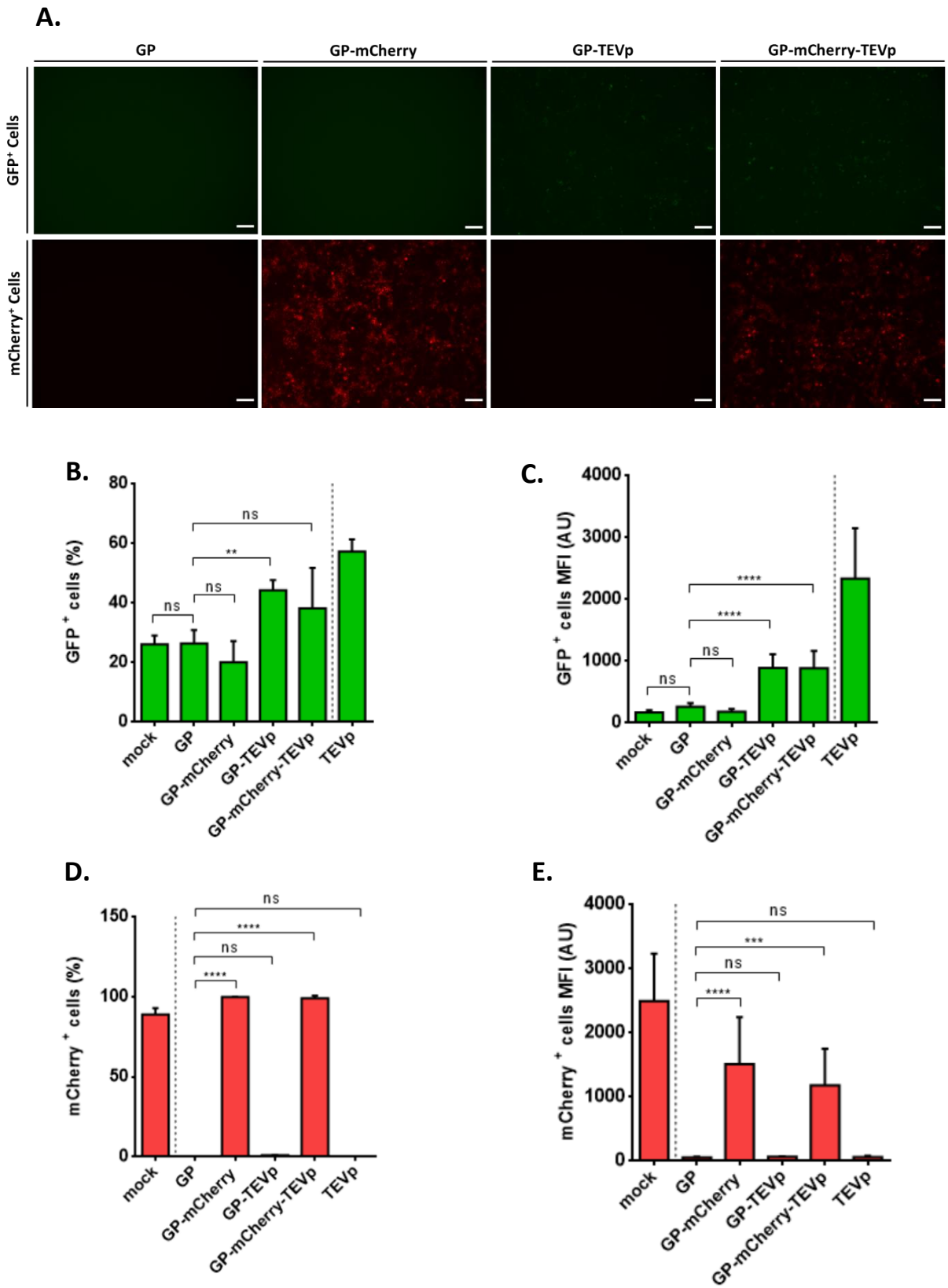

Figure 3. 10 – **Retrovirus-like particles characterization through transient sensor activation.** 293T cells co-transfected with ccGFP10, ccGFP11 and either a mock plasmid, GP, GP-mCherry, GP-TEVp, GP-mCherry-TEVp or TEVp were analyzed, 48 h post-transfection, by **(A)** fluorescence microscopy, and flow cytometry for **(B)** GFP positive cells (%) and **(C)** their mean fluorescence intensity (MFI) and for **(D)** mCherry positive cells (%) and **(E)** their mean fluorescence intensity (MFI). Data shown as mean ± SD of at least three independent experiments. **, $P < 0.01$; ***, $P < 0.001$; ****, $P < 0.0001$; ns, not significant, as indicated by ANOVA followed by Tukey's post-hoc test. AU, arbitrary units. Scale bar = 100 µm.

3.4 Stable reporter cell line establishment and characterization

After assessing biosensor activation by the chimeric polyproteins with all components in transient conditions, we also characterized the response in the previously established stable reporter cell population. As such, these cells were transiently transfected with each of the designed chimeric GP polyproteins and, 48 h later, analyzed by fluorescence microscopy and flow cytometry (**Figure 3.11**).

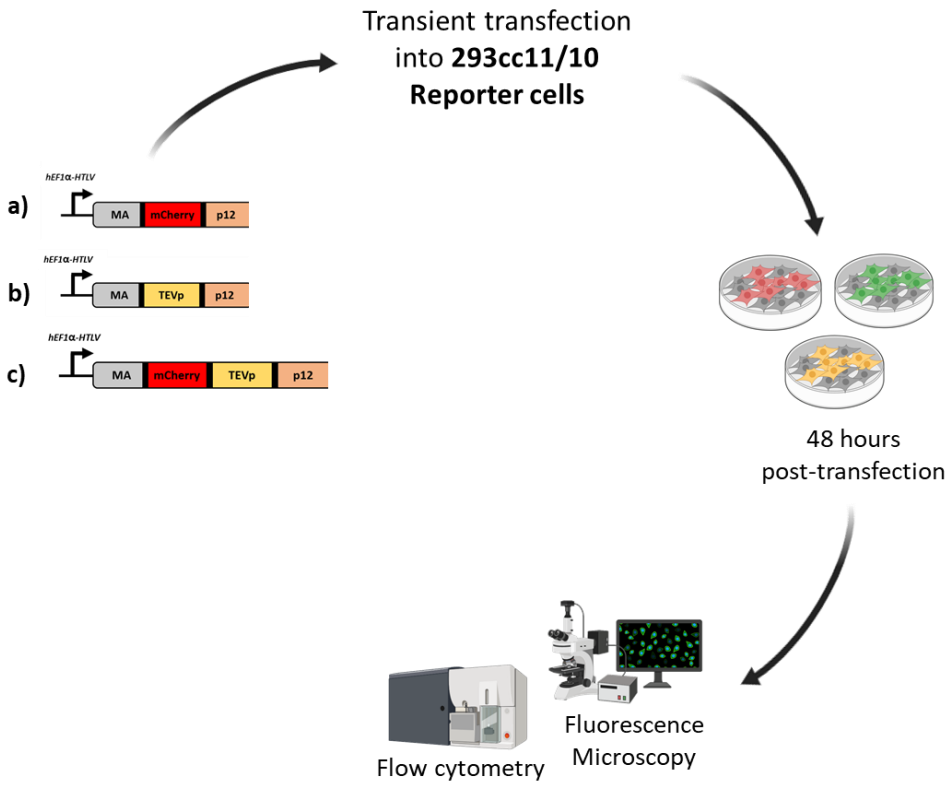

Figure 3. 11 – Schematic representation of the plasmids used for transient transfection of 293 reporter cells and posterior analysis. 293 reporter cells transfected with **a)** GP-mCherry, **b)** GP-TEVp or **c)** GP-mCherry-TEVp, were analyzed 48 h post-transfection by fluorescence microscopy and flow cytometry.

Fluorescence microscopy results showed no sensor activation for TEVp containing polyproteins and TEVp control transfections. Only a slight background fluorescence was detected (**Figure 3.12A**). Flow cytometry data corroborated these results by evidencing the same percentage of GFP positive cells and signal intensity (**Figure 3.12B**) for transfected and non-transfected 293cc11/10 reporter cells, meaning that in neither cases the sensor was activated.

Even though there was no activation, about 40% of both transfected and non-transfected cells presented GFP fluorescence, demonstrating these cells present sensor background. Indeed, these results showed that stable sensor expression in 293 cells resulted in an increase of approximately 2-fold of background fluorescence and intensity in comparison to transient sensor expression in 293T (**Figure 3.10B**). Also, the histogram data suggests the existence of two different populations of GFP positive cells.

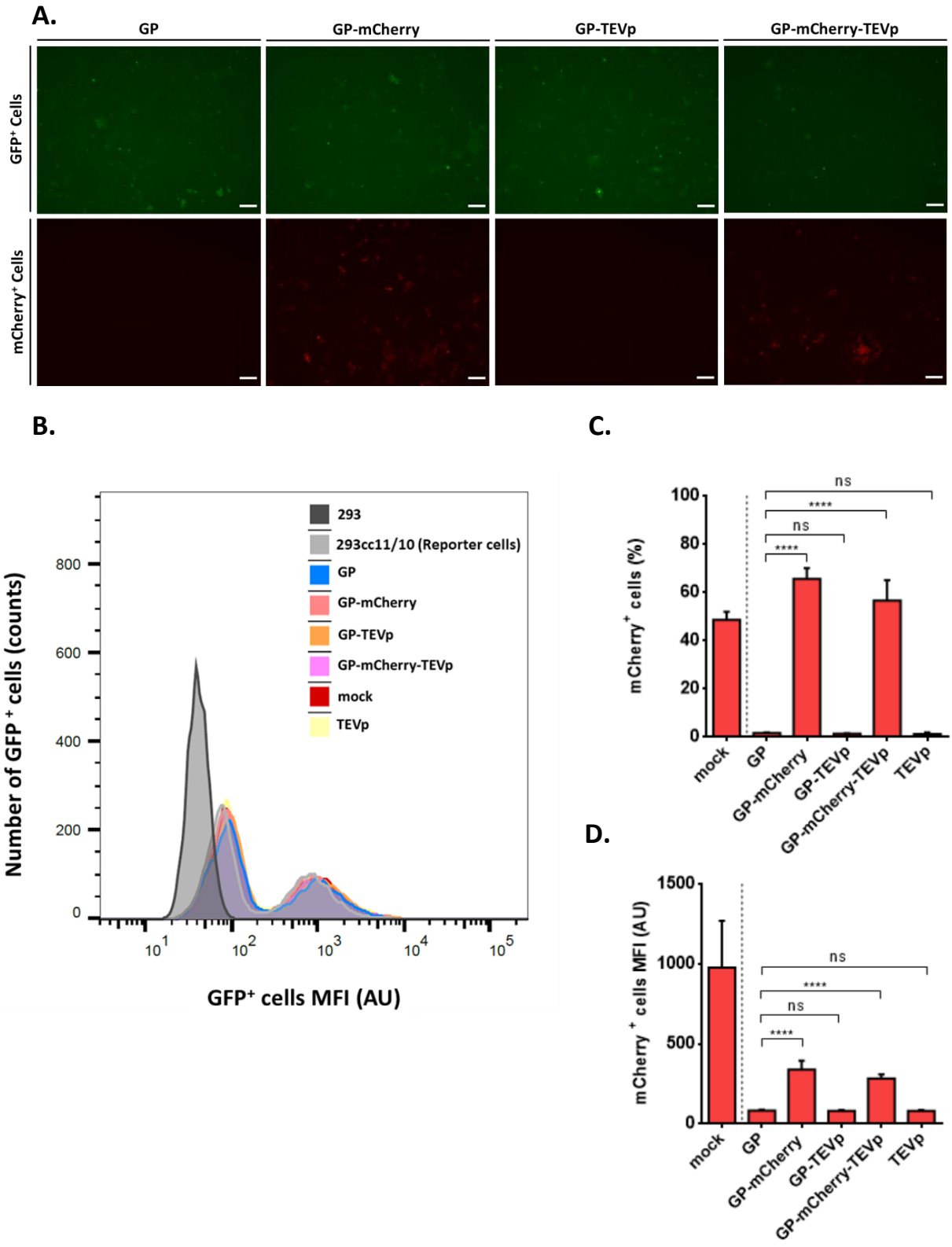

Figure 3. 12 – 293c11/10 reporter cell line transfection with chimeric polyprotein designs. 293cc11/10 established reporter cells transfected with mock, GP, GP-mCherry, GP-TEVp, GP-mCherry-TEVp or TEVp plasmids were analyzed, 48 h post-transfection, by **(A)** fluorescence microscopy, and flow cytometry for **(B)** number of GFP positive cells and their mean fluorescence intensity (MFI) and for **(C)** mCherry positive cells (%) and **(D)** their mean fluorescence intensity (MFI). Data shown as mean ± SD of at least three independent experiments. ****, P < 0.0001; ns, not significant, as indicated by ANOVA followed by Tukey's post-hoc test. AU, arbitrary units. Scale bar = 100 µm.

Concerning mCherry results, fluorescence microscopy evidenced a lower percentage of mCherry positive cells, and a significant decrease in fluorescence intensity when comparing to the transient transfections in 293T where transfection efficiencies were above 95% (**Figure 3.10D** and **Figure 3.10E**). These results were corroborated by flow cytometry where 49% ± 3 of mCherry positive cells for mock, 66% ± 4 for GP-mCherry and 57% ± 9 for GP-mCherry-TEVp were observed (**Figure 3.12C**). In addition, a clear decrease in signal intensity is observed when comparing mock (MFI 977 ± 293) with GP-mCherry (MFI 340 ± 57) and GP-mCherry-TEVp (MFI 284 ± 26) (**Figure 3.12D**).

3.5 Proof of concept: chimeric rVLPs transduction of 293cc11/10 reporter cells

Having thoroughly characterized the chimeric retroviral polyproteins and rVLPs production, and despite the lack of activation of the established reporter cells, we further characterized our virus- and cell-based platforms. Therefore, we produced, characterized, and then used the chimeric rVLPs to infect 293cc11/10 cells. For that, we used GP-mCherry-TEVp and GP-mCherry rVLPs. The latter, while not allowing assessment of proteolytic activity, may be better suited when only assessment of virus entry is desired.

For a first proof of concept of rVLPs transduction of sensor reporter cells, we transiently produced mCherry-TEVp and mCherry chimeric rVLPs, pseudotyped with the pantropic VSV-G envelope glycoprotein and carrying a transgene coding for the β-galactosidase enzyme (**Figure 3.13**).

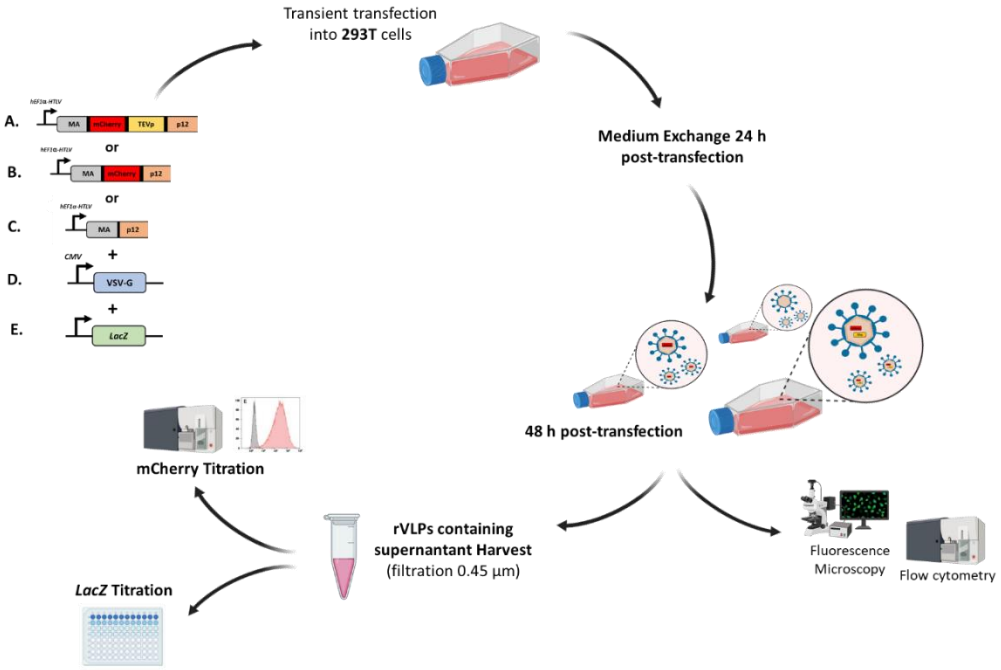

Figure 3. 13 – Production of vesicular stomatitis virus G enveloped proof of concept chimeric retrovirus-like particles. Plasmids coding for retrovirus *gag-pro-pol* bearing **(A)** mCherry-TEVp fusion, **(B)** mCherry or **(C)** retrovirus original *gag-pro-pol* (control) were transiently co-transfected into 293T cells with **(D)** VSV-G and **(E)** *LacZ* transgene plasmids. Forty-eight hours later the desired rVLPs were harvested and cells analyzed by fluorescence microscopy and flow cytometry. rVLPs were titrated using mCherry fluorescence and *LacZ* transgene.

Following production, the collected viral supernatants were quantified by flow cytometry (based on mCherry fluorescence) or by enzyme-based histochemical staining (based on β-galactosidase activity). While the former titration method quantifies rVLPs with potential for entry into cell hosts (transducing particles), the latter method quantifies the subset of those particles entering the cell host that are fully matured and able to integrate the transgene (integrative particles).

The number of total transducing particles given by mCherry titration was in every case superior to the number of integrative particles, given by *LacZ* titration (**Table 3.1**). Regarding transducing particles titration, similar values were obtained for both mCherry and mCherry-TEVp containing rVLPs, suggesting similar levels of produced particles with the ability to enter into host cells. However, when assessing titer by enzyme-based histochemical staining, major differences were observed. Indeed, and compared to the parental GP rVLPs, while GP-mCherry rVLPs showed similar levels of particles with potential to integrate the transgene, the introduction of TEVp into the retroviral polyprotein led to a decay of 2 orders of magnitude in the particles with integrative potential.

Table 3. 1 – Vesicular stomatitis virus G pseudotyped retrovirus-like particles titers obtained by mCherry and *LacZ* titration methods.

Retrovirus-like particle	Titration method	
	mCherry (TU/mL)	*LacZ* (IP/mL)
GP	-	5.7×10^{4} *
GP-mCherry	3.68×10^{6}	4.9×10^{4}
GP-mCherry-TEVp	2.33×10^{6}	8.0×10^{2}

*GP integrative particle titers of a representative experiment.

To understand the kinetics of protein delivery into the target cells and assess biosensor activation upon transduction, rVLPs containing supernatants were used to transduce the developed reporter cells – 293cc11/10 (**Figure 3.14A**). Transduced cells were then monitored by flow cytometry during 72 h. This experiment envisioned to study rVLPs infection kinetics elucidating when maximum infection efficiency and fluorescent signal intensity were reached for mCherry and sensor's GFP activation. Hence, enabling to assess the time points better suited for cell analysis to establish optimized protocols.

Relatively to TEVp delivery and subsequent sensor activation, the low percentages of GFP positive cells and signal intensity values showed, as previously verified by transient transfection of the reporter cells, absence of sensor activation (**Figure 3.14B** and **Figure 3.14C**).

The results obtained for mCherry delivery demonstrated an increase in transduced cells over 8 h, reaching a steady state of roughly 100% transduced cells at 10 h post-transduction (**Figure 3.14D**). Regarding signal intensity, a similar initial pattern was observed, evidencing a linear increase in MFI of mCherry positive cells until 8 h post-infection (**Figure 3.14E**). An increase in MFI of transduced cells was also observed occurring up to 24 h post-transduction, although at a lower rate. Finally, at 48 h, a sharp decrease in fluorescent signal intensity was observed, followed by a smaller decline at 72 h.

These results have showed an equal behavior for mCherry, and mCherry and TEVp containing rVLPs. However, regarding signal intensity, GP-mCherry-TEVp design presented slightly inferior values in comparison to GP-mCherry, observed from 8 h post-transduction onwards.

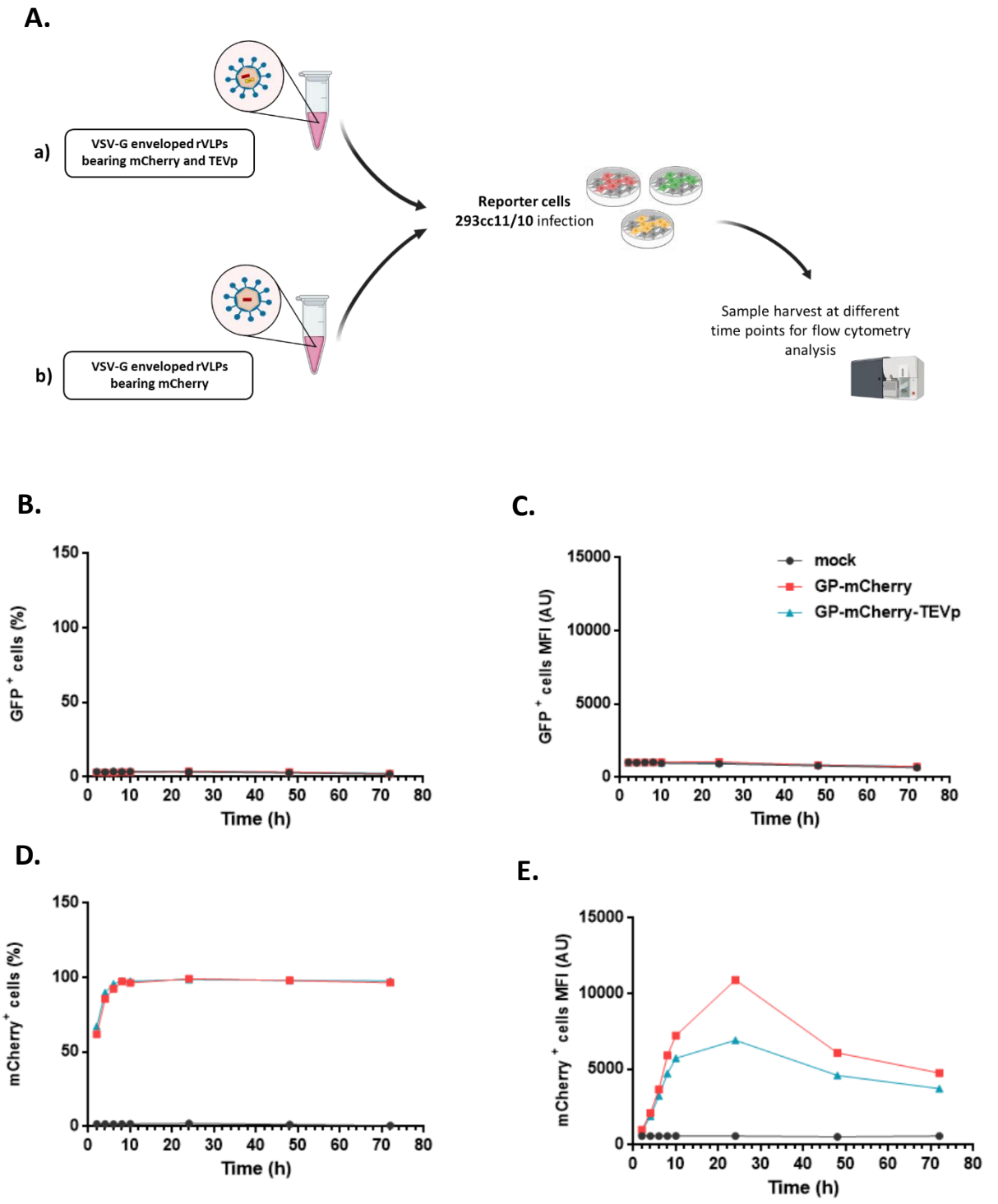

Figure 3. 14 – Protein delivery and biosensor activation kinetics in retrovirus-like particles. (A) Vesicular stomatitis virus G enveloped retrovirus-like particles bearing **a)** mCherry and TEVp or **b)** mCherry were infected with a multiplicity of infection of 3 in 293cc11/10 reporter cells. Samples were harvested 2, 4, 6, 8, 10, 24, 48 and 72 h post-infection and analyzed by flow cytometry for **(B)** GFP positive cells (%) and **(C)** their MFI and **(D)** mCherry positive cells (%) and **(E)** their respective MFI. Mock represents a supernatant obtained from 293T cells not producing rVLPs. Data represents a single experiment. AU, arbitrary units

4 Discussion and conclusion

The dramatic increase in the emergence and re-emergence of epidemic viruses, like ZIKV and CHIKV, observed over the past decades has brought deep concerns for society. The infectious nature of these viruses has resulted in worldwide outbreaks, causing severe debilitating conditions or even death to thousands of people. Established transmission chains coupled to human population growth, urbanization and long-distance travelling are the main causes behind this alarming situation. However, the lack of knowledge regarding these two arboviruses, evidences the world was not and still is not prepared to deal with this threat. In fact, the absence of knowledge about virus biology and pathogenesis and also the lack of methods to detect and quantify these viruses have a major impact in vaccine and antiviral development.

With this in mind, the scope of this thesis was focused on two main goals. The first one was to develop a cell-based platform to detect and quantify viral pathogens. For that, a genetically encoded split-GFP biosensing system triggered by viral protease activity was developed in mammalian cells. The second main goal was to develop a safe and efficient retroviral-like particle based protein presentation/delivery platform to screen an in-house library of peptides targeting envelope glycoproteins (and therefore inhibiting virus entry) and/or the viral protease (inhibiting virus life cycle). While the ultimate goal is to screen ZIKV and CHIKV glycoproteins and proteases, herein we developed a first proof of concept using VSV-G enveloped rVLPs bearing the highly efficient TEV viral protease.

4.1 Design and validation of split-GFP sensors activated by viral protease proteolysis

To develop the biosensing system exploiting split-GFP features, three different strategies consisting in structural distortions into one (single distortion) or both (dual distortion) GFP complementary fragments were designed: eGFP11, cyGFP11 and ccGFP10+ccGFP11 (**Figure 3.1**). The implemented structural distortions prevented fragment complementation and fluorescence emission until viral protease processing. To validate these strategies and understand which one presented the best performance, the developed sensors were transiently expressed in 293T together with a mock or the proof of concept viral protease – TEVp – and assessed for total fluorescence (**Figure 3.3A**).

Regarding distortion introduced by eglin c embedment – eGFP11 – no fluorescence was observed by fluorescence microscopy in the presence of TEVp (**Figure 3.3B**) and a SNR of 0.6 ± 0.04 was obtained when analyzed by flow cytometry (**Figure 3.3C**). These results suggest that the sensor was not being activated, possibly because TEVp could not efficiently reach the cleavage site for proteolytic processing, and thus, fragments remained separated. Interestingly, this strategy presented more background fluorescence in the presence of a mock plasmid than in the presence of TEVp. Moreover, of the three developed strategies, eGFP11 was the one that presented the highest background fluorescence. This suggests that embedding of GFP11 into eglin c is not fully efficient at altering the native spatial conformation of the GFP fragment, leaving room for fragment self-assembly and fluorescence reestablishment.

Relatively to strategy cyGFP11, a considerable fluorescent signal and a lower background fluorescence than eGFP11 was observed by fluorescence microscopy (**Figure 3.3B**), which translated an increased SNR of 20 ± 3 when analyzed by flow cytometry (**Figure 3.3C**). Although lower than eGFP11, the still observable background suggests that, in a similar fashion to eGFP11, intein cyclization is not entirely efficient at structurally distorting the GFP11 fragment.

Finally, and when analyzed at the fluorescence microscope, the ccGFP10+ccGFP11 strategy showed the lowest background fluorescence (**Figure 3.3B**). This suggests that dual distortions presented a better performance in preventing GFP fragment self-assembly than single distortions. Despite the similar fluorescence pattern observed between cyclization and coiled-coils strategies through fluorescence microscopy, the low background fluorescence, coupled to high fluorescence emission after proteolytic cleavage, led to an outstanding increase in SNR, up to 97 ± 21, when analyzed by flow cytometry (**Figure 3.3C**). The 162-fold and 5-fold increase in sensor performance when compared to eGFP11 and cyGFP11 strategies, demonstrated this was the best strategy to establish a biosensor with low background and high signal.

4.2 Design, validation, and characterization of chimeric retrovirus polyproteins

After knowing which was the best design for a biosensor, strategies to develop chimeric rVLPs with monitorable infection and sensor activation for antiviral peptide screening were established. Two different strategies were designed (**Figure 3.4**): a single strategy, comprised by two different rVLPs – one harboring an mCherry to monitor infection and another TEVp for sensor activation – and a dual strategy comprised by a single rVLP with both proteins – giving simultaneously indications of whether the cells were infected and whether the sensor was activated. While the dual rVLP provides an optimal design, introduction of the two coding sequences – mCherry and TEVp – might lead to impairment of GP functionality and virus production. Indeed, Voelkel and colleagues previously showed that introduction of foreign coding sequences was possible in between MA and P12 proteins (as we did), but still at the expense of lower virus production [116]. As such, before moving to rVLPs production, the different strategies of the chimeric rVLPs were functionally validated and characterized.

In a first phase, plasmids corresponding to each strategy were transfected into 293T cells to validate the respective constructions. The optimum fluorescent signal intensities obtained for GP-mCherry and GP-mCherry-TEVp constructions demonstrated that mCherry protein was fully functional, suggesting an efficient processing by the retroviral protease (**Figure 3.6C** and **Figure 3.6D**). Moreover, the similar behavior obtained for GP-mCherry and GP-mCherry-TEVp suggests that the introduction of another coding sequence (TEVp) and flanking restriction sites did not negatively impact mCherry activity. To verify if retrovirus protease was indeed correctly processing the polyprotein, releasing mCherry and TEVp as single proteins, a western blotting on total protein extracts from the transiently transfected 293T cells was performed. The obtained results showed that, in addition to the expected single mCherry protein (28 KDa), several other different sized proteins were present in both GP-mCherry and GP-mCherry-TEVp extracts (**Figure 3.7**). These results suggested that mCherry was being released not only as single protein but also in fusion to other neighboring proteins of RV *gag-pro-pol*

polyprotein. This effect may result in lower single mCherry protein concentrations and may affect its performance by interfering with proper folding and chromophore maturation. A possible solution to avoid this potential functionality impairment would be to resort to mCherry protein variants like the mScarlet or the superfolder SfCherry [117,118]. These proteins were projected to present great performance as fusion partners demonstrating high brightness and stability. Although protein intensity given by western blot results suggests that the single protein mCherry was the form present in a greater amount, overall, these results demonstrate that RV *gag-pro-pol* polyprotein is not being fully processed by the retrovirus protease, leading to partially processed by-products. On the other hand, it is also known that retrovirus only fully achieve maturation after cell release. Therefore, further analyses of polyprotein processing on purified particles are required to further elucidate the degree of its impairment by the insertion of mCherry and mCherry-TEVp.

To finalize chimeric rVLPs characterization, the impact of protein insertion in rVLP titers was assessed. For that, the number of physical particles present in transfected cells supernatant was determined by performing an ELISA targeting rVLPs capsid protein p30. The concentrations obtained for each chimeric *gag-pro-pol* evidenced that introducing mCherry or TEVp in the *gag-pro-pol* polyprotein resulted in a decrease in production relatively to parental control, showing that foreign protein insertions into the RV polyprotein originates titer reductions (**Figure 3.8B**). Among the three tested designs, GP-mCherry was the construction that presented the most similar yields to the control, demonstrating that mCherry insertion was the one affecting less significatively particle production yields. On the other hand, GP-TEVp and GP-mCherry-TEVp constructions were responsible for a sharper and similar decline, evidencing the role of TEVp in production impairment. As GP titers are normally translated in values reaching an order of 10^9 physical particles/mL, 9% of that value (relative titer obtained for GP-mCherry-TEVp) could still present a good working range. As GP-mCherry-TEVp did not present a substantial titer reduction in comparison to single TEVp strategy, and considering it allows the concomitant monitoring of cell entry and proteolytic activity, it still constitutes the most valuable candidate for our virus-based platform.

Having validated the chimeric polyproteins processing, their ability to function as good indicators of transfection/infection and to activate the optimal biosensors was evaluated. For that, each chimeric RV *gag-pro-pol* coding plasmid was co-transfected with the split-GFP coiled-coils distorted biosensor in 293T cells. The obtained results not only showed GP-mCherry-TEVp has a similar behavior as an indicative of transfection in comparison to GP-mCherry (**Figure 3.10D** and **Figure 3.10E**) but also showed similar sensor activation when comparing to GP-TEVp (**Figure 3.10B** and **Figure 3.10C**). Despite the larger size of GP-mCherry-TEVp polyprotein and additional coding sequence and processing site in between GP relatively to single strategies, this dual strategy comprises an equally competent approach. Statistically different results are observed between rVLPs harboring TEVp and the TEVp plasmid positive control (only expressing TEVp), which showed higher percentages of sensor activation and even higher signal intensity values. Although being an experimental control, these differences could be expected since TEVp and RV *gag-pro-pol* polyprotein are codified by totally different plasmids. Besides having different sizes, transcription is induced by different promotors – CMV for TEVp vs hEF1α-HTLV for RV *gag-pro-pol*. Also, while in the case of TEVp the resultant product is a

single protein, for *gag-pro-pol* the product is a polyprotein that needs to be processed to release TEVp as a single protein, causing, comparatively, a decrease in expression and activity. In the absence of TEVp, an increase in sensor background relatively to previous sensor distortion schemes characterization, was noticed (**Figure 3.3B**). However, while the characterization of the biosensors was performed in a Sysmex Partec flow cytometer, the characterization of the chimeric polyproteins was performed in a FACSCelesta flow cytometer, equipped with more powerful and sensitive lasers and detectors. Like previously observed for TEVp positive control, mock control (a negative control for sensor's assessment but a positive control for transfection monitoring) presented higher signal intensities than rVLPs harboring mCherry. Once again, theses variances may be explained by plasmids different designs. Not only the mock control constitutes a much smaller plasmid but also the mCherry is transcribed as a single protein in contrast to GP constructions, where it is found in the context of a polyprotein.

After successful validation and characterization of the different possible designs for chimeric RV polyproteins, we proceeded with one more step of characterization using the established stable sensor population. With this, we were not only characterizing the cell line, but also evaluating the applicability of the designed RV polyproteins in our viral pathogen detection and quantification system. For that, transfections with GP, GP-mCherry, GP-TEVp and GP-mCherry-TEVp were performed for sensor activation and performance assessment. The obtained results showed no sensor activation in TEVp presence (**Figure 3.12B**). While it might be hypothesized that the TEVp in the chimeric polyprotein is not functional, its functionality was already shown in transient co-transfection with the biosensors (**Figure 3.10B** and **Figure 3.10C**). As such, absence of sensor activation in stable cells should not be correlated with lack of TEVp activity but to the sensor reporter cells (the 293cc11/10). This issue might possibly be correlated with low fragment expression or the application of a not ideal fragment ratio expression in these cells.

4.3 Retrovirus-like particles production and characterization

Overall, the dual strategy – chimeric RV polyprotein expressing both mCherry and viral protease – showed similar functionality to polyproteins expressing only mCherry or TEVp, although with lower particle production (**Figure 3.10** and **Figure 3.8B**). As such, as it allows to assess simultaneously virus entry and viral proteolytic activity, we further characterized these particles for protein presentation (envelope glycoproteins) and delivery (TEVp as proof of concept). As a backup strategy, we also characterized chimeric rVLPs bearing only the mCherry reporter as they allow tracking of virus entry and showed good particle productivity (**Figure 3.8B**). Chimeric rVLPs were transiently produced with each of the GP-mCherry or GP-mCherry-TEVp plasmids, and, for this initial proof of concept, making use of the pantropic VSV-G envelope glycoproteins, since this envelope assures high infectability of target cells. After production, rVLPs were titrated using mCherry fluorescence and *LacZ* transgene expression to acknowledge respectively titers of transducing and integrative particles (**Figure 4.1**). As a naturally occurring process, rVLPs assembly originates several different particles, which are roughly divided into total physical ones, transducing particles, and integrative particles. While physical particles comprise all particles, whether they are immature or lacking any component (such as the envelope or

the transgene), transducing particles englobe all the particles able to enter the host cell (having at least a fully functional envelope). Integrative particles represent an even smaller subset of the latter as they are able to integrate the transgene into the host cell genome. For that, complete functionality of the particle – such as envelope incorporation, complete processing of the GP polyprotein and, correct packaging of the transgene – is necessary.

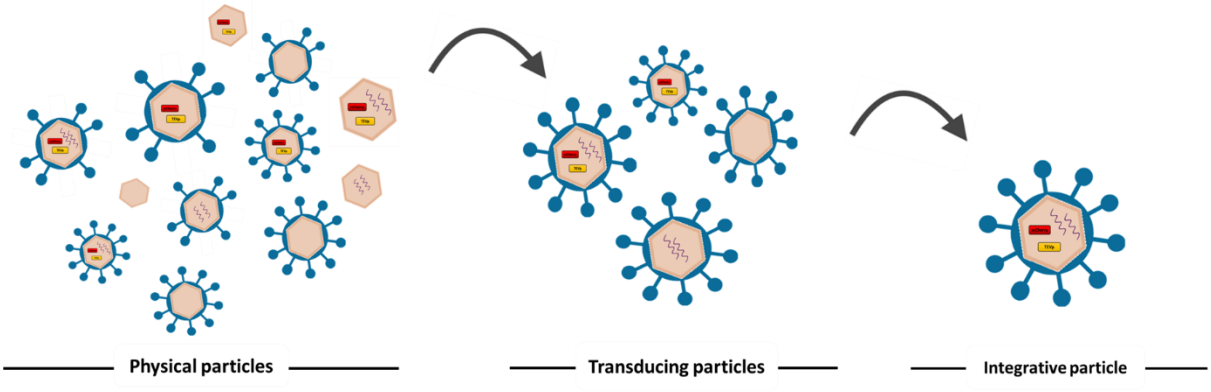

Figure 4. 1 – Schematic representation of physical, transducing, and integrative particles and their differences. During retrovirus-like particle assembly, three different types of particles are produced: physical, transducing, and integrative particles. While physical particles englobe all the possible produced forms, whether they are immature or lacking any component, transducing particles are the ones able to entry a target cell, and thus present an intact envelope. Integrative particles represent a small subset of transducing particles that are totally functional and thus able to integrate the transgene.

The similar values obtained for GP-mCherry and GP-mCherry-TEVp transducing titers, suggest once again that the introduction of an additional coding sequence (TEVp) did not affect rVLP total particle production. Moreover, the similarity between integrative titers of the parental control and GP-mCherry suggests that mCherry insertion also did not affect production of integrative particles. However, GP-mCherry-TEVp integrative particle titers were severely affected, leading to a decrease of approximately 100-fold in integrative particle titer. These results suggest that addition of TEVp to the RV polyprotein may impair the correct polyprotein maturation, thus affecting transgene integration.

It is important to highlight that in a transducing particle the viral envelope must be intact allowing for correct glycoprotein attachment and consequent cell entry. However, not all particles that are able to enter the cell are perfectly assembled rVLPs since some of them may not be correctly matured and may or may not have encapsulated viral genome. As such, particle titration by mCherry fluorescence may not include the mCherry proteins resulting from partially processed polyproteins. As previously mentioned, partial polyprotein processing may interfere with chromophore maturation, and thus signal intensity, lowering mCherry MFI and its detection. However, it is important to point out that to correctly verify if the polyprotein is being completely and correctly processed or not, western blots of purified rVLPs must be performed. In addition, it is noteworthy to keep in mind that these productions were performed with proof of concept envelopes, meaning that the different nature of ZIKV or CHIKV envelopes of the chimeric rVLPs to be produced in the future may introduce different variants in the production's quality outcome.

For the final purpose of chimeric rVLPs, which is viral entry and protease targeting antiviral testing, particles do not necessarily need to be integrative, providing that they are able to enter the cell and present a correctly processed GP.

Finally, to understand the kinetics of protein presentation and delivery, the previously established reporter cell population was infected with the characterized stocks of chimeric rVLPs and monitored for 72 h. Absence of GFP fluorescence when evaluating TEVp delivery revealed once again absence of sensor activation, which may be explained by the previously discussed factors in section 4.2. Results obtained through mCherry monitoring revealed successful infection efficiencies, achieving the highest value (100%) approximately 10 hours post-transduction. Additionally, such monitoring permitted to understand that mCherry fluorescent signal intensity increased in a linear form, reaching the highest point at 24 h post-infection. These findings not only evidenced rVLPs integrity, but also permitted to understand that at 24 h post-infection we could assess transduction and signal intensity at their best performances.

With this information we could develop protocols with optimized analysis points not only for titration purposes but also for the envisioned antiviral screenings. Notwithstanding, it is important to point out that this study was performed with proof of concept rVLPs, which bear a different type of envelope. Hence, despite providing an estimate, values may moderately differ when evaluating the final chimeric particles.

Overall, we could conclude from this work that rVLPs provide functional particles to be used in cell entry assays. Indeed, their suitability for pseudotyping makes them excellent tools not only for antiviral screenings but also for antibody neutralizing assays, thus also providing an excellent platform for vaccine development tests also. These functional particles flexibility to incorporate mCherry reporter protein showed to be a good strategy for particle entry monitoring during cell entry-based assays. Incorporation of proteases within rVLPs showed however to be more challenging as this may hamper particle production and maturation. From the developed biosensor platforms based on split-GFP distortion schemes, coiled-coils was the one that presented the best performance in transient transfections. However, coiled-coils activation seemed to be inefficient in stable cells. Hence, further optimizations or alternative biosensor designs should be considered to detect with sensitivity the protease or other viral enzymes activity. Finally, it is important to point out that the combined use of sensor reporter cells and pseudotyped rVLPs delivering viral enzymes provides a very flexible platform with an enormous potential in virus fundamental and applied research.

Part of this work resulted in an already published peer reviewed scientific article in “Sensors” scientific Journal: Guerreiro, M.R.; Fernandes, A.R.; Coroadinha, A.S. Evaluation of Structurally Distorted Split GFP Fluorescent Sensors for Cell-Based Detection of Viral Proteolytic Activity. Sensors 2021, 21, 24.

4.4 Future perspectives

In the future, two different work lines can be pursued. On one hand we should switch TEVp by ZIKV or CHIKV proteases and test them to activate new coiled-coil sensors harboring cleavage sites specifically recognized by these proteases. On the other hand, as the proof of concept stable expression system was not successful, we could continue this work with GP-mCherry single strategy design and confine antiviral screenings for viral entry targeting compounds. The short-term chosen approach is in fact the last one. For that, chimeric rVLPs harboring a mCherry and displaying ZIKV or CHIKV envelope glycoproteins would first be developed. Before proceeding to the desired tests, an in-house library of peptides with potential antiviral capacity will go through a series of selection steps to eliminate non-specific peptide binders and select the ones with affinity and specificity for the targets. After selection, rVLP susceptible cells would be incubated with different concentrations of the selected peptides and posteriorly challenged with the developed tool. With this, it would be possible to find the peptides that are able to bind the envelope glycoproteins and consequently prevent their attachment to the cell receptors, inhibiting a crucial step for viral entry. If they succeed in viral entry inhibition, cells would not present any kind of fluorescence (**Figure 4.2 A**). However, if they fail as antivirals, cells would display red fluorescence, indicating rVLPs infection (**Figure 4.2 B**).

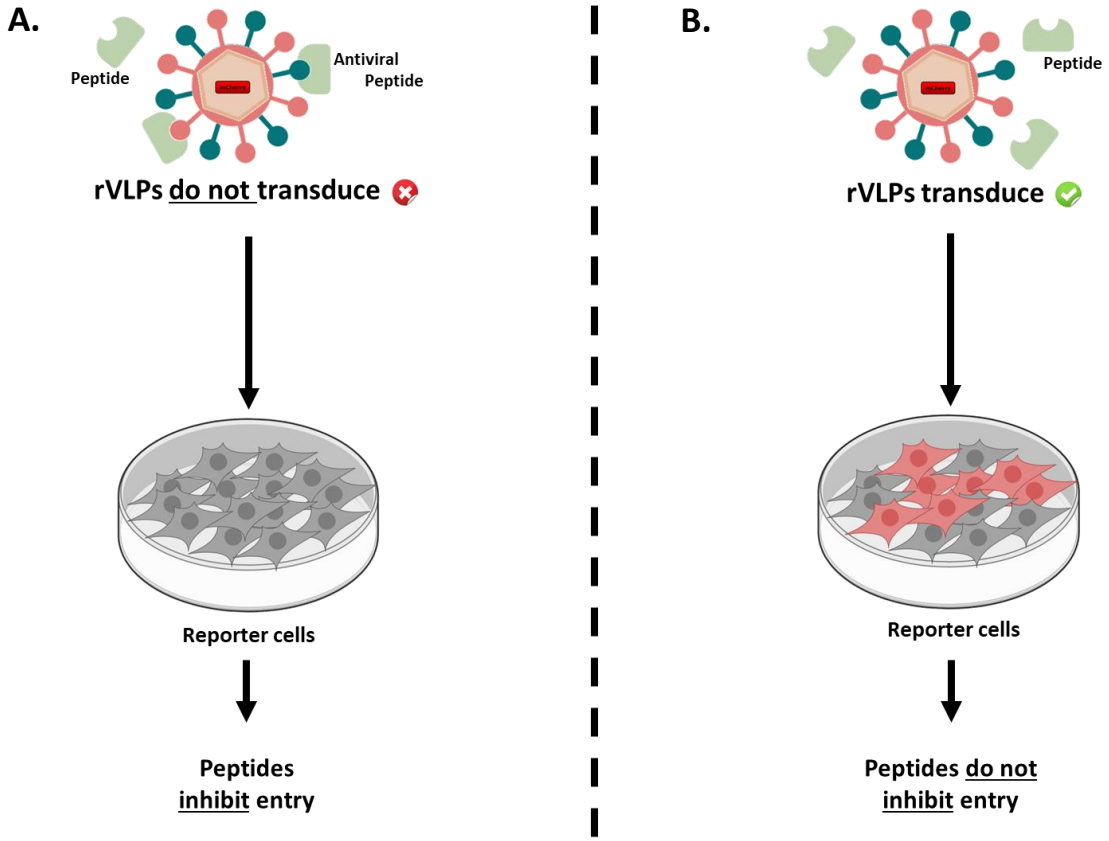

Figure 4. 2 – Future work. In the future work, mCherry chimeric retrovirus-like particles with envelopes expressing Zika or Chikungunya virus envelope proteins will be developed for antiviral screenings targeting envelope glycoproteins. When these particles are challenged with an in-house library of peptides with potential antiviral activity, two outcomes are expected: (**A)** peptides have antiviral effect, inhibiting viral entry and consequently preventing any fluorescent signal; (**B)** peptides do not have antiviral properties, allowing viral entry into the target cells and the emission of mCherry fluorescence.

5 References

1. Gubler, D. J. The global emergence/resurgence of arboviral diseases as public health problems. *Arch. Med. Res.* **33**, 330–342 (2002).

2. Weaver, S. C., Charlier, C., Vasilakis, N. & Lecuit, M. Zika, Chikungunya, and Other Emerging Vector-Borne Viral Diseases. *Annu. Rev. Med.* **69**, 395–408 (2018).

3. Genetic and Rare Diseases Information Center (GARD). *Neglected Diseases*. https://rarediseases.info.nih.gov/files/neglected_diseases_faqs.pdf.

4. Patterson, J., Sammon, M. & Garg, M. Dengue, zika and chikungunya: Emerging arboviruses in the new world. *Western Journal of Emergency Medicine* vol. 17 671–679 (2016).

5. Petersen, L. R., Jamieson, D. J., Powers, A. M. & Honein, M. A. Zika Virus. *N. Engl. J. Med.* **374**, 1552–1563 (2016).

6. Galán-Huerta, K. A., Rivas-Estilla, A. M., Fernández-Salas, I., Farfan-Ale, J. A. & Ramos-Jiménez, J. Chikungunya virus: A general overview. *Med. Univ.* **17**, 175–183 (2015).

7. Musso, D. & Gubler, D. J. Zika Virus Fact Sheet. *WPRO Fact Sheets* **29**, 1- (2016).

8. Failloux, A. B. The emergences of arboviruses: Chikungunya and zika. *Bull. Acad. Natl. Med.* **200**, 1589–1603 (2016).

9. Song, B. H., Yun, S. I., Woolley, M. & Lee, Y. M. Zika virus: History, epidemiology, transmission, and clinical presentation. *J. Neuroimmunol.* **308**, 50–64 (2017).

10. World Health Organization (WHO). *Global overview ZIKA EPIDEMIOLOGY UPDATE*. (2019).

11. Spitz, D. Zika: the continuing threat. *Bull World Heal. Organ* doi:10.2471/BLT.19.020119.

12. World Health Organization (WHO). *Countries and territories with current or previous Zika virus transmission*. https://www.who.int/ith/Zika_map.pdf (2017).

13. Tappe, D. *et al.* First case of laboratory-confirmed Zika virus infection imported into Europe, November 2013. *Eurosurveillance* **19**, 20685 (2014).

14. WHO, W. H. O. *Situation Report: Zika virus Microcephaly, Guillain-Barré syndrome* . http://apps.who.int/iris/bitstream/10665/250626/1/WHO-ZIKV-SRF-16.4-eng.pdf?ua=1 (2016).

15. Arsuaga, M., Bujalance, S. G., Díaz-Menéndez, M., Vázquez, A. & Arribas, J. R. Probable sexual transmission of Zika virus from a vasectomised man. *The Lancet Infectious Diseases* vol. 16 1107 (2016).

16. D'Ortenzio, E., Matheron, S. & Yazdanpanah, Y. Evidence of sexual transmission of Zika Virus. *New England Journal of Medicine* vol. 374 2195–2198 (2016).

17. Health Organization Regional Office for Europe, W. *ZIKA VIRUS Technical report Interim Risk Assessment WHO European Region*. http://www.euro.who.int/pubrequest (2016).

18. European Centre for Disease Prevention and Contro. *Zika Annual Epidemiological Report for 2018*. (2019).

19. European Centre for Disease Prevention and Control. Epidemiological update: Outbreaks of Zika virus and complications potentially linked to the Zika virus infection, 13 October 2016.

https://www.ecdc.europa.eu/en/news-events/epidemiological-update-outbreaks-zika-virus-and-complications-potentially-linked-32.

20. Caglioti, C. *et al.* Chikungunya virus infection: An overview. *New Microbiol.* **36**, 211–227 (2013).

21. European Centre for Disease Prevention and Control (ECDC). Factsheet about chikungunya. https://www.ecdc.europa.eu/en/chikungunya/facts/factsheet.

22. Burt, F. J., Rolph, M. S., Rulli, N. E., Mahalingam, S. & Heise, M. T. Chikungunya: A re-emerging virus. *Lancet* **379**, 662–671 (2012).

23. Centers for disease control and prevention (CDC). Geographic Distribution | Chikungunya virus | CDC. https://www.cdc.gov/chikungunya/geo/index.html.

24. Bodenmann, P. & Genton, B. Chikungunya: an epidemic in real time. *Lancet* **368**, 258 (2006).

25. Mudur, G. Failure to control mosquitoes has led to two fever epidemics in India. *BMJ* **333**, 773 (2006).

26. Taubitz, W. *et al.* Chikungunya Fever in Travelers: Clinical Presentation and Course. *Clin. Infect. Dis.* **45**, e1–e4 (2007).

27. Beltrame, A. *et al.* Imported chikungunya infection, Italy [6]. *Emerging Infectious Diseases* vol. 13 1264–1266 (2007).

28. Sambri, V., Cavrini, F., Rossini, G., Pierro, A. & Landini, M. P. The 2007 epidemic outbreak of Chikungunya virus infection in the Romagna region of Italy: A new perspective for the possible diffusion of tropical diseases in temperate areas? *New Microbiologica* vol. 31 303–304 (2008).

29. Rezza, G. *et al.* Infection with chikungunya virus in Italy: an outbreak in a temperate region. *Lancet* **370**, 1840–1846 (2007).

30. Wahid, B., Ali, A., Rafique, S. & Idrees, M. Global expansion of chikungunya virus: mapping the 64-year history. *International Journal of Infectious Diseases* vol. 58 69–76 (2017).

31. Tomasello, D. & Schlagenhauf, P. Chikungunya and dengue autochthonous cases in Europe, 2007-2012. *Travel Medicine and Infectious Disease* vol. 11 274–284 (2013).

32. Delisle, E. *et al.* Chikungunya outbreak in Montpellier, France, September to October 2014. *Eurosurveillance* **20**, 21108 (2015).

33. WHO, W. H. O. WHO | Chikungunya – France. *WHO* (2017).

34. Ganesan, V. K., Duan, B. & Reid, S. P. Chikungunya virus: Pathophysiology, mechanism, and modeling. *Viruses* **9**, 1–14 (2017).

35. da Cunha, R. V. & Trinta, K. S. Chikungunya virus: Clinical aspects and treatment. *Mem. Inst. Oswaldo Cruz* **112**, 523–531 (2017).

36. Newman, C., Friedrich, T. C. & O'connor, D. H. Macaque monkeys in Zika virus research: 1947-present A brief history of Zika virus. doi:10.1016/j.coviro.2017.06.011.

37. Sirohi, D. & Kuhn, R. J. Zika Virus Structure, Maturation, and Receptors. *J. Infect. Dis.* **216**, S935–S944 (2017).

38. SIB Swiss Institute of Bioinformatics. Zika Virus. *Viral Zone* https://viralzone.expasy.org/6756.

39. Agrelli, A., de Moura, R. R., Crovella, S. & Brandão, L. A. C. ZIKA virus entry mechanisms in human cells. *Infect. Genet. Evol.* **69**, 22–29 (2019).

40. Saxena, S. K., Elahi, A., Gadugu, S. & Prasad, A. K. Zika virus outbreak: an overview of the experimental therapeutics and treatment. *VirusDisease* **27**, 111–115 (2016).

41. Acosta-Ampudia, Y. *et al.* Autoimmune neurological conditions associated with zika virus infection. *Front. Mol. Neurosci.* **11**, (2018).

42. Zeller, H., Van Bortel, W. & Sudre, B. Chikungunya: Its history in Africa and Asia and its spread to new regions in 2013-2014. *J. Infect. Dis.* **214**, S436–S440 (2016).

43. Firth, A. E., Chung, B. Y. W., Fleeton, M. N. & Atkins, J. F. Discovery of frameshifting in Alphavirus 6K resolves a 20-year enigma. *Virol. J.* **5**, (2008).

44. SIB Swiss Institute of Bioinformatics. Alphavirus. *Viral Zone* https://viralzone.expasy.org/625.

45. Silva, L. A. & Dermody, T. S. Chikungunya virus: Epidemiology, replication, disease mechanisms, and prospective intervention strategies. *J. Clin. Invest.* **127**, 737–749 (2017).

46. Sunit Kumar Singh and Salini Krishnan Unni. Chikungunya virus: host pathogen interaction. *Rev. Med. Virol.* **21**, (2011).

47. Jose, Joyce Snyder, Jonathan E Kuhn, R. J. A structural and functional perspective of alphavirus replication and assembly. *Futur. Microbiol.* 837–856 (2010) doi:10.2217/fmb.09.59.A.

48. Froshauer, S., Kartenbeck, J. & Helenius, A. Alphavirus RNA replicase is located on the cytoplasmic surface of endosomes and lysosomes. *J. Cell Biol.* **107**, 2075–2086 (1988).

49. Chen, K. C. *et al.* Comparative analysis of the genome sequences and replication profiles of chikungunya virus isolates within the East, Central and South African (ECSA) lineage. *Virol. J.* **10**, 2–9 (2013).

50. Soonsawad, P. *et al.* Structural Evidence of Glycoprotein Assembly in Cellular Membrane Compartments prior to Alphavirus Budding. *J. Virol.* **84**, 11145–11151 (2010).

51. Arévalo, M. T., Huang, Y., Jones, C. A. & Ross, T. M. Vaccination with a chikungunya virus-like particle vaccine exacerbates disease in aged mice. *PLoS Negl. Trop. Dis.* **13**, 1–18 (2019).

52. Higgs, S., Vanlandingham, D. L. & Powers, A. M. *Chikungunya and Zika viruses : global emerging health threats - Chapter 11. Chikungunya and Zika Virus Vaccines*.

53. Poland, G. A., Ovsyannikova, I. G. & Kennedy, R. B. Zika Vaccine Development: Current Status. *Mayo Clin. Proc.* **94**, 2572–2586 (2019).

54. Weaver, S. C., Osorio, J. E., Livengood, J. A., Chen, R. & Stinchcomb, D. T. Chikungunya virus and prospects for a vaccine. *Expert Rev. Vaccines* **11**, 1087–1101 (2012).

55. Fuenmayor, J., Gòdia, F. & Cervera, L. Production of virus-like particles for vaccines. *N. Biotechnol.* **39**, 174–180 (2017).

56. Buonaguro, F. M. & Buonaguro, L. Virus-like particles in vaccine development. *Virus-like Part. Vaccine Dev.* **9**, 1–136 (2014).

57. Grgacic, E. V. L. & Anderson, D. A. Virus-like particles: Passport to immune recognition. *Methods* **40**, 60–65 (2006).

58. Mohsen, M. O., Zha, L., Cabral-Miranda, G. & Bachmann, M. F. Major findings and recent advances in virus–like particle (VLP)-based vaccines. *Semin. Immunol.* **34**, 123–132 (2017).

59. Lua, L. H. L. *et al.* Bioengineering virus-like particles as vaccines. *Biotechnol. Bioeng.* **111**, 425–440 (2014).

60. Garg, H., Sedano, M., Plata, G., Punke, E. B. & Joshi, A. Development of Virus-Like-Particle Vaccine and Reporter Assay for Zika Virus. *J. Virol.* **91**, (2017).

61. Metz, S. W. *et al.* Effective Chikungunya Virus-like Particle Vaccine Produced in Insect Cells. *PLoS Negl. Trop. Dis.* **7**, (2013).

62. Kaczmarczyk, S. J., Sitaraman, K., Young, H. A., Hughes, S. H. & Chatterjee, D. K. Protein delivery using engineered virus-like particles. doi:10.1073/pnas.1101874108.

63. Jennifer Kouznetsova, Wei Sun, Carles Martínez-Romero, Gregory Tawa, Paul Shinn, Catherine Z Chen, Aaron Schimmer, Philip Sanderson, John C McKew, W. Z. & A. G.-S. Identification of 53 compounds that block Ebola virus-like particle entry via a repurposing screen of approved drugs. *Emerg. Microbes Infect.* **3**, (2014).

64. Yan, D., Wei, Y. Q., Guo, H. C. & Sun, S. Q. The application of virus-like particles as vaccines and biological vehicles. *Appl. Microbiol. Biotechnol.* **99**, 10415–10432 (2015).

65. Garg, H., Mehmetoglu-Gurbuz, T. & Joshi, A. Virus Like Particles (VLP) as multivalent vaccine candidate against Chikungunya, Japanese Encephalitis, Yellow Fever and Zika Virus. *Sci. Rep.* **10**, 1–13 (2020).

66. Abdelnabi, R., Neyts, J. & Delang, L. Chikungunya virus infections: time to act, time to treat. *Curr. Opin. Virol.* **24**, 25–30 (2017).

67. Mumtaz, N., van Kampen, J. J. A., Reusken, C. B. E. M., Boucher, C. A. B. & Koopmans, M. P. G. Zika Virus: Where Is the Treatment? *Curr. Treat. Options Infect. Dis.* **8**, 208–211 (2016).

68. Saiz, J. C. & Martín-Acebes, M. A. The race to find antivirals for zika virus. *Antimicrob. Agents Chemother.* **61**, 1–9 (2017).

69. X., de L., L., N. & R.N., C. Antiviral treatment of chikungunya virus infection. *Infect. Disord. - Drug Targets* **9**, 101–104 (2009).

70. Cheng, F., Murray, J. L. & Rubin, D. H. Drug Repurposing: New Treatments for Zika Virus Infection? *Trends Mol. Med.* **22**, 919–921 (2016).

71. Kang, C. B., Keller, T. H. & Luo, D. Zika Virus Protease: An Antiviral Drug Target. *Trends Microbiol.* **25**, 797–808 (2017).

72. Kaur, P. & Chu, J. J. H. Chikungunya virus: An update on antiviral development and challenges. *Drug Discov. Today* **18**, 969–983 (2013).

73. Bassetto, M. *et al.* Computer-aided identification, design and synthesis of a novel series of compounds with selective antiviral activity against chikungunya virus. *Antiviral Res.* **98**, 12–18 (2013).

74. Delvecchio, R. *et al.* Chloroquine, an endocytosis blocking agent, inhibits zika virus infection in different cell models. *Viruses* **8**, 1–15 (2016).

75. Mohsin Khan, S.R. Santhosh, Mugdha Tiwari, P.V. Lakshmana Rao, and M. P. Assessment of In Vitro Prophylactic and Therapeutic Efficacy of Chloroquine Against Chikungunya Virus in Vero Cells. *J. Med. Virol.* (2010) doi:10.1002/jmv.

76. Delogu, I. *et al.* In vitro antiviral activity of arbidol against Chikungunya virus and characteristics of a selected resistant mutant. *Antiviral Res.* **90**, 99–107 (2011).

77. Pohjala, L. *et al.* Inhibitors of alphavirus entry and replication identified with a stable Chikungunya replicon cell line and virus-based assays. *PLoS One* **6**, (2011).

78. Geraerts, M., Willems, S., Baekelandt, V., Debyser, Z. & Gijsbers, R. Comparison of lentiviral vector titration methods. *BMC Biotechnol.* **6**, 1–10 (2006).

79. Virocyt. An Overview of Virus Qunatification Techniques. *Axiomathes* 7 (2013) doi:10.1007/s10516-014-9260-9.

80. Agbulos, D. S., Barelli, L., Giordano, B. V. & Hunter, F. F. Zika virus: Quantification, propagation, detection, and storage. *Curr. Protoc. Microbiol.* **2016**, 15D.4.1-15D.4.16 (2016).

81. Paemanee, A., Wikan, N., Roytrakul, S. & Smith, D. R. Infectious Viral Quantification of Chikungunya Virus - Virus Plaque Assay. *Chikungunya Virus Methods Protoc.* **1426**, 179–193 (2016).

82. Pankaj, K. Virus Identification and Quantification. *Mater Methods* **3**, 1–22 (2013).

83. Ryu, W.-S. Diagnosis and Methods. *Mol. Virol. Hum. Pathog. Viruses* 47–62 (2017) doi:10.1016/b978-0-12-800838-6.00004-7.

84. Alera, M. T. *et al.* Zika virus infection, philippines, 2012. *Emerging Infectious Diseases* vol. 21 722–724 (2015).

85. Way, H. J., Bowen, E. T. W. & Platt, G. S. Comparative studies of some African arboviruses in cell culture and in mice. *J. Gen. Virol.* **30**, 123–130 (1976).

86. Digoutte, J. P., Calvo-Wilson, M. A., Mondo, M., Traore-Lamizana, M. & Adam, F. Continuous cell lines and immune ascitic fluid pools in arbovirus detection. *Res. Virol.* **143**, 417–422 (1992).

87. Zannoli, S. *et al.* Diagnostics and laboratory techniques. in *Chikungunya and Zika Viruses: Global Emerging Health Threats* 293–315 (Elsevier, 2018). doi:10.1016/B978-0-12-811865-8.00009-X.

88. Mardekian, S. K. & Roberts, A. L. Diagnostic Options and Challenges for Dengue and Chikungunya Viruses. *Biomed Res. Int.* (2015) doi:10.1155/2015/834371.

89. Chalfie, M., Tu, Y., Euskirchen, G., Ward, W. W. & Prasher, D. C. Green fluorescent protein as a marker for gene expression. *Science (80-.).* **263**, 802–805 (1994).

90. Manicassamy, B. *et al.* Analysis of in vivo dynamics of influenza virus infection in mice using a GFP reporter virus. *Proc. Natl. Acad. Sci. U. S. A.* **107**, 11531–11536 (2010).

91. Elliott, G. & O'Hare, P. Live-Cell Analysis of a Green Fluorescent Protein-Tagged Herpes Simplex Virus Infection. *J. Virol.* **73**, 4110–4119 (1999).

92. Mueller, S. & Wimmer, E. Expression of foreign proteins by poliovirus polyprotein fusion: analysis of genetic stability reveals rapid deletions and formation of cardioviruslike open reading frames. *J. Virol.* **72**, 20–31 (1998).

93. Gläsker, S. *et al.* Virus replicon particle based Chikungunya virus neutralization assay using Gaussia luciferase as readout. *Virol. J.* **10**, 1–10 (2013).

94. Deng, C. L. *et al.* Development of neutralization assay using an eGFP chikungunya virus. *Viruses* **8**, 1–16 (2016).

95. Shan, C. *et al.* An Infectious cDNA Clone of Zika Virus to Study Viral Virulence, Mosquito Transmission, and Antiviral Inhibitors. *Cell Host Microbe* **19**, 891–900 (2016).

96. Gadea, G. *et al.* A robust method for the rapid generation of recombinant Zika virus expressing the GFP reporter gene. *Virology* **497**, 157–162 (2016).

97. Frumence, E., Viranaicken, W., Gadea, G. & Desprès, P. A GFP reporter MR766-based flow

cytometry neutralization test for rapid detection of zika virus-neutralizing antibodies in serum specimens. *Vaccines* **7**, (2019).

98. Ruggli, N. & Rice, C. M. Functional cDNA clones of the Flaviviridae: strategies and applications. *Advances in virus research* vol. 53 183–207 (1999).

99. Tamura, T. *et al.* Characterization of Recombinant Flaviviridae Viruses Possessing a Small Reporter Tag. *J. Virol.* **92**, (2018).

100. Stripecke, R. *et al.* Immune response to green fluorescent protein: Implications for gene therapy. *Gene Ther.* **6**, 1305–1312 (1999).

101. Steel, J. J., Franz, A. W. E., Sanchez-Vargas, I., Olson, K. E. & Geiss, B. J. Subgenomic reporter RNA system for detection of alphavirus infection in mosquitoes. *PLoS One* **8**, 1–12 (2013).

102. McFadden, M. J. *et al.* A fluorescent cell-based system for imaging zika virus infection in real-time. *Viruses* **10**, 13–18 (2018).

103. Arias-Arias, J. L., MacPherson, D. J., Hill, M. E., Hardy, J. A. & Mora-Rodríguez, R. A fluorescence-activatable reporter of flavivirus NS2B–NS3 protease activity enables live imaging of infection in single cells and viral plaques. *J. Biol. Chem.* **295**, 2212–2226 (2020).

104. Addgene. Addgene: Lentiviral Guide. https://www.addgene.org/guides/lentivirus/.

105. Coroadinha, A. S. *et al.* The use of recombinase mediated cassette exchange in retroviral vector producer cell lines: Predictability and efficiency by transgene exchange. *J. Biotechnol.* **124**, 457–468 (2006).

106. Scientific, T. & Phusion. *Phusion High-Fidelity DNA polymerase product information*.

107. Korbie, D. J. & Mattick, J. S. Touchdown PCR for increased specificity and sensitivity in PCR amplification. *Nat. Protoc.* **3**, 1452–1456 (2008).

108. Clontech (Takara). *In-Fusion® HD Cloning Kit User Manual*. *In-Fusion Cloning* vol. 1 https://www.google.com/%5Cnpapers2://publication/uuid/41E4AB88-9309-4873-A108-046E03DED691 (2012).

109. Zhu, B., Cai, G., Hall, E. O. & Freeman, G. J. In-Fusion™ assembly: Seamless engineering of multidomain fusion proteins, modular vectors, and mutations. *Biotechniques* **43**, 354–359 (2007).

110. Dull, T. *et al. A Third-Generation Lentivirus Vector with a Conditional Packaging System*. *JOURNAL OF VIROLOGY* vol. 72 (1998).

111. Cabantous, S., Terwilliger, T. C. & Waldo, G. S. Protein tagging and detection with engineered self-assembling fragments of green fluorescent protein. *Nat. Biotechnol.* **23**, 102–107 (2005).

112. Callahan, B. P., Stanger, M. J. & Belfort, M. Protease Activation of Split Green Fluorescent Protein. *ChemBioChem* **11**, 2259–2263 (2010).

113. Sakamoto, S. *et al.* Creation of a caspase-3 sensing system using a combination of split-GFP and split-intein. *Chem. Commun.* **49**, 10323–10325 (2013).

114. To, T. L. *et al.* Rational Design of a GFP-Based Fluorogenic Caspase Reporter for Imaging Apoptosis In Vivo. *Cell Chem. Biol.* **23**, 875–882 (2016).

115. Cesaratto, F., Burrone, O. R. & Petris, G. Tobacco Etch Virus protease: A shortcut across biotechnologies. *J. Biotechnol.* **231**, 239–249 (2016).

116. Voelkel, C. *et al.* Protein transduction from retroviral Gag precursors. *Proc. Natl. Acad. Sci. U. S. A.* **107**, 7805–7810 (2010).

117. Bindels, D. S. *et al.* MScarlet: A bright monomeric red fluorescent protein for cellular imaging. *Nat. Methods* **14**, 53–56 (2016).

118. Pedelacq, J. D. & Cabantous, S. Development and applications of superfolder and split fluorescent protein detection systems in biology. *Int. J. Mol. Sci.* **20**, (2019).

6 Supporting information

Table 6.1 – Primers and templates for plasmid construction.

CLONING PRIMERS				
Final Plasmid	**Insert**			**Cloning vector**
	Coding for	**Source**	**Primer sequence (5'– 3')**	
pRRLSIN.cPPT.CMV.TEVp.EMCVIRES.Zeo.WPRE	TEVp	pRRLSIN.EF1a.TEVp.IRES.Puro.WPRE.v2	**Fw**: CGTCAGATCCGCTAGCCACCATGGGCGAGAG **Rv:** CGGGCTCGATGGATCCTTAGTTCATCAGCTGTGTGGCCTC	pRRLSIN.cPPT.CMV.Adenain-MVGLG-VIc.EMCVIRES.Zeo.WPRE opened with NheI and BamHI
pRRLSIN.CMV.eENLYFQS.IRES.Puro.WPRE.v2	eGFP11-ENLYFQS	pRRLSIN.CMV.eLRGAG.v2.IRES.Puro.WPRE.v2	**Fw:** CGTCAGATCCGCTAGCCGCCACCATGACCGAGTTT **Rv:** GGTGATGCCAGCGGCGTT	pRRLSIN.CMV.eLRGAG.v2.IRES.Puro.WPRE.v2 opened with NheI and BamHI
			Fw: GCCGCTGGCATCACCGAAAATTTGTACTTTCAAAGTTACAATAGAGTGCGGGTGTTCTAC **Rv:** CGGGCTCGATGGATCCTCAGCCCACGTGT	
pRRLSIN.CMV.cENLYFQS-GFPS11.IRES.Puro.WPRE.v2	cyGFP11-ENLYFQS	pRRLSIN.CMV.cLRGAG-GFPS11.IRES.Puro.WPRE.v2	**Fw:** CGTCAGATCCGCTAGCCGCCACCATGATCAAGATCG **Rv:** ACTTTGAAAGTACAAATTTTCGTTGAAGCAGTTGCTGGCGA	pRRLSIN.CMV.cLRGAG-GFPS11.IRES.Puro.WPRE.v2 opened with NheI and PstI
			Fw: TTGTACTTTCAAAGTAGGGACCACATGGTGCTG **Rv:** CGGGCTCGATGGATCTCTGCAGTCACAGGTCCTCTTCGGAGATCA	
pRRLSIN.CMV.E5-GFPS10-ENLYFQS-GGS-K5.IRES.Zeo.WPRE.v2	ccGFP10-ENLYFQS	pRRLSIN.CMV.E5-GFPS10-GLRGAG-GGS-K5.IRES.Zeo.WPRE.v2	**Fw:** TCTGGAAAAGGGATCCTCGAAGG **Rv:** TAGACCCCCCGAATTCACTTTGAAAGTACAAATTTTCTTTCTCGTTTGGGTCTTTGCTCA	pRRLSIN.CMV.E5-GFPS10-GLRGAG-GGS-K5.IRES.Zeo.WPRE.v2 opened with BamHI and EcoRI

pRRLSIN.CMV.K5-GFPS11-ENLYFQS-E5.IRES.Puro.WPRE.v2	ccGFP11-ENLYFQS	gBlocks gene fragments (synthesized)	CGTCAGATCCGCTAGCCGCCACCATGGGGGGGTCTAAAGTATCTGCGCTCAAGGAAAAGGTATCAGCGCTCAAAGAGAAAGTGAGTGCTCTGAAAGAGAAAGTATCTGCTTTGAAGGAAAAAGTCTCCGCCTTGAAAGAAAGGGACCACATGGTCCTTCACGAGTACGTTAACGCCGCAGGAATCACCGAAAATTTGTACTTTCAAAGTGAGGTTAGTGCGCTGGAAAAGGAGGTTTCAGCTCTGGAAAAAGAAGTTAGTGCATTGGAAAAAGAAGTATCTGCGCTGGAAAAGGAAGTTTCTGCCCTGGAGAAGTAACTGCAGAGATCCATCG	pRRLSIN.CMV.K5-GFPS11-GLRGAG-E5.IRES.Puro.WPRE.v2 opened with NheI and PstI
pMLV-GP-mCherry	HTLV (Left Fragment)	pMLV-GP	**Fw:** GACTGTTACCACTCCCTTAAGTTTGA **Rv:** ATAAAGGGAGGATCGAGGCGG	pMLV-GP opened with AflII
	mCherry	pPuro_mCherry	**Fw:** CGCCTCGATCCTCCCTTTATCCTGCTCTGACACCTATGGTGAGCAAGGGCGAGGAG **Rv:** AGAGAAGGAGTGAGGGCTGGATAAAGGGAGGATCGAGGCTTGTACAGCTCGTCCATGCCG	
	p30 (Right Fragment)	pMLV-GP	**Fw:** CCAGCCCTCACTCCTTCTCTAGG **Rv:** CCTGCGATAGGCTTCCTTAAGTCTC	
pMLV-GP-TEVp	HTLV (Left Fragment)	pMLV-GP	**Fw:** GACTGTTACCACTCCCTTAAGTTTGA **Rv:** ATAAAGGGAGGATCGAGGCGG	pMLV-GP opened with AflII
	TEVp	pRRLSIN.cPPT.CMV.TEVp.EMCVIRES.Zeo.WPRE	**Fw:** CGCCTCGATCCTCCCTTTATCCTGCTCTGACACCTATGGGCGAGAGCCTGTTCAAGG **Rv:** AGAGAAGGAGTGAGGGCTGGATAAAGGGAGGATCGAGGGTTCATCAGCTGTGTGGCCTCTTTC	

	p30 (Right Fragment)	pMLV-GP	**Fw:** CCAGCCCTCACTCCTTCTCTAGG **Rv:** CCTGCGATAGGCTTCCTTAAGTCTC	
pMLV-GP-mCherry-TEVp	HTLV (Left Fragment)-mCherry	pMLV-GP-mCherry	**Fw:** GACTGTTACCACTCCCTTAAGTTTGA **Rv:** AGGGGTCAGAGCGGGGTACAGAGAGCTTCTAGGCTTGTACAGCTCGTCCATGCCG	pMLV-GP opened with AflII
	TEVp-p30 (Right Fragment)	pMLV-GP-TEVp	**Fw:** TGTACCCCGCTCTGACCCCTATGGGCGAGAGCCTGTTCAAGG **Rv:** CCTGCGATAGGCTTCCTTAAGTCTC	

Table 6.2 – VCN-qPCR primers.

Target Sequence	Primers sequence (5'– 3')	Probe sequence (5'– 3')
LTR	**Fw:** GCTAACTAGGGAACCCAC **Rv:** GCTAGAGATTTTCCACACTGA	FAM/CTTGCCTTG/ZEN/AGTGCTTCAAGTAGTG /IBFQ
ALB	Integrated in the Thermofisher mix, unknown sequence	